Tissue Engineering of the Human Atrium – Approaching Mechanisms of Genesis and Control of Atrial Fibrillation

A thesis submitted to the University of Manchester
for the degree of Doctor of Philosophy
in the Faculty of Engineering and Physical Sciences

2010

By
Phillip R. Law
School of Physics and Astronomy

Contents

List of tables

List of figures

Abstract

The University of Manchester
Phillip Robert Law
Doctor of Philosophy
Tissue Engineering of the Human Atrium – Approaching Mechanisms of Genesis and Control of Atrial Fibrillation
1st September 2010

Cardiovascular disease is prevalent across the western world and is a major cause of morbidity and mortality, accounting for approximately a third of all fatalities. Investigating the heart by simulating its electrophysiology via the aid of mathematical models has advanced significantly over the past 60 years and is now a well established field. While much of the research focus is placed on the ventricles, the study of the atria is in comparison neglected. Therefore this Thesis is focused on the genesis and maintenance of atrial fibrillation (AF). A series of case studies are performed whereby established biophysically detailed mathematical models are implemented and modified to incorporate electrophysical alterations of atrial cells resulting from a variety of external conditions.

The opening section of this Thesis is dedicated to developing a background to the field, including a discussion into the clinical aspect of the diagnosis and management of AF. The suitability of two atrial cell models is discussed and the development of single cell, 1D, 2D, and 3D multi-scale simulation protocols are described in detail. In addition measurements taken to quantify the arrhythmogenic properties of the cells susceptibility to AF are outlined. The second section is focused on the incorporation of conditions thought to enhance atrial tissues ability to initiate and maintain the genesis of AF. Included is a case study into the missence S140G gene mutation, and elevated physiological levels of the hormone Homocystein. The third section investigates the effectiveness of well established and widely used pharmacological treatments such as Beta-Blockers. In addition possible avenues of investigations for the development of atrial specific drugs are explored. These include blocking of the ultra rapid potassium channel and a more novel target for therapy via the targeting of $5HT_4$ receptors; which is transcribed solely in the atria and alters the electrophysical properties of the L-type Calcium current. The final part of this Thesis is dedicated to the development of a 2D atrial sheet model which includes electrical and spatial heterogeneities via the inclusion of multiple cell types and basic fiber orientation respectively. This allows for an investigation into the role that heterogeneities play in role genesis and maintenance of AF.

The main finding of this Thesis is that alterations to the electrophysiology of atrial cells, due to external factors, can be successfully simulated via the implementation of mathematically detailed atrial cell models. It is concluded that simulations of the KENQ1 mutation and elevated levels of Homocystein successfully reproduce conditions which increase the onset of AF. Established treatments such as Beta-Blockers are found to have limited effectiveness. Possible theoretical treatments, such as the blocking of $I_{Kur,}$ are found to provide a small amount of therapeutic benefit. In contrast, investigations into the effects of Serotonin were inconclusive. The study into the 2D atria indicated the importance that heterogeneities play in atria. The conclusions show that models provide a powerful tool when investigating how changes to electrophysiology of cells are manifested at a multi-scale level. The models also have their limitations and require further advancement to improve their accuracy.

Declaration

No portion of the work referred to in this thesis has been submitted in support of an application for another degree or qualification of this or any other university or other institute of learning.

Copyright

i. The author of this thesis (including any appendices and/or schedules to this thesis) owns any copyright in it (the \Copyright") and s/he has given The University of Manchester the right to use such Copyright for any adminis-trative, promotional, educational and/or teaching purposes.

ii. Copies of this thesis, either in full or in extracts, may be made only in accordance with the regulations of the John Rylands University Library of Manchester. Details of these regulations may be obtained from the Librar-ian. This page must form part of any such copies made.

iii. The ownership of any patents, designs, trade marks and any and all other intellectual property rights except for the Copyright (the \Intellectual Prop-erty Rights") and any reproductions of copyright works, for example graphs and tables (\Reproductions"), which may be described in this thesis, may not be owned by the author and may be owned by third parties. Such Intel- lectual Property Rights and Reproductions cannot and must not be made available for use without the prior written permission of the owner(s) of the relevant Intellectual Property Rights and/or Reproductions.

iv. Further information on the conditions under which disclosure, publication and exploitation of this thesis, the Copyright and any Intellectual Property Rights and/or Reproductions described in it may take place is available from the Head of School of Physics and Astronomy (or the Vice-President).

Acknowledgements

I would like to thank my supervisor, Prof. Henggui Zhang of the Biological Physics Group Manchester, for his guidance throughout the course of my projects. In particular his advice on areas of further study and discussions on overcoming problems, both technical and physiological, were invaluable. I would also like to thank the other members of the Biological Physics group who's discussion into both physiological and computing problems were greatly appreciated. In particular I have a debt of gratitude to Dr. Sanjay Kharche and Dr. Jonathan Stott who I worked very closely with on multiple projects. Their help and guidance was a great asset in completing my PhD project.

My parents, Robert and Carol Law, and also my brother Michael W. Law who's love and supported was of great help to me throughout the course of the PhD.

My friends, who discussions allowed me to look at problems in an alternative light and provided additional background relating to clinical method of which I was unaware.

I would also like to thank the EPSRC for providing funding and guidance which allowed me to complete the PhD project.

I would also like to thank all those who helped in the drafting of the Thesis and their efforts in reducing the errors in the thesis text, however all remaining errors are my own.

The author

Phillip Law graduated with a Master of Physics (2:1) degree from the University of Manchester in 2006. His Masters project focused on the study of artificial gene-networks via the implementation of mathematical models. The techniques and experience gained in his Masters project laid the ground work before beginning his PhD on modelling the atria; this Thesis represents his first major research project.

Publications: (submitted and accepted): In chronological order

Sanjay Kharche, **Phillip Law**, Antony Workman, Andrew Rankin, Kathy Kane, Henggui Zhang (2010). "Computational Evaluation of Electrophysiological Effects of Beta-blockers on Chronic Atrial Fibrillation." (In Preparation)

P Law, S Kharche, J Higham, Henggui Zhang. (2010). "Anti-arrythmogenic Effects of Atrial Specific I_{Kur} Block: A Modelling Study" *Proc Physiol Soc* 19 PC 14

P Law, S Kharche, J Stott, Henggui Zhang. (2009). "Conduction Propagation Dysfunction with No Apparent Changes in Cellular Electrical Action Potentials in Human Atria: A Simulation Study." *Proc Physiol Soc* 1 PC11

Sanjay R Kharche, **Phillip. R. Law**, Henggui Zhang (2009). "Recent Advances in Biomedical Engineering."

Law, P., S. Kharche, et al. (2009). "Effects of elevated Homocysteine hormone on electrical activity in the human atrium: A simulation study." Conf Proc IEEE Eng Med Biol Soc **1**: 3936-9.

S Kharche, J Stott, **P Law**, H Zhang (2008). "Simulating the effects of atrial fibrillation in electrically heterogeneous human atria: a computer modeling study." *Computers in Cardiology* 35: 65-68.

S Kharche, J Stott, **P Law**, H Dobrzynski, H Zhang (2008). "Effects of atrial fibrillation on electrically heterogeneous human atria: a computer modeling study." *Proc Physiol Soc* 11 C20.

S Kharche, J Stott, **P Law**, H Zhang, JC Hancox (2007). **"**Computational evaluation of the effects of novel anionic currents on human atrial electrical behaviour." *Proc Physiol Soc* 8 PC8**.**

Acronyms

AF ..... Atrial Fibrillation
AFER ..... AF Electrical Remodelling
AP ..... Action Potential
APD ..... AP Duration
APD_{50} ..... APD, 50% repolarisation
APD_{90} ..... APD, 90% repolarisation
APDr ..... APD Restitution
APDr,50 ..... APDr, 50% Repolarisation
APDr,90 ..... APDr, 90% Repolarisation
AV ..... Atrioventricular
BB ..... Beta-Blockers
BCL ..... Basic Cycle Length
CRN ..... Courtemanche Atrial Cell Model
CV ..... Conduction Velocity
CVr ..... Conduction Velocity Restitution
DF ..... Dominent Frequency
DI ..... Diastolic Interval
dV/dT_{max} ..... Maximal Upstroke Velocity
ECG ..... Electrocardiogram
ERP ..... Effective Refactory Period
ERPr ..... ERP Restitution
LA ..... Left Atrium
LS ..... Life Span
MS ..... Minimum Substrate
NYG ..... Nygren Atrial Cell Model
OS ..... Over Shoot
PCL ..... Paceing Cycle Length
RA ..... RightAtrium
RP ..... Resting Potential
SA ..... Sinoatrial
SVW ..... Spatial VW
SR ..... Sinus Rhythm
VW ..... Vulnerability Window

I_{CaL} ..... L-Type Inward Ca^{2+} Current

I_{to} ..... Transient Outward K^{+} Current

I_{K1} ..... Inward Rectifier K^{+} Current

I_{Kur} ..... Ultra Rapid Delayed Rectifier K^{+} Current

I_{Kr} ..... Rapid Delayed Rectifier K^{+} Current

I_{Ks} ..... Slow Delayed Rectifier K^{+} Current

I_{Cap} ..... Sarcoplasmic Ca^{2+} Pump Current

I_{bNa} ..... Background Na^{+} Current

I_{bK} ..... Background K^{+} Current

I_{bCa} ..... Background Ca^{2+} Current

I_{NaK} ..... Na^{+}-K^{+} Pump Current

I_{NaCa} ..... Na^{+}-Ca^{+} Pump Current

I_{Na} ..... Fast Inward Na^{+} Current

Chapter 1

Introduction

Cardiac disease and its effect on underlying electrophysiology have been studied since the birth of modern medicine. However, the mechanisms which underpin the disease are still poorly understood, this provides a testament to the complex and multi-faceted nature of the condition. This thesis is primarily focused on the study of atrial fibrillation (AF), which is characterised by rapid uncoordinated contractions of the atrial myocardium. While AF is not in itself life threatening the paroxysmal nature of the condition and subsequent continual re-admittance of patients to hospital poses a considerable financial and time consuming burden to health care budgets (Boriani, Diemberger *et al.* 2004). The study of AF in the clinical setting is often costly and raises many ethical questions. The development of mathematical models which can simulate the onset of AF computationally provides a complimentary method by which the condition can be examined ethically and in a cost effective manner. In this introductory chapter I aim to give an overview of the clinical problem, a brief description of diagnosis techniques and current treatment methodology. In addition I have outlined current techniques for modifying atrial cell models and methods for quantifying the arrhythmogenic effects of these changes.

1.1 Why cardiac disease is a cause for concern

Cardiac disease in a major cause of morbidity and mortality across the western world contributing to approximately a third of all fatalities in the UK and US (Whiteley 2007). Recent evidence suggests cardiac disease is also a burgeoning problem in emerging economies such as China (Zhang 2009). Due to the paroxysmal nature of AF and associated long term treatment strategies there is a substantial burden on health care budgets in the UK and elsewhere around the world. Traditionally, cardiac disease was the reserve of the old (Aronow 2009; Wetzel, Hindricks et al. 2009). However, due to current lifestyle choices there is an increasing prevalence of the condition in an ever younger population dynamic. Therefore study into the genesis and maintenance of AF is crucial to developing new and cost effective strategies for treatment. In addition increased understanding of the underlying causes of AF allows preventative measures to be explored.

1.2 The anatomical structure of the heart

The human heart, which can be seen in Figure 1.1 weighs approximately between 250 and 300 grams. It located in the centre of your mediastinum and is contained in a membranous

sac called the pericardium, which protects the heart and anchors it in its surrounding. The heart is comprised of four chambers, two superior atria and two inferior ventricles. The atria function is to receive blood and pump it into the ventricles where there is a greater mechanical force to expel the blood to the rest of the body. The left ventricle and left atria (LA) combined is referred to as the left heart, and is responsible for pumping blood round the systemic circuit. The right atria (RA) and right ventricle is referred to as the right heart, and it pumps blood round the pulmonary circuit. Due to the increased force required to provide the power blood through the systemic circuit the left ventricle is larger in volume than the right. Back flow is potentially harmful (Trichon, Felker et al. 2003) and is prevented by a series of four valves, the tricuspid and mitral valves, which are located between the atria and ventricle in the right and left heart respectively, and the pulmonary and aortic valves which are located on the entrance on the opening of the aorta and the pulmonary artery (Gray 1918).

1.3 The electrophysiology of a heartbeat

A heartbeat begins with an initiation of an excitation wave from a specialised group of cells in the right atrium collectively known as the sinoatrial (SA) node (Chen, Joung et al. 2009). The node is located in the superior lateral wall of the RA near the opening of the superior vena-cava (Gray 1918). These cells spontaneously depolarise at regular intervals, thus the SA-node acts as the hearts pacemaker. Once the cells depolarise the resultant electrical wave travels through the RA and then on to the LA causing them to beat in rapid succession. After the wave transverses the atrium it enters the atrioventricular (AV) node at which point the speed of propagation is reduced due to a combination of cell diameter (2-3μm) and complex intracellular circuitry. The slowing of the wave is of significance as it allows the ventricles to beat approximately $1/10^{th}$ of a second after the atrium, allowing time for the blood to be pushed into the ventricle before its beat. Once the wave has passed the AV node it is rapidly transmitted through the bundle of His along the left and right bundle branches and through the Purkinje network. This network is comprised of specialized cells in which conduction velocity is increased significantly. The rapid velocity of the wave along the Purkinje fibres allows the action potential be to be distributed throughout the entire ventricular wall to ensure simultaneous contraction; one full heartbeat typically takes approximately one second. AF occurs when the normal conduction pathway of the electrical wave is disrupted. Dependant on how the conduction

pathway is altered directly effects how AF in manifested in the patient. This explains why patients with AF show a range in the severity of their symptoms. When a patient initially develops AF the symptoms are relatively minor. However, untreated the condition increases in severity over time.

1.4 The action potential of a cardiac myocyte and wave propagation

The tissue of the myocardium is constructed from multiple cell types. However, the cell which provides the mechanical force required for a heartbeat is the cardiac myocyte (Yin, Zhang et al. 2005). It is the combined mechanical force of these cells contracting in a coordinated manner which provides the power required to pump the interstitial fluid around the body. A typical resting potential (RP) of an atrial cell is approximately -80 mV, where the net charge entering and exiting the cell across the cell membrane remains negligible. (Courtemanche, Ramirez et al. 1998; Nygren, Fiset et al. 1998). Cardiac myocytes are arranged in strands with each cell connected to its neighbour via gap junctions. As a neighbouring myocyte depolarises ions pass into the cell resulting in elevated membrane potential. If membrane potential is elevated sufficiently the ion-channel responsible for the rapid flow of sodium ions into the cell will open causing membrane potential to become positive. At such elevated potentials multiple ion-channels become active which control the flow of potassium and calcium ions across the cell membrane. The flow of these ions across the cell membrane alters the potential of the cell over time and is observed as an action potential (AP); a typical example of which is shown in Figure 1.2. It is during an AP that a myocyte will contract. The topography of the AP is created as different ion-channels and pumps transport the various ions across the cell membrane. The shape of an AP can provide an insight into individual ion-channel behaviour. Gap junction coupling between adjacent myocytes provides a mechanism that allows the cells to contract sequentially in quick progression. This creates an excitation wave which propagates around the structure of the heart, resulting in a successful heartbeat.

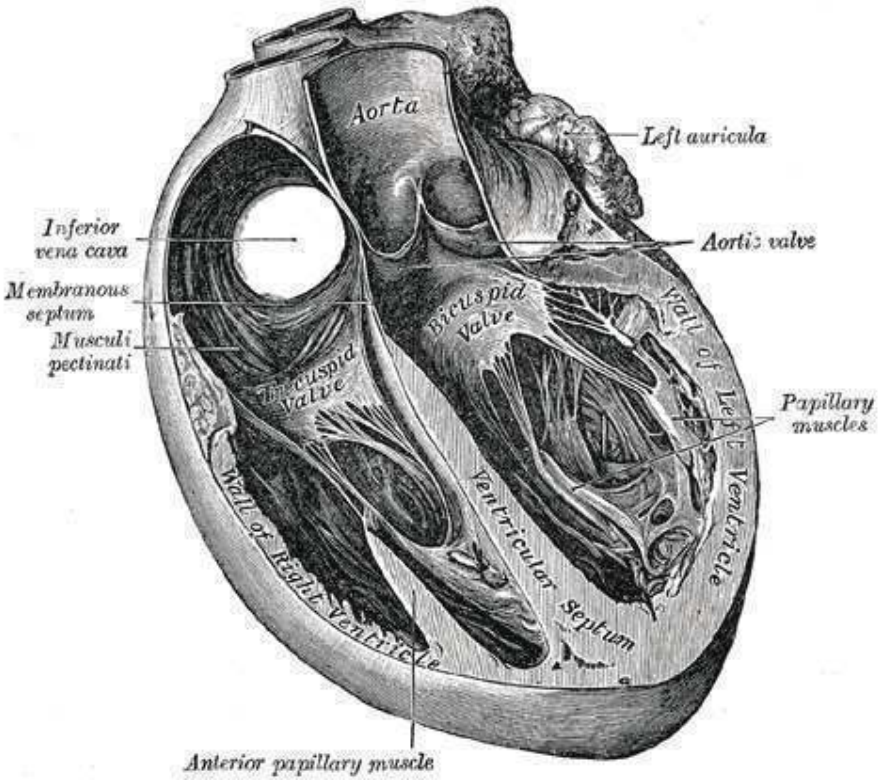

Figure 1.1 Anatomical structure of the mammalian heart with points of interest indicated which include the atria, ventricles, tricuspid and bicuspid valves, aorta, and inferior vena cava (Gray 1918).

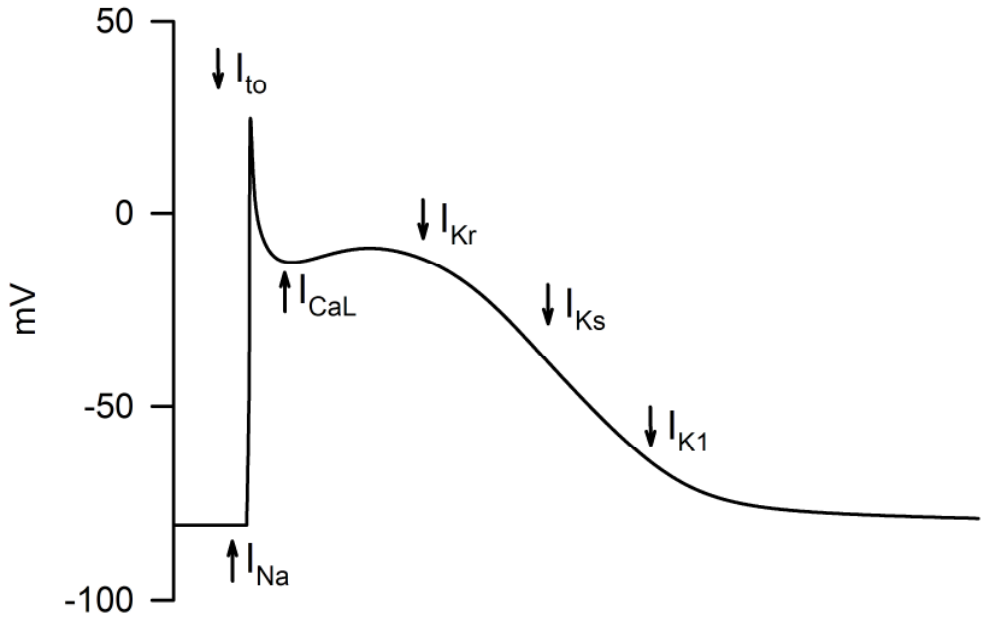

Figure 1.2 Schematic of the human AP simulated using the Courtemanche *et al* model with major inward (↑)and outward (↓) currents responsible for the depolarization and repolarisation of the atrial myocytes indicated.

1.5 The clinical problem

The aim of computational cardiology is to develop understanding of cardiac physiology with the ultimate aim of improving current clinical treatment techniques and aid pharmacological development. Therefore this section of the introduction provides a background into the history of AF along with current clinical methodology behind diagnosis and treatment options available.

1.5.1 Historical perspective

The first recoded case of AF was identified in the yellow emperor's classic of internal medicine (Huang 1949) which was written in approximately 2000 BC, where an irregular pulse was associated with a poor prognosis for the patient. However, the first document case of AF described as 'fibrillation of the auricles' was identified in 1628 by William Harvey (Harvey and Lederle Laboratories. 1987). Although AF had been observed there was no reliable way of identifying a patient with AF. Before a treatment could be considered an accurate diagnosis method was required. The invention of the stethoscope in 18th century provides some aid to the clinician it was not until the early 1900's with the invention of the ECG that an accurate method for the diagnosis of AF was devised. ECGs remain the clinicians' primary apparatus for diagnosis to this day. The ECG provided an accurate method for the diagnosis of AF. However, treatment of AF still provided an obstacle for clinicians. While there had been anecdotal evidence that the properties of the digitalis leaf (Digitalis purures) brought some relief to patients with sever heart failure the mechanism by which application of the leaf help relieve the symptoms was unknown, it was in fact first pharmacological intervention treatment method discovered.

Even as recently as a few decades ago the treatment options for AF were limited. The standard treatment recommended for a patient identified to be in an AF episode was to perform a cardioversion, either pharmacologically via administration of either Quinidine, or via DC shock. Patients in permanent AF were prescribed digitalis as a rate control treatment method (CK Friedberg 1966; P Wood 1968). The treatment of AF has improved significantly in recent years, both in management and prevention of AF. There is now a wide array of treatment options available to the clinician to achieve the best outcome for the patient. These include anti-coagulation drugs, surgical interventions, and a range of rate and rhythm control drugs (Van Wagoner 2007).

1.5.2 Associated risk factors for AF

The increased incidence of AF has long been associated with an ageing population. However, a detailed analysis of the risk factors associated with the condition were not fully studied until 1948 in the Framingham study (Dawber, Moore et al. 1957). This longitudinal study focused on the town of Framingham in Massachusetts, USA. The aim was to quantify the risk factors for the onset of AF in a large sample of population over an extended period of time, the study is now on its third generation. Over the past fifty years the study had identified numerous risk factors including smoking, hypertension, diabetes, high blood cholesterol, and obesity (Kannel and McGee 1979; Castelli, Garrison et al. 1986; Kannel, Cupples et al. 1991; Gillman, Kannel et al. 1993). While the study had provided insight into how lifestyle choices increase the risk of AF it did not focus on other biologically inherent mechanisms which result in the genesis of AF. More recent clinical studies have showed how genetic defects, hormone imbalances, and AF induced electrical remodelling (AFER) can facilitate the genesis of AF (Kharche, Garratt et al. 2008; Knight 2009; Law, Kharche et al. 2009).

1.6 The genesis of AF

AF is self perpetuating in nature and has multiple contributing factors. The schematic in Figure 1.3 outlines the hypothesis that "AF begets AF" and shows how remodelling of the atria occurs both electrically and structurally. Typically electrical remodelling occurs on relatively short time period. In contrast, structural remodelling tends to occurs over an extended period of time. Initiation of a patient's first AF episode is likely to begin due to an ectopic beat, which may be the result of underlying etiology. If the atrial tissue is healthy, exhibiting normal AP duration (APD) and therefore normal atrial effective refractory period (ERP) any re-entrant waves born as a result of the ectopic beats are broken up and normal sinus rhythm (SR) is resumed; this is known as paroxysmal AF. Such episodes may be short and the patient may be unaware that this has occurred. However, the underlying mechanism which resulted in the ectopic beat remains. Therefore, AF is likely to reoccur. If these episodes reoccur at regular enough intervals then the initiation of re-entry is likely to increase in frequency and lengthen in period. This is due to AFER which results from prolonged periods of rapid pacing causing remodelling of the major ionic currents. As a consequence the myocyte exhibits a permanently reduced APD and ERP (Wijffels, Kirchhof et al. 1995). Reduced ERP shortens the wavelength at which atrial tissue can sustain re-entry, resulting in an increased susceptibility to AF genesis.

Structurally, prolonged periods of rapid pacing result in a decrease in contractibility of the atrial myocytes thereby decreasing the ability of the atria to expel blood, this would possibly cause thrombosi to be formed. These place the patient at increased risk of strokes or cause a myocardial infarction. In addition rapid pacing results in hypertrophy due to increases in the atrial myocytes size, alterations to the extracellular matrix in terms of increased fibroblast density, and chamber dilation due to hypertrophy. Increased atrial size allows greater substrates for re-entrant waves to be sustained before being terminated.

1.7 Current clinical methods for diagnosis of AF

The invention of the ECG provided clinicians with a reliable tool for the detection of abnormalities in the electrophysiology of the heart and is still the mainstay of the diagnosis procedure. However, for an ECG to be an accurate diagnosis tool it requires a skilled clinician. Modern advances in computing have allowed for the clinician diagnosis skills to be augmented, providing more accurate and powerful diagnoses tool (Slocum, Sahakian et al. 1992) . However, due to the complex multi-faceted nature of the genesis of AF it is vital to know the underlying mechanism through which AF is born to implement the most effective treatment. There is still no single technique for identifying the underlying etiology for the onset of AF. Therefore, the diagnosis of AF remains one of exclusion resulting from a careful evaluation, including thorough collection of medical history, physical examination, blood pressure measurement, laboratory tests, ECG, and possibly, chest x-ray and exercise testing (Kozlowski, Budrejko et al. 2009).

1.8 Clinical treatment of AF

Clinical treatment of AF is dependant on progression and the underlying etiology. In Figure 1.3 which shows how “AF begets AF” numbered entries indicate the various treatment options available and when they should be implemented to be of most effect. For a patient initially admitted to hospital who is identified to be suffering from an AF episode the standard method for restoring SR is to apply a cardioversion, thereby resetting the electrical activity in the myocardium so that normal SR be resumed (Reiffel 2009). This in normally achieved by pharmacological methods or by a direct DC shock to the torso. However, cardioversion provides only a short them solution as the underlying mechanism which resulted in the genesis of the arrhythmia is still present. If normal SR can be restored with a cardioversion then the patient is referred to as being in persistent AF, if the patient reverts back into AF soon after a cardioversion that patient is know to be in permanent AF.

Patients diagnosed with AF are at risk of blood clots, which place the patient at increased risk of stroke. Therefore it is standard to provide the patient with a anticoagulants (Sobieraj-Teague, O'Donnell et al. 2009). The long term options for the management of AF are aimed at maintaining normal SR; these are referred to as rhythm control strategies. The treatment strategy which a clinician chooses in outlined in the NICE guidelines and a representative flow chart is shown in Figure 1.4. The success of these treatments are limited and in trials it had been concluded that anti-arrhythmic drugs administered after cardioversion still result in 70-85 % of patients developing further complications with in a year (Lafuente-Lafuente, Mouly et al. 2006) (Segal, McNamara et al. 2000; Olshansky, Rosenfeld et al. 2004). Surgical intervention can also be implemented in rhythm control strategies and had been found to be a successful treatment option (Levy 2006). AF may be initiated via an ectopic beat origination from auto-rhythmic cells located in the pulmonary vein (Haissaguerre, Jais et al. 1998). Surgical intervention aimed at ablating this region to remove the focal point of any ectopic beat may provide a possible 'cure' for the condition. If rhythm control options are deemed no longer possible the patient may be moved to a rate control strategy. In rate control the contraction of the ventricles is managed either by pharmacological means, or surgically via the ablation of the AV node and replacement by a biventricular pacemaker. This allows for precise control of the rate of ventricular contractions (Abraham, Fisher et al. 2002; Bode and Schutte 2009). The addition of mini-defibrillators to the artificial pacemaker allow for the immediate cardioversion of the heart, limiting the risk of possible stroke from the AF episode.

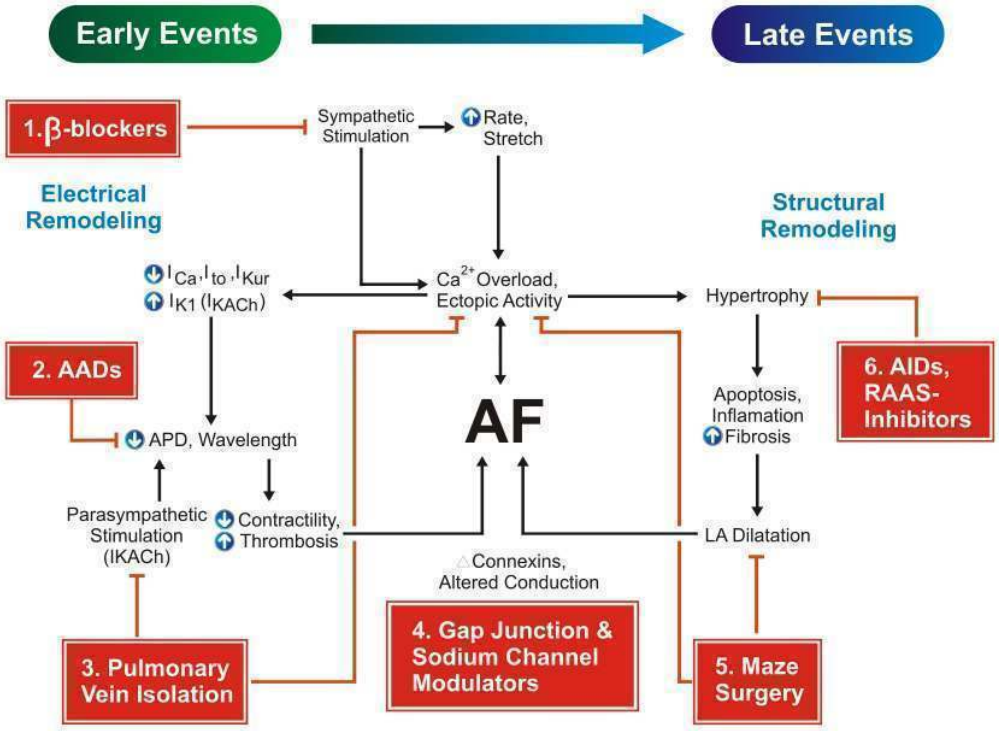

Figure 1.3 Schematic showing the mechanisms for AF and targets for possible therapeutic treatments. Electrical remodeling (left side) typically occurs on short time scales and structural remodeling (right side) occurs over longer periods. The initiation AF due to an ectopic beat results in rapid pacing of the atrial cells allowing AFER to occur. The shortening of APD and atrial ERP increase the tissues susceptibility to AF being initiated. Structural remodeling occurs as rapid pacing results causing hypertrophy and LA dilation, increasing the myocardial volume and therefore increasing the tissues susceptibility to re-entry. Possible treatments options and are numbered and indicate present and future treatment interventions, these include β-Blockers, antiarrhythmic drugs (AADs), pulmonary vein isolation, gap junction and sodium channel modulators, maze surgery, anti-inflammatory drugs (AIDs), rennin-angiontensin-aldosterone system (RAAS).

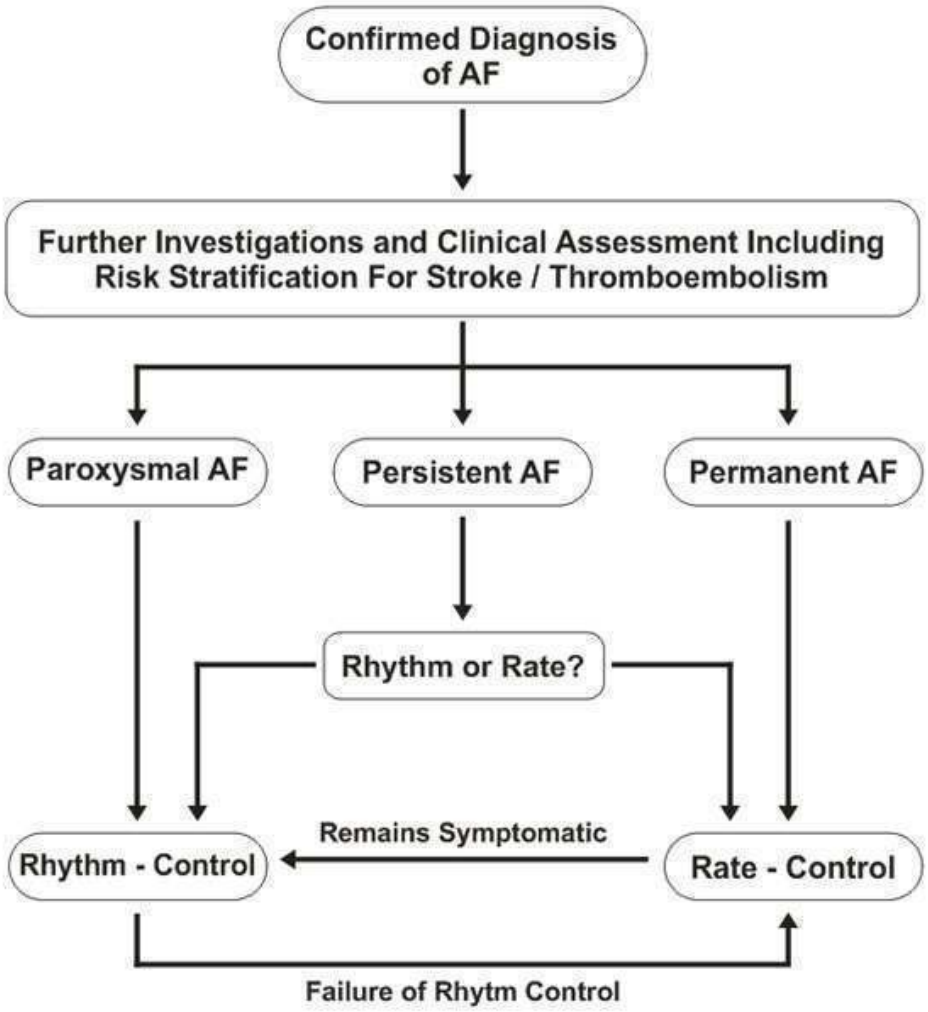

Figure 1.4 Diagram showing NICE treatment guidelines for management of AF via rate or rhythm control. Treatment is chosen depending on the categorisation of AF. Paroxysmal AF: short periods of re-entry until the atria returns to SR independent of intervention. Persistent AF: AF occurs until cardioversion is performed. Permanent AF: Atria return to AF shortly after a cardioversion is performed.

1.9 The role of computer simulation and mathematical modelling

Multiple risk factors and several roots to the initiation of AF combined with the self perpetuating nature of the condition means the diagnosis and treatment of AF remains a challenge. Understanding the mechanisms underpinning the genesis and maintenance of AF are vital to developing successful clinical diagnosis and treatment techniques. While the conditions behind AF are complex the treatment options available remain simple in design as can be seen in Figure 1.4, when compared to Figure 1.3, which provides a glimpse into the overall complexity of the condition. Traditionally clinicians have opted for a multi-treatment approach relying on their experience to determine which options are best for the patient. Such treatment methodology while effective may lead to unnecessary treatments being prescribed, with implications to the patient in terms of side effects, and an increased treatment cost. Current scientific methods for studying AF are split between clinical trials, research on cellular electrophysiology, and more recently computer simulation. These research methods have provided key information that has led to a much more profound understanding of the arrhythmogenesis and cardiac physiology in general. The role of computer modelling in particular provides a powerful tool for the study of cardiac electrophysiology due to its relatively inexpensive setup costs and limited ethical considerations required for its application. Biophysically detailed mathematical models allow for results recorded from single cell wet lab experiments to be incorporated into these models. This allows simulations to be performed as a multi-scalar level providing a detailed dissection and analysis of how changes in the electrophysiology of the cell manifest themselves at a multi-cellular level and therefore provides possible insight into future direction for experimental studies.

1.10 Modelling single ion-channels by means of ionic current formulations

The first electrophysiological model was constructed by Hodgkin and Huxley on the giant squid axon (Hodgkin and Huxley 1952). Developments of atrial cell models are based on knowledge of underlying electrophysiology, primarily which ion-channel proteins are actively transcribed in the cell allowing the flow of ions to cross the cell membrane. Ion-channels are pore-forming proteins which regulate the flow of Ca^{2+}, K^{+}, and Na^{+} ions across the bi-lipid cell membrane. Each of these ions has multiple associated ion-channels each with its own unique properties which include, time kinetics, voltage dependent activation and deactivation. All of these properties can be modelled mathematically in accordance with available experimental data.

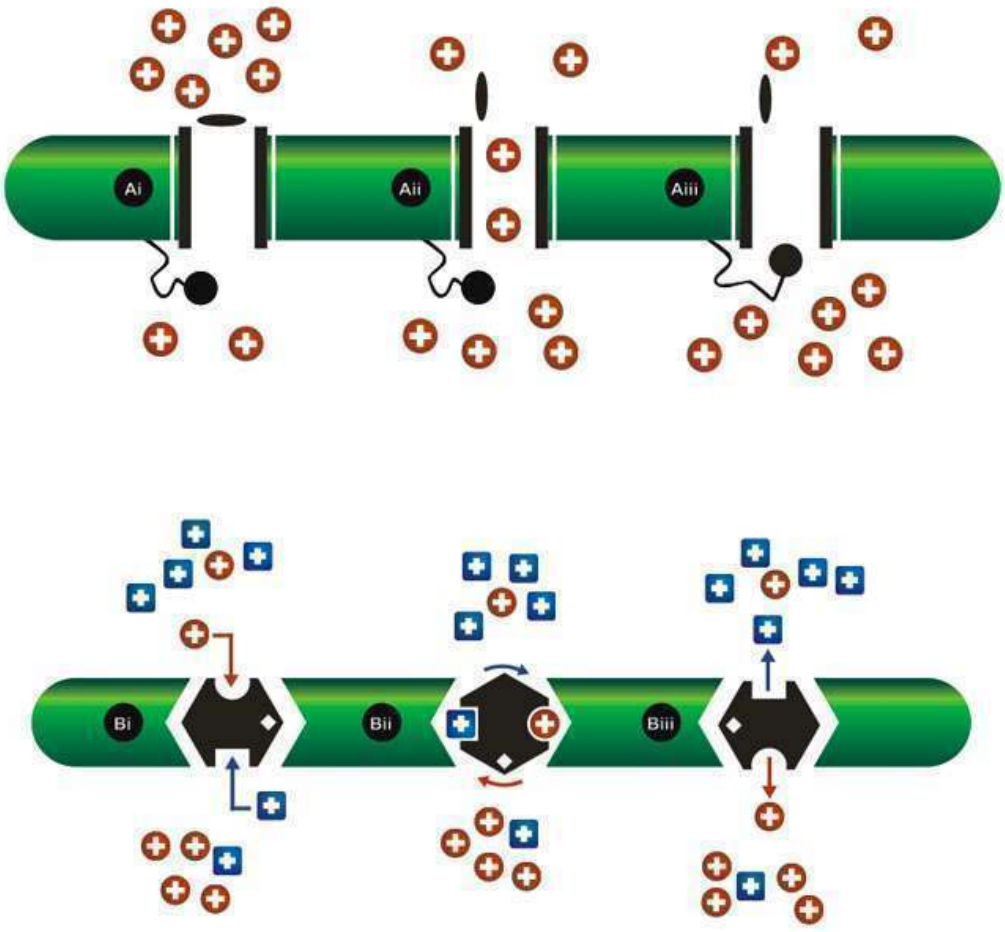

Figure 1.5 Schematic showing a gated ion-channel (A) and pump (B) imbedded in a cell membrane, where positive ions are shown as red circles and negative ions are shown as blue squares. Panel A shows an activation gate (represented as a lozenge) and an inactivation gate (represented as a ball on a chain) Ai: Shows an ion-channel with a net positive charge above the cell membrane, the activation gate, located at the top of the channel is closed preventing the flow of ions. Aii: Activation and inactivation gates are open allowing the flow of ions across the cell membrane. Aiii: As ions flow through the channel net charge across the membrane is altered resulting in the inactivation gate to close, preventing the flow of ions back through the cell membrane. Panel B shows the function of an exchanger pump whereby the protein structure allows for the passing of ions across the membrane against the ionic gradient. An exchanger pump allows ion to be exchanged with an oppositely charged partner from the other side of the membrane. Bi: A positive charged ion and negatively charged ion enter the pump from above and below the cell membrane respectfully. Bii: Ions are exchanged through the pump. Biii: Ions exit the pump on the opposite side from which they entered.

1.10.1 Ion-channels and pumps

An individual ion-channel is responsible for the transfer of a specific ion type across the cell membrane in the direction of the concentration gradient. However, there is also a sub-category of ion-channel which allows the flow of ions regardless of direction of this gradient; these are referred to as pumps. As pumps allow the flow of ions against the concentration gradient, they require a greater energy consumption to function. Ion-channels are also catagorised by their effect on the net charge of the cell. Inward current are those which allow positive ions to enter the cell or negatively charged ions to exit, resulting in an increase in cell membrane potential. Conversely, outward current are those which result in a net ionic charge exiting the cell thereby reducing membrane potential. Ion-channels are further classified by the ions they transport. The simplest form of ion-channel, which relies on the ionic concentration gradient alone is know as a leakage current, and has a fixed conductance value. However, ion-channels currents which are modified by the potential difference across the cell membrane are known as voltage-gated channels. These channels have activation (allowing the flow of ions) or deactivation (preventing the flow of ions) gates. There may also be a time-dependant component to the activation and deactivation of ion-channels. A schematic of these ion-channels can be seen in Figure 1.5. In addition to ion-channel flow being regulated by there voltage dependant ion-channel, they can also be modulated by the presence of various hormones or chemicals. For example the I_{KATP} ion-channel is responsible for the flow of potassium currents and can be modulated by the presence of the ATP hormone (Ehrlich 2008). The alteration of ion-channels in accordance with various external factors may be part of the body's mechanisms to provide a natural cardiac protective effect and are of interest as they can be exploited in the development of drug therapies.

1.10.2 Hodgkin-Huxley simulation

The first model of the ion-channels was proposed by Alan Lloyd Hodgkin and Andrew Huxley in 1952 on their work on the giant squid axon; for which they received the noble prize in 1963 (Hodgkin and Huxley 1952). In their paper they conducted voltage clamp experiments on the nerve endings of a giant squid axon. Their work concluded that the total current of a cell could be modeled by the following equations.

$$I(V,t) = g_{\max} n^a m^b (V - E_k)$$
$$n(V,t) = \frac{1}{\tau_n}(n_\infty - n) \quad (1.1)$$
$$m(V,t) = \frac{1}{\tau_m}(m_\infty - m)$$

Where I is the total membrane current for a specific ion-channel, V is the membrane potential, *t* is the time, g_{max} is the maximal conductance, n is the activation gate probability, m is the inactivation gate probability, a and b are integer values representing the number of activation and inactivation gates respectively, τ_n and τ_m are the activation and inactivation time constants respectively, and n_∞ and m_∞ are the probability that the n and m gates will be open if the system is allowed to run for an infinite amount of time, i.e. reach a steady state. Using this modelling technique they concluded that experimental data collected from patch clamp recording of the squid axon could be fitted accurately to a hypothetical curve. Hodgkin and Huxley found that using the values of 3 and 1 for a and b respectively provided an accurate fit. It was subsequently discovered that this corresponded to the number of gates each individual ion-channel possessed. These simulation techniques remain the foundation of many of the current cardiac models available in the literature

1.10.3 Markov chains

While there has been much success in utilising the Hodgkin-Huxley type formulation to develop detailed cell models (Courtemanche, Ramirez et al. 1998; Nygren, Fiset et al. 1998) the simplified gated hypothesis of an ion-channel either being open or closed state is not physiologically accurate. Cellular biologists have concluded that a single ion-channel can exist in multiple closed and open states. Therefore recent modelling practices have utilisised a Markov chain hypothesis to simulate ion-channel function. An example Markov chain formulated for simulating I_{Kur} in a canine model is described in Equation 1.2 (Sridhar, da Cunha et al. 2007).

$$C_1 \underset{\beta^1}{\overset{\alpha^1}{\rightleftarrows}} C_2 \underset{\beta^2}{\overset{\alpha^2}{\rightleftarrows}} O \quad (1.2)$$

This model permits the ion-channel to be in one of three states, two closed (C1 and C2) and one open (O). Each individual ion-channel can exist in only one state and progresses to

another state at a rate of α or β. It is possible to model the ion-channel deterministically via a series of ODEs. However, solving a set of ODEs describing a markov chain formulation is problematic. The large range of timescales present in the ODE system result in the equations being extremely stiff in nature, and therefore require advanced numerical techniques to solve. In addition modelling ion-channels deterministically does not provide a realistic representation of ion-channel kinetics. Modelling the system in a truly stochastic manner requires a solution method such implementing the Gillespie algorithm (Gillespie 1977) whereby the progression of the state of the channel is described by the drawing of a random number.

1.11 Atrial cell models

Two well established biophysically detailed computer models of human atrial cell APs by Courtemanche et al. (Courtemanche, Ramirez et al. 1998) (hereafter referred to as CRN) and Nygren et al. (Nygren, Fiset et al. 1998) (hereafter referred to as NYG) were used in this study. Both models were developed in the same year and are based on similar physiological data. However, the construction methods by which the models took and differenced to the underlying physiology on which the cell models are based resulted in dramatic difference in the AP simulated and the stability of the models; simulated APs and ionic currents for the CRN and NYG models can be see in Figure 1.7. Although based on similar experimental data, the spike-and-dome AP produced by the CRN model and the triangular AP produced by the NYG model are strongly regulated by the respective ionic currents and biophysical properties considered in the two models. Intracellular ion dynamics are also different between the two models, with the NYG model incorporating a cleft space. With detailed mathematical descriptions of ionic currents and intracellular ion dynamics, the CRN model consists of a 24 variable non-linear coupled ODE system and has been widely used in computational studies (Zhang, Garratt et al. 2005; Seemann, Hoper et al. 2006; Kharche, Garratt et al. 2008). The 29 variable ODE Nygren model, based on the previous LMCG model (Lindblad, Murphey et al. 1996), also consists of biophysically detailed descriptions of cell membrane ion currents and intracellular ion dynamics. The NYG model is parametrically tuned for stable APs at a pacing frequency of 1 Hz under basal conditions. It has been used in our previous computational studies, and has been shown by others to be functionally similar to the CRN model (Zhang, Garratt et al. 2005). Conductance parameters in the CRN model can be manipulated to reproduce the NYG model AP (Syed, Vigmond et al. 2005). However, prolonged pacing of the NYG

model, even at low pacing rates, gave rise to errant spontaneous APs. The pacing protocols in simulations using both models were therefore altered to avoid such modelling defects.

1.12 Multi-scale tissue simulations

While developing electrophysiological models from available experimental data is capable of reproducing APs. There remains the issue of performing simulations to quantify how changes to the underlying electrophysiology can manifest themselves as AF. This section outlines simulation protocols for performing single cell, 1D, 2D, and 3D multi-scale simulations using the CRN and NYG models. It is noted that the NYG model was used only in simulating the effects of Beta-Blockers (BB) in Chapter 5. The only alteration in the simulation protocols for the NYG model was the stimulation strength and duration to elicit an AP was altered to -1.3 nA for 6 ms respectfully. In addition, due to the observed instability of the NYG model at prolonged pacing the 4^{th} AP was measures instead of the 10^{th} as described in CRN simulations.

1.12.1 Simulation of AP

An AP profile from an isolated atrial myocyte was simulated by using a standard pacing protocol (Kharche, Seemann et al. 2007) whereby a series of 10 supra-threshold stimuli of 2 nA/pF and duration of 2 ms are applied to the cells, which can be seen in Figure 1.6A. Each stimulus was applied to the cell at a pacing cycle length (PCL) of 1000 ms. Such a pacing regime was deemed sufficient to allow the cell models to reach a consistent AP profile. The 11^{th} AP was therefore used for measuring the properties of the AP and all major currents. Multiple measurements of the AP profile were taken to quantify its morphology and study how alterations in these values indicate the possible geneses of AF; quantities measured and are indicated in Figure 1.6B. These include AP duration, APD_{50} and APD_{90}, which are defined as the time taken from the initial excitation stimuli until the AP reached 50% and 90% repolarisation respectfully. The RP was measured as the steady state value of the cell membrane potential, which was taken to be the value immediately preceding the final AP. Over shoot (OS) is is recorded as the peak membrane potential. Maximal upstroke velocity (dV/dt_{max}) is defined as the maximum gradient of the upstroke of the AP. Simulated CRN and NYG are shown in Figure 1.7.

1.12.2 Construction of APD restitution curves

APD restitution (APDr) measures the excitation behaviour of atrial cells subjected to premature pulses immediately after a previous excitation (Franz, Karasik et al. 1997; Qi,

Tang et al. 1997; Kim, Kim et al. 2002; Burashnikov and Antzelevitch 2005; Cherry, Hastings et al. 2008). Recent experimental and modelling studies have shown the correlation between the maximal slope of APDr greater than unity and instability of re-entrant excitation waves in 2D and 3D tissues (Xie, Qu et al. 2002; Banville, Chattipakorn et al. 2004; ten Tusscher, Mourad et al. 2009). In our study, APDr is computed using a standard S1-S2 protocol whereby a series of 10 conditioning pulses (S1) at a PCL of 1000 ms followed by a premature stimulus pulse (S2) are applied. S1 and S2 have the same stimulus amplitude and duration of 2 nA/pF and 2 ms respectively. The time interval between the final conditioning excitation and onset of the premature excitation emulates atrial diastolic interval (DI), or the time the atrial tissue has for recovery from the previous excitation of the premature AP. The APD is measured and plotted in respect of the DI to obtain APDr curves. DI is defined as the time duration from the end of the 10^{th} conditioning AP excitation (defined as the time at which the 10^{th} excitation reached 90% repolarisation) and the upstroke (defined as the time at which the AP excitation reached maximal upstroke velocity) of the premature 11^{th} excitation. Maximal slopes (MS) is defined as the peak gradient of the APDr curves. The cut off PCL is defined as the shortest DI at which the cell can illicit a successful AP. The pacing protocol along with constructed CRN and NYG APDr curves are shown in Figure 1.8. At large DI, APDr curves have negligible slopes and show AP profiles under physiological rates of pacing. At low DI, however, the slopes gradients are noticeably increased.

1.12.3 Construction of ERP restitution curves

Shortening of atrial APD and ERP are well recognised features of atrial electrical activities during AF. ERP is generally measured by using cellular or tissue preparations (Workman, Kane et al. 2001; Laurent, Moe et al. 2008). In these simulation studies, the experimental protocol as described by Workman et al. (Workman, Kane et al. 2001) was adopted whereby ERP and ERP restitution (ERPr) was computed using a S1-S2 protocol with stimulus strength and duration of 2 nA/pF and 2 ms respectively. A series of 10 premature stimulus pulses (S1) are applied at a given PCL, an 11^{th} premature stimulus (S2) with variable time delay (ΔT) is applied. ERP is defined as minimal time between S1 and S2 by which will elicit a successful AP; successful being defined as an AP which has an amplitude of at least 80% of the magnitude of the preceding AP. The constructed ERPr curve shown in Figure 1.9 was constructed by plotting ERP as a function of the variable PCL.

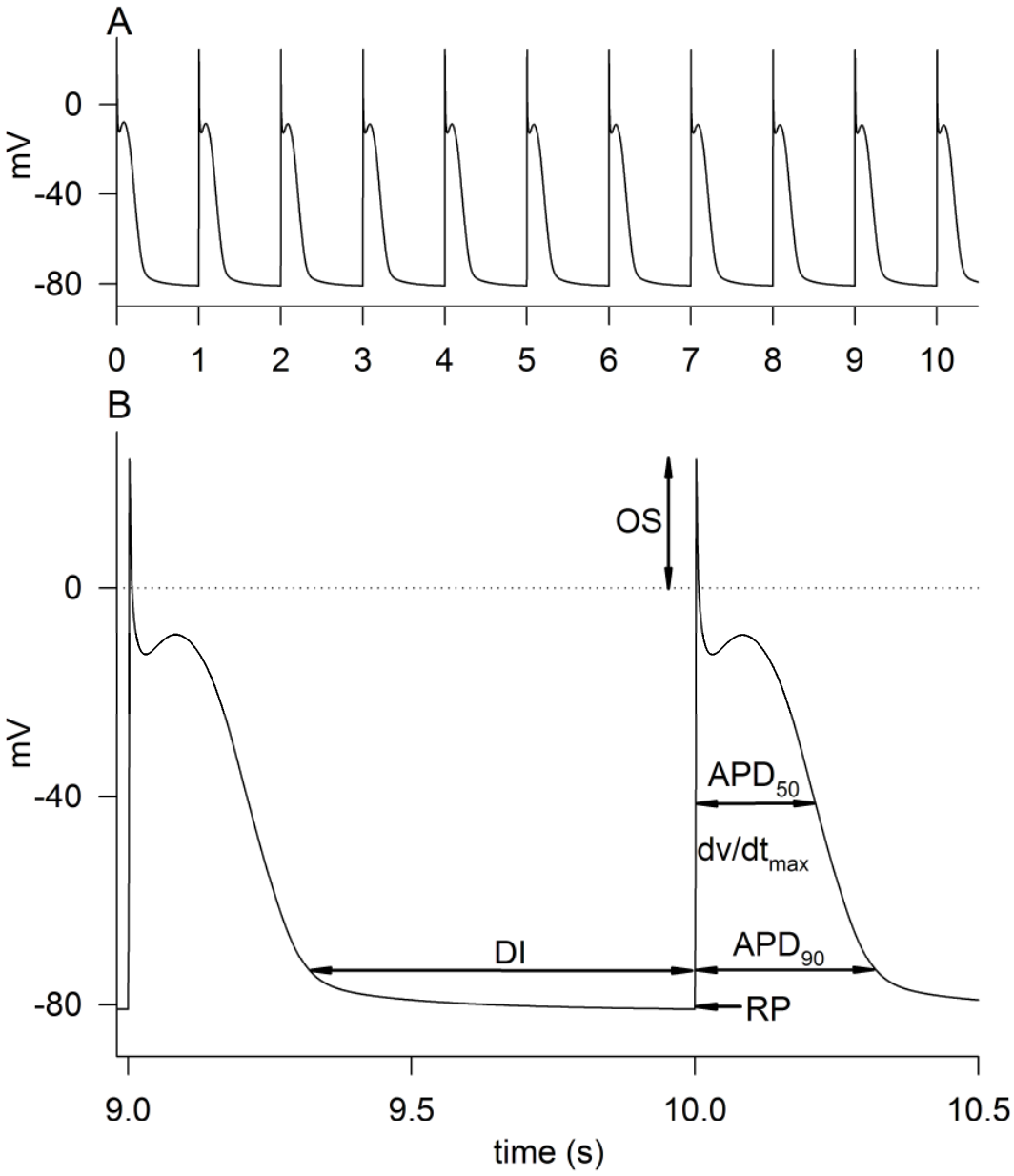

Figure 1.6 Simulated AP pacing protocol using the CRN model and identification of important physiological measurements. A: A train of 10 conditioning pulses at a PCL of 1000 ms and initiation of a final 11th AP which is recorded for measurements. B: Final two APs from panel A where the measurements DI, RP, OS, $dV/dt_{max,}$, APD_{50}, and $APD_{90.}$ are indicated.

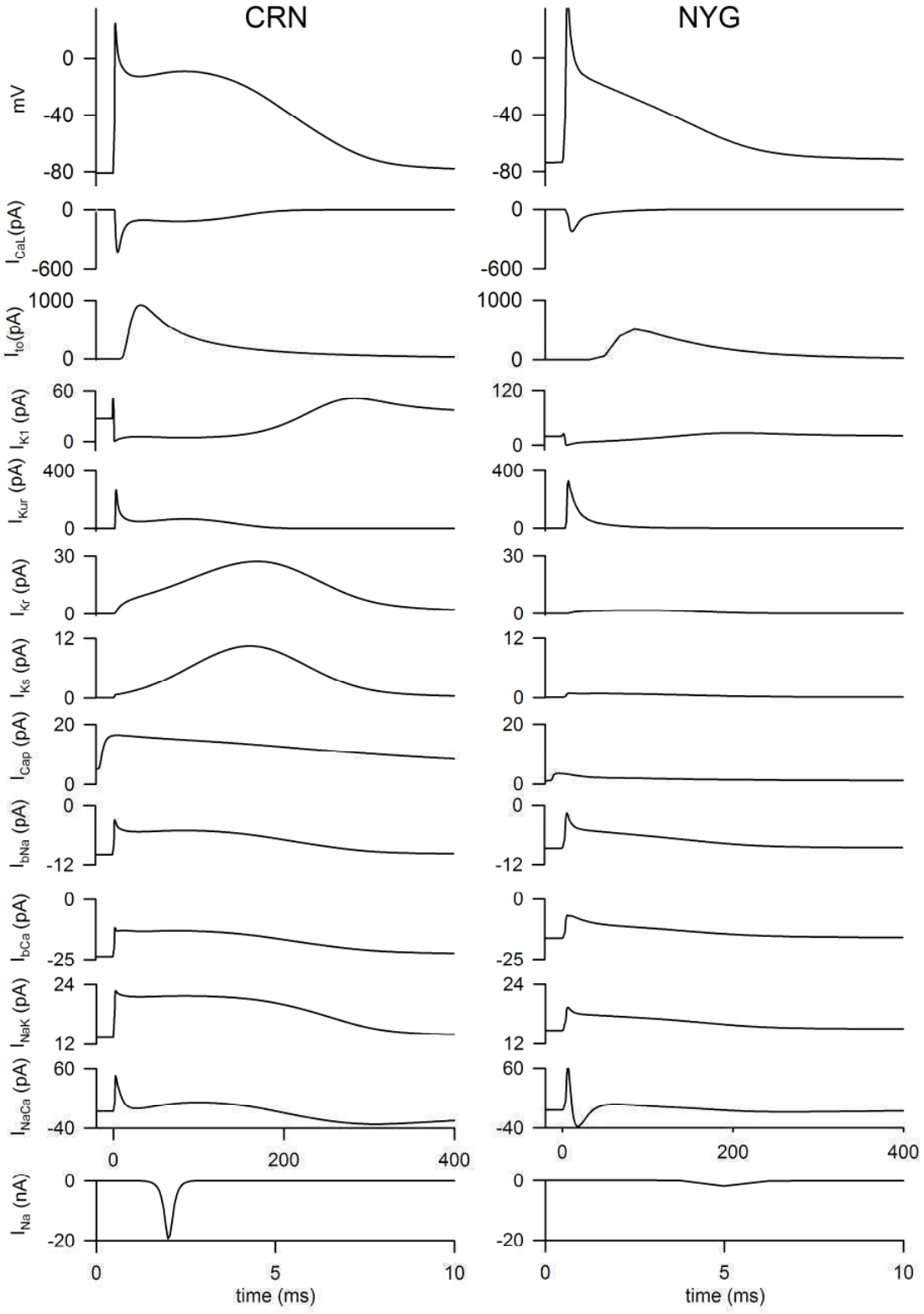

Figure 1.7 Simulated AP and current traces from the CRN (left column) and NYG (right column) representing the 11th AP from a cell is paced at 1 Hz.

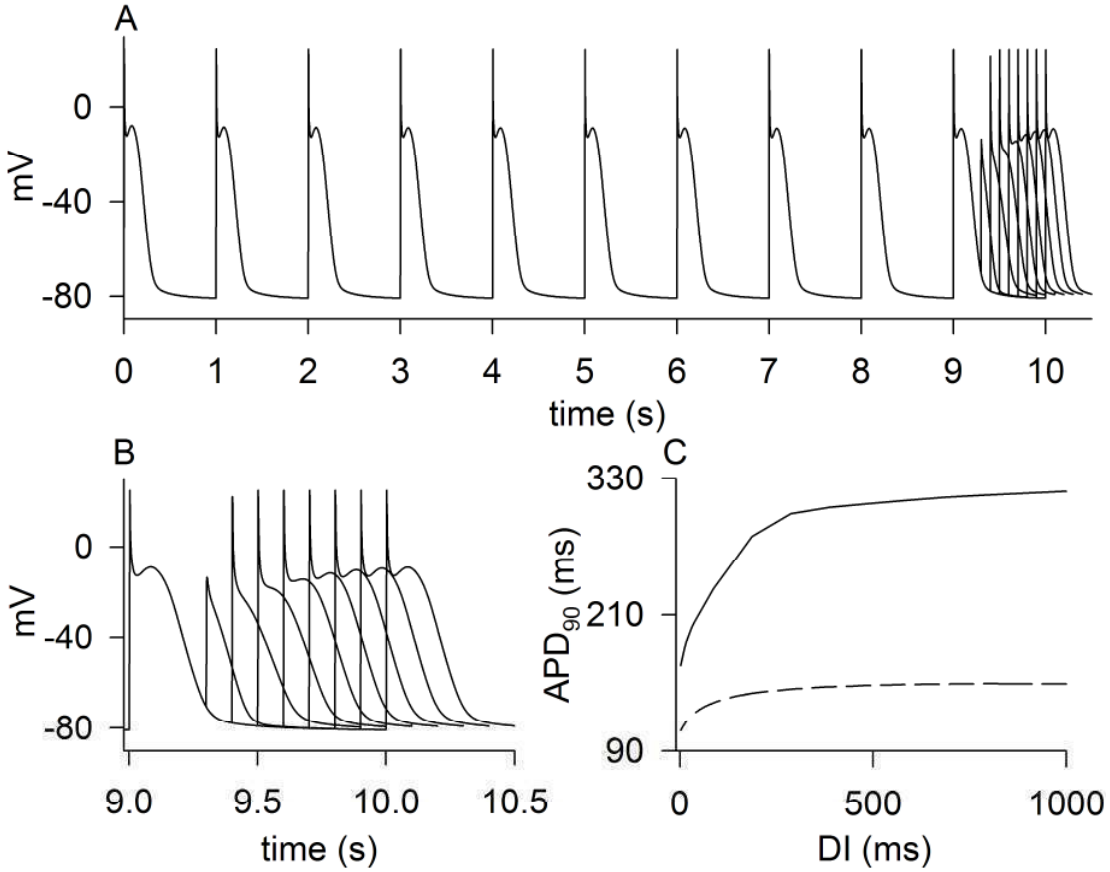

Figure 1.8 Simulation protocol for the construction of the APDr,90 curve and representative curves for the CRN and NYG models A: Train of 10 preconditioning pulses followed by several premature elicited APs as various DIs. B: Final 1.5 s of simulation protocol showing the 10^{th} and 11^{th} APs, where APD is observed to shorten in relation to the reduction of DI. C: Constructed APRr,90 curves for the CRN (solid line) and NYG (dashed line) model.

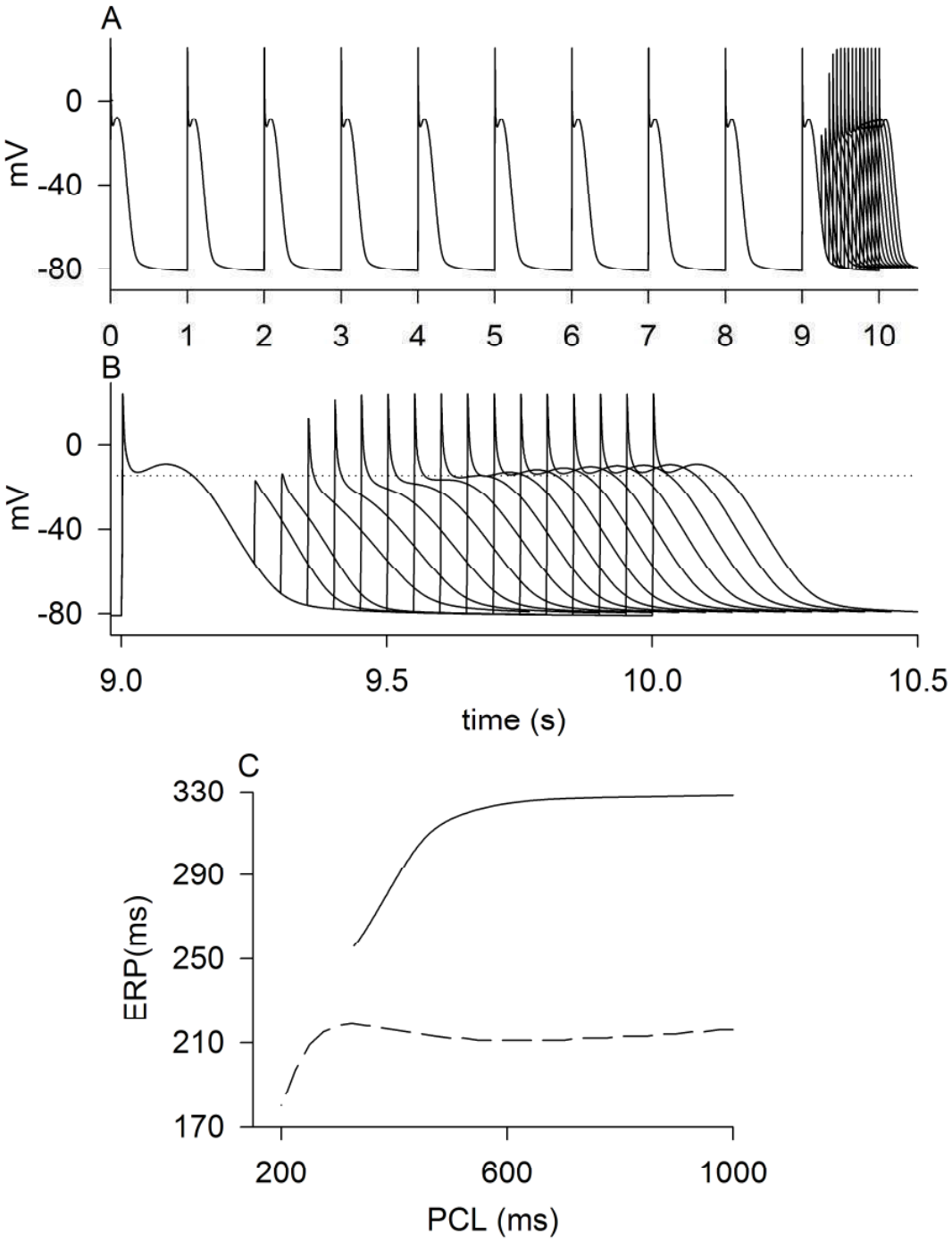

Figure 1.9 Simulation protocol for the construction of the ERPr curves and representative curves for NYG and CRN models. A: Train of 10 preconditioning pulses followed by several premature elicited APs. B: Final 1.5 s of simulation protocol showing the 10^{th} and 11^{th} APs where the dotted line represents 80% of the amplitude of the 10^{th} AP. Amplitude of the 11^{th} AP is observed to shorten due to premature stimuli. ERP is measured as the shortest time at which the tissue can elicit an AP with amplitude of 80% of the previous C: Constructed ERPr curves for the CRN (solid line) and NYG (dashed line) model.

1.12.4 Simulation of spatially extended tissues

1D strands of tissue were modeled by incorporating the single cell models into a parabolic partial differential equation (PDE) to construct mono-domain spatial models of electrical propagation. The PDE has the form:

$$C_m \partial u / \partial t = D\nabla^2 u - I_{ion} \tag{1.3}$$

Where u is cell membrane potential, C_m is cell membrane capacitance, D is the electrotonic diffusion coupling between cells simulating the gap junction coupling, u is the membrane potential, and I_{ion} is the membrane current. D was taken to be 0.031 mm^2/ms (Biktashev 2002) to give a physiological conduction velocity (CV) of 0.27 mm/ms for a solitary wave propagating through atrial tissue. Intracellular distance, represented by the spatial step of the spatially extended models, was taken to be 0.1 mm. Such a space step closely relates to physiological spacing between human atrial cells and gave stable numerical solutions independent of spatial step size. Such a formulation is sufficient for our purposes as we do not consider any extracellular potentials, fluids or indeed mechanical activity, for which more complex bi-domain formulations have to be adopted (Potse, Dube et al. 2006; Whiteley 2007; Vigmond, Weber dos Santos et al. 2008; Linge, Sundnes et al. 2009; Morgan, Plank et al. 2009).

1.12.5 Construction of CV restitution curves in a 1D strand of atrial tissue

CV restitution (CVr) curves are computed by measuring the speed of propagation of the excitation wave front along the simulated 1D homogenous strand of atrial tissue using a standard protocol and can be seen in Figure 1.10 (Zhang, Kharche et al. 2008). A series of 10 conditioning pulses were elicited and allowed to propagate across the strand. The wave was initiated by stimulating the end three cells with stimulus strength of 2 nA/pF for 2 ms. Conditioning pulses (S1) were applies at a PCL of 1000 s after which a premature pulse (S2) was applied. The velocity of propagations of the wave from the S2 stimulus is computed by calculated from the time for the excitation wave front to reach the center of the strand. The CV of the second propagation wave is plotted as a function of the inter-pulse duration to construct the CVr curve.

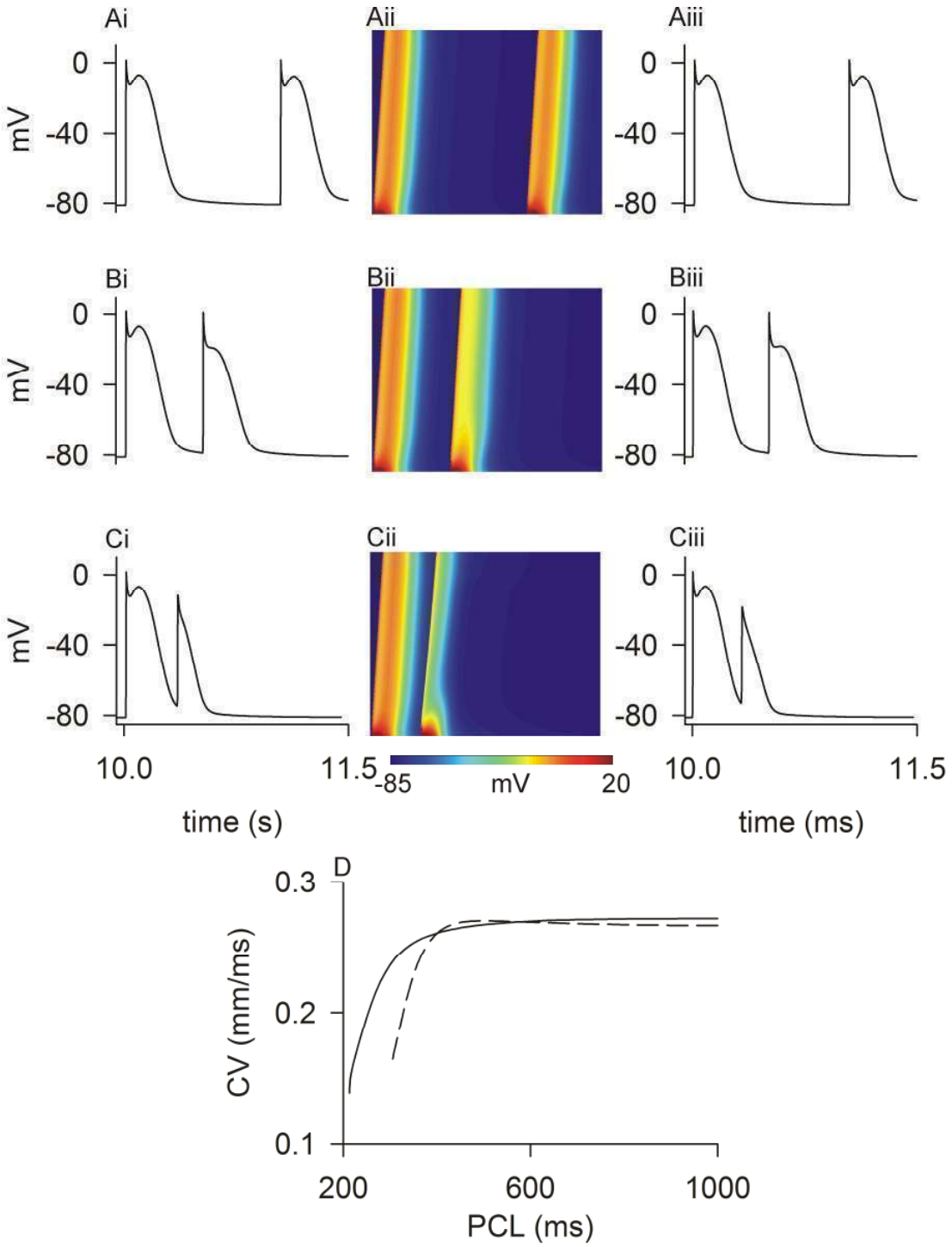

Figure 1.10 Simulation protocol for the construction of CVr curves and representative curves for the CRN and NYG models. Where rows A, B, and C show the propagation of the excitation wave along a 1D strand at inter pulse durations 1000 ms, 500 ms, and 320 ms respectfully. Panels i and iii shows a representative voltage time plot for the 50^{th} and 150^{th} nodes respectfully. Panel ii shows an image representing the propagation of the wave along the 1D strand with respect to time. Panel D shows constructed CVr curves for the CRN (solid line) and NYG (dashed line) model.

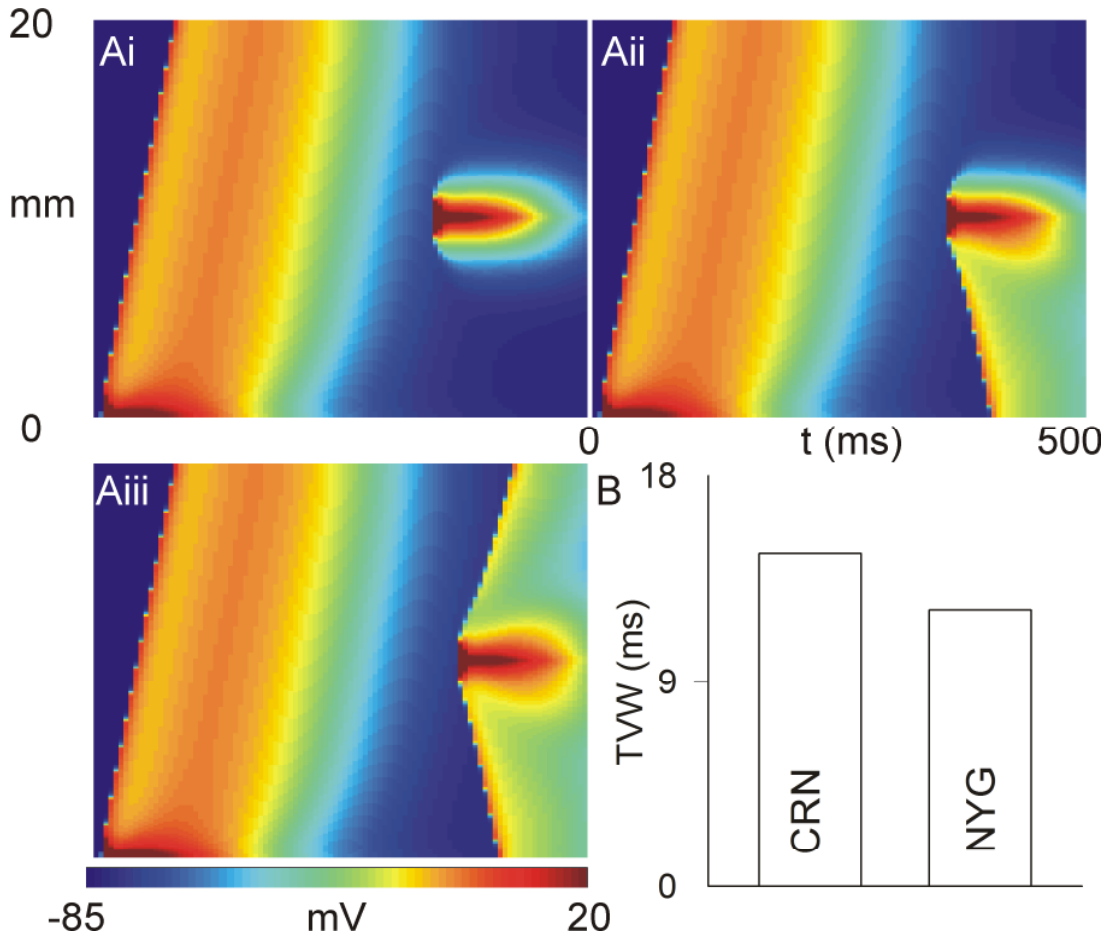

Figure 1.11 Temporal vulnerability window (TVW) simulations and calculated results for the CRN and NYG models. The method for TVW computation is shown in panels A. A conditioning pulse propagating from bottom to top of the 1D virtual strand, with a premature stimulus resulting in either bi-directional block (Ai), uni-directional block (Aii) or bi-directional propagation (Aiii) depending on when during the repolarisation phase it was applied. B: Shows the calculated TVW for the CRN and NYG models.

1.12.6 Calculation of temporal and spatial vulnerability window

Genesis of re-entrant circuits require tissue to sustain uni-directional block (Quan and Rudy 1990). Uni-directional conduction block in atria can lead to genesis of re-entrant excitation waves. Temporal vulnerability window (TVW) measures the vulnerability of cardiac tissue to genesis of uni-directional conduction block. TVW is computed by allowing a single solitary wave to propagate from one end of the 1D tissue to the other. After certain duration and in the repolarisation phase in the middle of the tissue, a premature pulse is applied. The time window during which the premature pulse elicits uni-directional propagation block is termed as the TVW. Figure 1.11 illustrates the protocol and also shows the measured TVW calculated for the CRN and NYG models.

Spatial vulnerability window (SVW) is quantified by using 2D homogeneous models of human atrial tissue. SVW is computed as the minimal atrial substrate size that can sustain re-entrant waves. To this end, a sufficiently long pulse as shown in Figure 1.12 is applied in the repolarisation tail of the conditioning pulse, giving rise to a figure of "8" re-entrant waves. The minimum length that sustains such re-entry is termed as minimum substrate (MS). The calculated SVW for the CRN and NYG models is also give in Figure 1.12.

1.12.7 2D tissue modelling, spiral wave re-entry

Models of 2D idealized homogenous atrial tissue were constructed to study the behaviour of re-entrant waves. Using the PDE described in Equation 1.3 to construct mono-domain spatial models of electrical propagation. The 2D sheets were taken to be 37.5 mm x 37.5 mm approximating the size of the human atria. In simulations, re-entrant waves are initiated by using a cross-field stimulation protocol. After allowing a planar wave to sufficiently propagate through the 2D sheet, a cross-field stimulus is applied so as to initiate re-entry (Kharche, Seemann et al. 2007). Upon initiation of a re-entrant wave in the middle of the tissue, the re-entrant waves are allowed to evolve. In total 6 s of electrical activity in the 2D sheets was simulated and characterized by re-entrant wave tip trajectories, life spans (LS), and a time series plot of the membrane potential of selected nodes whereby a frequency analysis yielded the PSD indicating the dominant frequencies (DF) of the electrical excitations. The 2D simulations using the CRN model are shown in Figure 1.13.

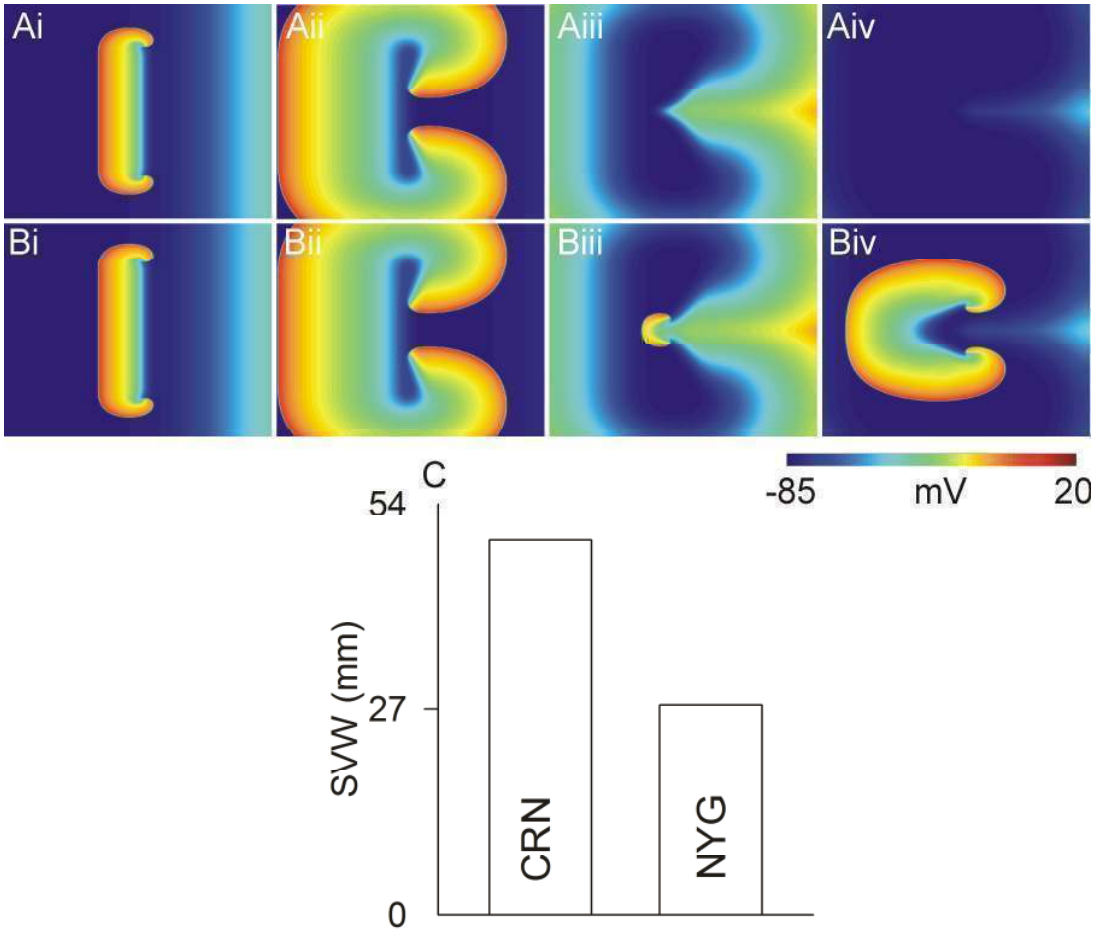

Figure 1.12 SVW simulations and calculated values for the CRN and NYG models. The 2D Panels shown in rows A and B illustrate the simulation protocol. In panels A the stimulus is of insufficient length to initiate re-entry. In panels B the stimulus is of sufficient length initiates a figure of eight re-entry. The critical value of the stimulus length at which re-entry is initiated is measured as the MS. C: Shows calculated MS for the CRN and NYG models.

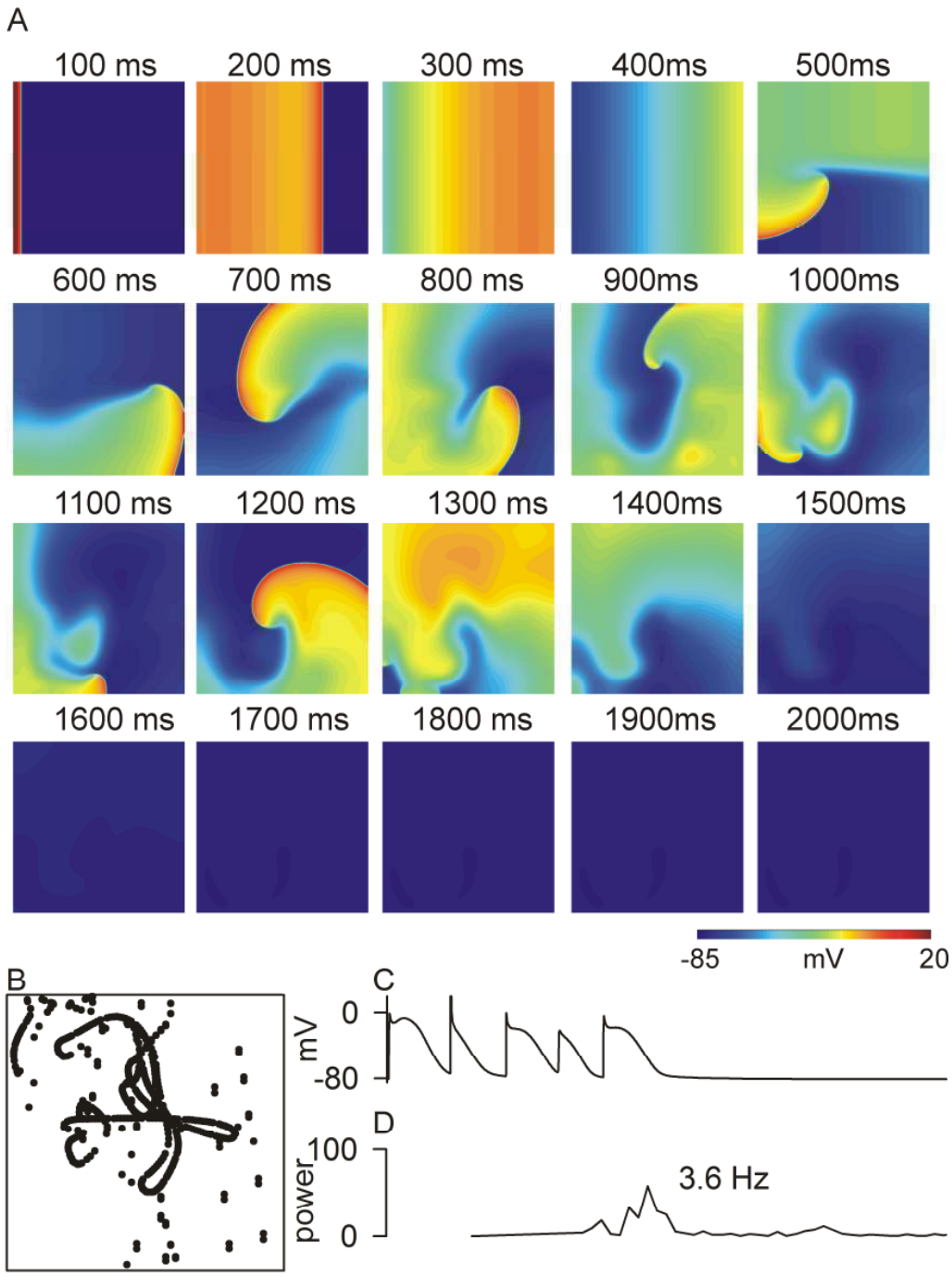

Figure 1.13 Simulation of re-entry in a 2D idealised sheets of virtual atrial tissue. A: Representative frames from 2D simulations using the CRN model B: Spiral wave tip trace C: AP trace taken from a representative cell in the 2D atrial sheet, re-entry is observed to terminate after 1.4 s. D: Corresponding PSD for the representative AP trace in panel C, where the frequency of maximum power is shown as 3.6 Hz.

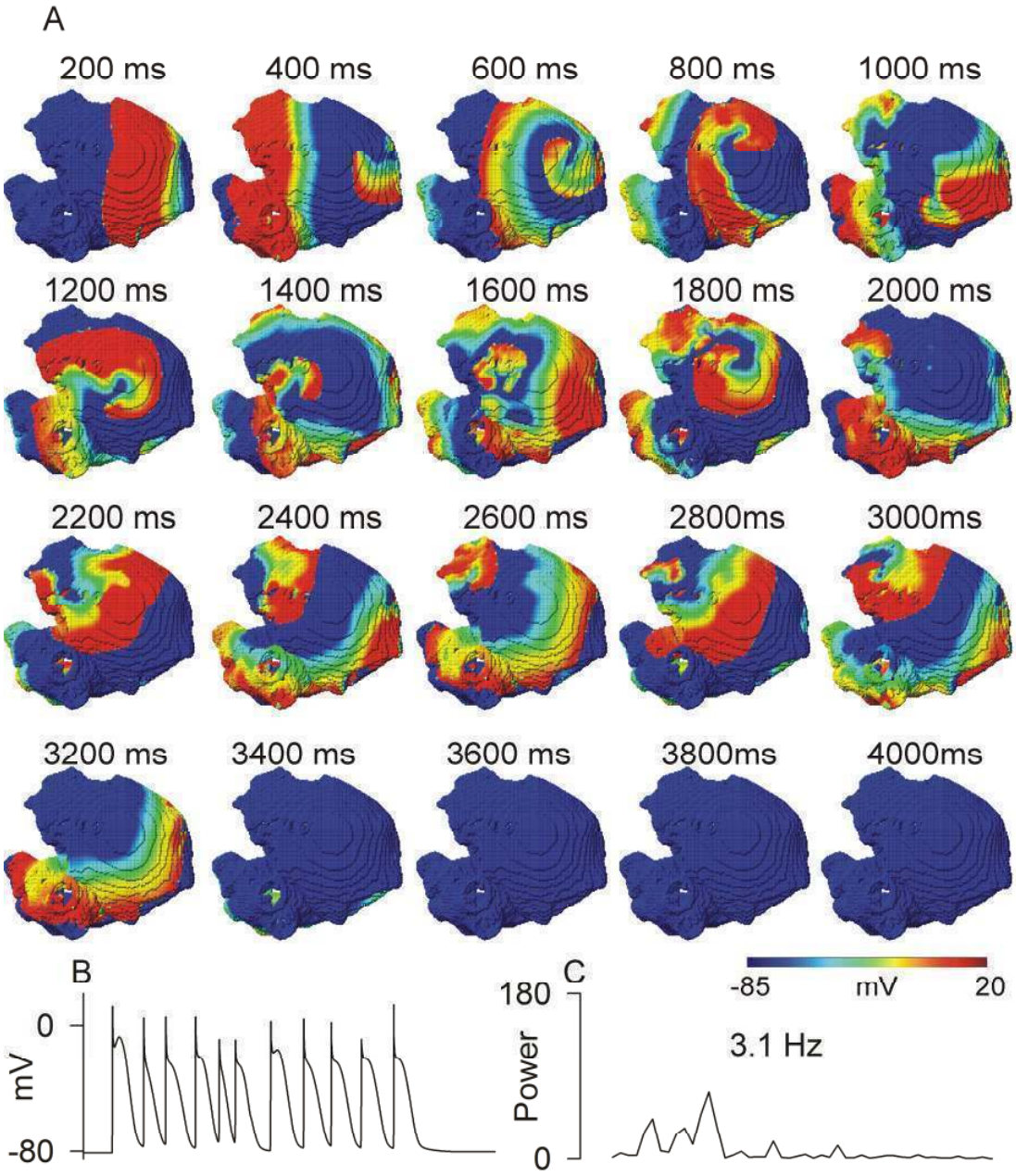

Figure 1.14 3D scroll wave simulations. A: Representative frames from 3D simulations using the CRN model B: AP trace taken from a representative cell in the 3D atrial geometry, re-entry is observed to terminate after 4.2 s D: Corresponding PSD for the representative AP trace in panel C, where the frequency of maximum power is shown as 3.1 Hz.

1.12.8 3D scroll waves in the atria

The 3D anatomically detailed spatial model of human female atria as was developed in a previous study (Seemann, Hoper et al. 2006). It is based on the anatomical geometry of the human atria reconstructed from the visible human project (Ackerman, 1991; Ackerman and Banvard 2000). The anatomical model consists of electrically homogeneous atrial tissue, the SA node and conduction pathways. The SA node is the main pacemaker wherefrom cardiac electrical excitation originates. The conduction pathways are electrically and structurally heterogeneous and assist in normal conduction of electrical excitation in the human atrium. In our studies, we investigate re-entrant waves and therefore do not consider SA node electrical activity, nor the heterogeneity associated with the conduction pathways. All cells in our 3D anatomical model simulations are considered to be electrically homogeneous. The 3D model has a spatial resolution of 0.33 mm x 0.33 mm x 0.33 mm. Although the 3D simulations have a small dependence on such a space step, the total simulated time of electrical activity was less than 6 s and no apparent differences were observed in preliminary simulations at 0.1 mm and 0.33 mm up to such time scales. The re-entrant waves were initiated using a protocol similar to the 2D case. The planar S2 stimulus was applied at a location in the RA to reduce boundary effects and interference from anatomical obstacles. The RA was chosen to be ideal as it offers minimal anatomical defects interfering with the initial evolution of the re-entrant waves. The activity of the atria were characterised by LS of re-entrant waves, time-traces were recorded from selected nodes, and frequency analysis was preformed to construct a PSD to determine of DF of the re-entrant waves. Results under control conditions are shown in Figure 1.14 where lifespan was measure to be around 4.2 s and a DF of 3.1 Hz was calculated.

1.12.9 Numerics, algorithms and visualisation

The simulations in this thesis were performed by utilising a simulation toolkit custom deigned for performing multi-scale simulations (Kharche, Seemann et al. 2007). As the CRN model consists of multiple timescales the ODE system is stiff. However, the toolkits integration method of an explicit Euler method with a time step of 0.05 ms was found to provide a sufficiently stable solution when implemented. The toolkit also utilises check pointing wherever possible to limit computational expense of the simulations. The 1D and 2D spatially extended PDE models were solved using the explicit Euler method with a 3

and 5 node Laplacian operator in 2D respectively; a time step was 0.005 ms and space step 0.1 ms proved sufficient for a stable solution. In the 3D case a 7-node approximation for the Laplacian operator was implemented and the space step was taken to be the anatomical model spatial resolution of 0.33 mm, which gave stable solutions with a time step of 0.05 ms. The 2D and 3D spatial models are large with 140625 and more than 26 x 10^6 nodes respectively. Parallelisation is therefore an important part of cardiac simulations. Solvers that used shared memory parallelism (OpenMP) and large distributed memory parallelism (MPI) were developed in our laboratory (Kharche, Seemann et al. 2008). The local high performance computing facilities with 208 CPUs system with distributed memory connected by a single rail Quadrics QsNetII interconnector and with MPI was used. The full geometrical model demands very large amounts of contiguous memory. 3D Atrial tissue geometry occupies about 8% geometry of the total data set, due to atrium being thin walled with large holes of atrial chambers and vena caves. We re-structured the computer code such that only atrial nodes, *i.e.* only 8% of the total 26 million nodes and related information are stored in the computer memory. This improved efficacy of memory usage. By re-numbering the real atrial nodes we are not storing any data points that are not atrium. The memory required is reduced to less than 10 GB in the 3D case, and the required computer floating point operations (flops) are also reduced.

The 3D simulations produce large data sets of more than 30 GB. Traditionally this output is then post-processed to obtain measures quantifying the simulation, e.g. scroll wave filament meander, and to visualise the dynamics of the electrical propagations. Each output file consists of a binary data file of approximately 150 MB size. Efficient visualisation of the 3D data was developed created by using the visualisation package Advanced Visualisation System (AVS) developed by Manchester Visualisation Centre. This is versatile high level graphical software with a high level of functionality. 3D figures were produced using diamond shaped glyphs, each of which was colour coded with a scalar value, namely the value of voltage at that location. For smaller visualisation jobs, *e.g.* 2D visualisation, we have used MATLAB due to its functionality and transparent scripting. Development of visualisation scripts using MATLAB is relatively straightforward with a high level of functionality. MATLAB is also available to our laboratory locally. Having successfully developed 2D visualisation pipelines using MATLAB, AVS as a high level visual programming environment is also versatile and the results obtained using MATLAB can be replicated by AVS.

1.10 Simulating disease and AF

Several ion-channel dysfunctions are associated with AF (Abriel and Kass 2005; Abriel 2007). In addition the effects of age have been studied in a tissue specific study by Zhao et al. (Zhao, Trew et al. 2009). There is a large amount of interest in the modelling community to simulate how changes in the electrophysiology of a cell due to such external factors are manifested as AF. The effects of multi-channel dysfunction induced AF has been studied in our laboratory (Kharche and Zhang 2008). Initiation of re-entrant waves is often due to triggers, and the underlying mechanisms have also been investigated in a limited way (Tveito and Lines 2008). In a novel cellular automata modelling study, Reumann et al. and others (Haghjoo 2007; Reumann, Bohnert et al. 2007) showed the existence of "snakes" and "worms" in the human atrium. Simulation facilitates the dissection of the underlying electrophysiological causes (Zhang, Garratt et al. 2005) of tissue and organ level AF (Kharche, Garratt et al. 2008). Simulation studies remain focused on investigating the causes of initiation and stabilisation of re-entrant waves (Xie, Qu et al. 2002). Although attempts have been made to simulate the whole atrium in anatomical and biophysical detail (Blanc, Virag et al. 2001), it has not been achieved to sufficient accuracy to be clinically relevant. Small animal research also plays an important role in understanding of cardiac electrophysiology and the simulation of AF is no exception. The ability to simulate pharmacological intervention, for example the effects of I_{Na} block which results reduction of APD (Kneller, Kalifa et al. 2005), also provides an aim for modellers.

Table 1.1. Quantitative summary of the multi-scale simulations for the CRN and NYG atrial cell models.

Model	Quantity	CRN	NYG
Cell	Resting potential (mV)	-80.80	-73.7
	APD_{90} (ms)	314.2	221.3
	APD_{50} (ms)	210.6	134.4
	Overshoot (mV)	24.7	29.5
	dV/dt_{max} (mV/ms)	217.1	141.7
	APDr maximal slope	1.3	0.64
	ERP (ms) (stimulus interval ~ 1 s)	327.9	216.0
	Cut off BCL (ms)	328.6	200.0
1D	CV (mm/ms)	0.26	0.27
	Cut off S2 (ms)	320	213
	TVW (ms)	14.6	12.1
	Wavelength (mm)	81.7	60.2
2D	LS (s)	1.4	-
	DF (Hz)	3.6	-
	Tip meander area (cm^2)	5.25	-
	SVW (mm)	49.2	27.5
3D	LS (s)	4.2	-
	DF (Hz)	3.1	-

Chapter 2

Simulating the arrhythmogenic effects of the KCNQ1 (S140G) gene mutation in human atria

2.1 Introduction to the KCNQ1 gene mutation

Whilst the underlying mechanisms for the genesis of AF are yet unclear, organic cardiac disease (Danicek, Theodorovich et al. 2008; Tanabe, Kawamura et al. 2009) and AF induced electrical remodelling of ion-channels (Bosch, Zeng et al. 1999; Workman, Kane et al. 2001; Ashcroft 2006) are believed to be among major factors responsible for initiating and sustaining AF. These underlying risk factors increase in prevalence with age and are the primary reasons why the incidence of AF rises substantially in the elderly. Lone AF patients, who have no underlying disease indicating an increased risk of AF, are still at risk of sudden episodes of AF. Lone AF is also observed in much younger demographics. These patients have characteristic solitary gene defects which predispose them to the condition (Fox, Parise et al. 2004; Campuzano and Brugada 2009). Recent experimental studies have identified several gene mutations in familial AF patients (Yang, Xia et al. 2004; Xia, Jin et al. 2005; Olson, Alekseev et al. 2006; Otway, Vandenberg et al. 2007). These mutations have been identified to alter the electrophysiology of key ion-channels responsible for repolarisation of atrial myocytes. Recently a mutation has been identified in familial AF patients in the KCNQ1 gene that encodes the pore forming α-subunit of the cardiac slow-delayed rectifier potassium channel (I_{Ks}) (Lundby, Ravn et al. 2007; Ravn, Aizawa et al. 2008; Restier, Cheng et al. 2008). Chen *et al.* (Chen, Xu et al. 2003) clinically identified a familial missense mutation of KCNQ1 at nucleotide 418 from adenine to guanine, which results in a change of amino acid from serine to glycine at 140 (S140G mutation). Functional analysis of the co-expression of wild type (WT) and S140G mutant type (MT) KCNQ1 with KCNE1 revealed a mutation induced increase of I_{Ks} (Chen, Xu et al. 2003). I_{Ks} is an important outward potassium current regulating late repolarisation of action potentials (APs) in cardiac cells. Abnormality of I_{Ks} has been found in various cardiac diseases including long QT (Lundby, Ravn et al. 2007; Zhang, Yin et al. 2008) and short QT (Bellocq, van Ginneken et al. 2004) syndromes. It has been shown that gain-in-function of I_{Ks} due to KCNQ1 V93I mutation in SQT-2 syndrome dramatically abbreviates human ventricular AP duration (APD) and augments intra-ventricular heterogeneity increasing susceptibility to arrhythmia (Zhang, Kharche et al. 2008). However, the mechanisms by which the gain-in-function of I_{Ks} caused by the KCNQ1 S140G mutation promote and perpetuate atrial arrhythmia have not been elucidated. The aim of

this study was to quantify the pro-arrhythmogenic effects of the KCNQ1 S140G mutation in the human atria at cell, tissue and whole-organ levels.

2.2 Methods

This section outlines the modification of the CRN model (Courtemanche, Ramirez et al. 1998) to simulate the alterations to I_{Ks} due to the KCNQ1 mutation. Experimental data provided by (Chen, Xu et al. 2003) allowed the mutation to be simulated as an addition of a voltage dependant leakage current. Simulations were performed as described in Chapter 1 to quantify the arrhythmogenic effects of the mutation at the single cell, 1D strand, and 2D idealized atrial sheet levels, as well as in an anatomically detailed 3D atria.

2.2.1 Model of I_{Ks} and atrial cell APs

The CRN model (Courtemanche, Ramirez et al. 1998) was used in this simulation study. It was chosen as it incorporates available human atrial cell and membrane data and reproduces human atrial electrical APs and APD rate dependence. The model has been found to be well suited to study re-entrant arrhythmias in human atrium (Pandit, Berenfeld et al. 2005; Seemann, Hoper et al. 2006; Kharche, Garratt et al. 2008). In the CRN model, the I_{Ks} potassium (K^+) current is modeled as:

$$I_{Ks} = g_{Ks} n^2 (V - E_k) \tag{2.1}$$

where g_{Ks} is the current conductance (CRN Control g_{Ks} = 0.129 nS/pF), n is the activation gate, V is the membrane voltage, and E_k is the K^+ reversal potential. The steady state properties of the activation gate, n, are described in the original CRN model. The model was modified to incorporate changes in I_{Ks} due to the KCNQ1 S140G mutation (Chen, Xu et al. 2003), as shown in Figure 2.1A. These changes include (i) a large increase of I_{Ks} current density; and (ii) a large I_{Ks} at hyperpolarized potentials not seen under WT conditions. Upon analysis of the experimental I-V data (Hong, Piper et al. 2005), equation (2.1) was modified by adding a non-gated voltage dependent leakage component, to model mutant I'_{Ks} as:

$$I'_{Ks} = I_{Ks} + \varphi g_{Ks} \left(V - E'_{rev}\right) \tag{2.2}$$

where g_{Ks} has the same value as in the Control case, I_{Ks} is the current conductance, E'_{rev} is the reversal potential of the leakage component, which was estimated to be -75.3 mV. φ is a scaling factor between 0 (WT; Control) and 1 (MT; homozygous), enabling simulation of possible intermediate heterozygous mutant conditions.

Modifications to I_{Ks} for the mutant condition were validated by the reproduction of experimental I_{Ks} I-V relationships (Chen, Xu et al. 2003) and I_{Ks} time traces during voltage clamp under the WT ($\varphi = 0$) and the MT ($\varphi = 1$) conditions. Following experimental voltage clamp protocol as given in Chen *et al.* (Chen, Xu et al. 2003), the cell membrane potential was first held at -80 mV for 1 s, and then clamped at test potentials ranging from -130 mV to 50 mV, each for a duration of 3 s. Amplitudes of I_{Ks} at the end of the voltage clamp pulses were plotted as a function of the step voltages to obtain I-V relationships (Figure 2.1A). Experimental and simulated time traces of I_{Ks} during voltage clamp are shown in Figure 2.1, B-E. In both the WT and MT cases, the simulated I_{Ks} I-V relationships closely approximate experimental data. In the following, simulation results are presented for $\varphi = 0$ (WT), $\varphi = 0.1$ (10% MT), $\varphi = 0.25$ (25% MT) and $\varphi = 1$ (MT) conditions.

2.3 Results

This section provides a detailed description of the results obtained from performing multi-scale simulations on the electrophysiological effects of the KCNQ1 S140G mutation. A summary of the functional effects of the mutation on simulated human atrial electrical activity are listed in Table 2.1.

2.3.1 Effects of increased I_{Ks} on atrial APs

Increased I_{Ks} due to the KCNQ1 S140G mutation abbreviated human atrial APs as shown in Figure 2.2A. The measured APD was 314.2 ms under WT condition and 22.4 ms under the MT condition. The APD reduction was due to the mutation induced increase in I_{Ks} (Figure 2.2B), and is associated with a decrease in the delayed rectifier K^+ current, I_{Kr} (Figure 2.2C) and I_{to} (Figure 2.2D). A marginal reduction of the L-type calcium current, I_{CaL}, (Figure 2.2F) was observed. Since the mutation was seen to cause such a dramatic abbreviation of the APD, the effects of intermediate increases in the leakage component of I_{Ks}, mimicking homozygous conditions, were investigated by gradually increasing φ. An increase in φ resulted in a monotonic decrease in the APD (Figure 2G). At $\varphi = 0.1$ (10%) and $\varphi = 0.25$ (25%), the measured APD was 147.5 ms and 79.32 ms respectively.

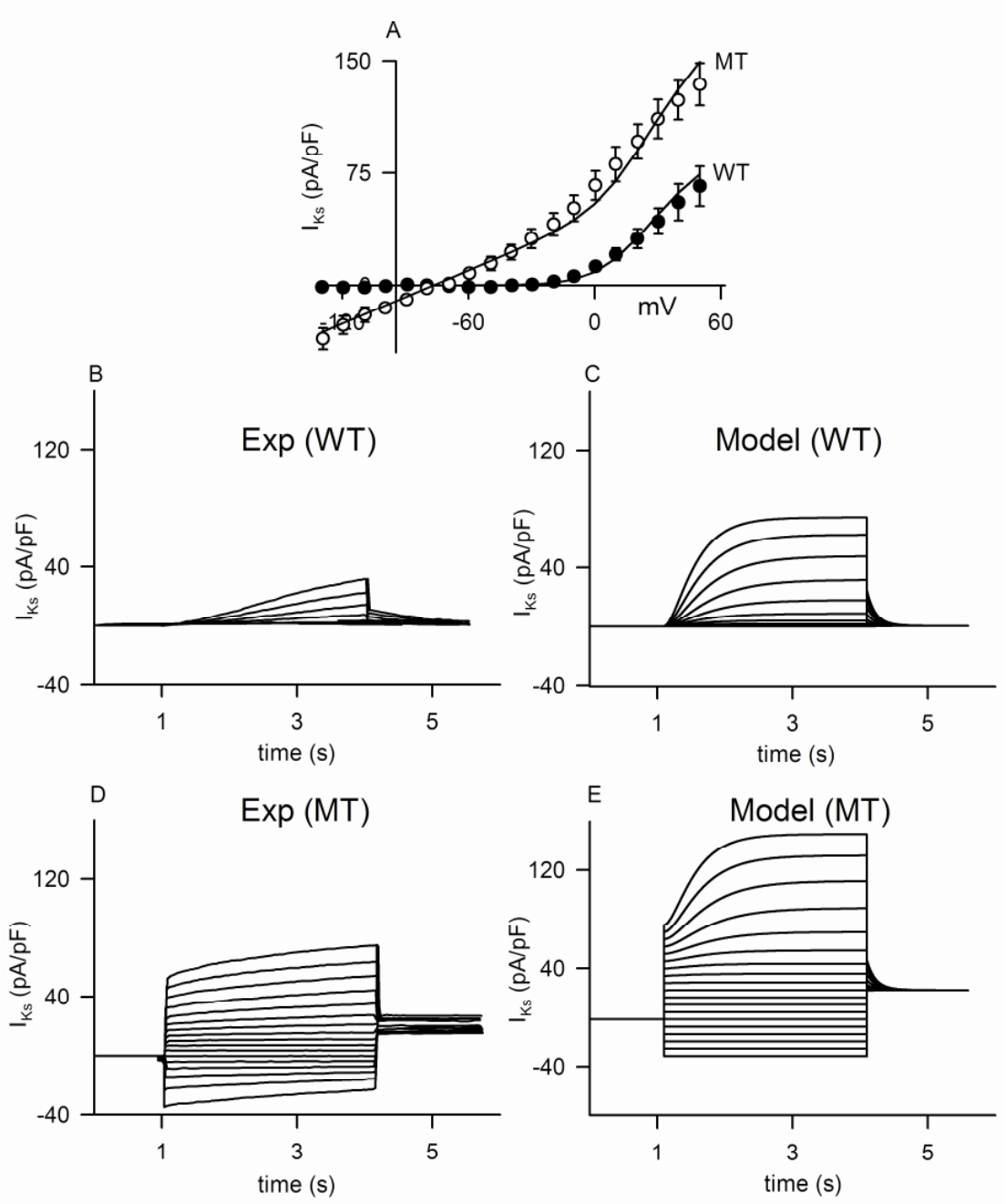

Figure 2.1 Experimental and simulated I_{Ks} under WT and MT conditions where experimental data are from Chen *et al.* (Chen, Xu et al. 2003). A: Experimental I_{Ks} I-V relationships under WT (solid circles) and S140G mutant I_{Ks} (open circles) superimposed upon simulated I-V relationships for WT and MT cases (solid lines). B: Experimental I_{Ks} current traces under WT conditions. C: Simulated current traces under WT conditions. D: Experimental current traces under MT conditions. E: Simulated current traces under MT conditions.

Table 2.1. Quantitative summary of the effects of the KCNQ1 (S140G) mutation.

Model	Quantity	WT	MT (φ=0.1)	MT (φ=0.25)	MT
Cell	Resting potential (mV)	-80.80	-80.01	-78.74	-76.88
	APD_{90} (ms)	314.2	147.5	79.3	22.4
	Overshoot (mV)	24.7	24.07	23.05	18.11
	dV/dt_{max} (mV/ms)	217.1	214.17	208.58	193.44
	APDr maximal slope	1.3	0.6	0.38	0.05
	ERP (ms) (stimulus interval ~ 1 s)	327.9	169.1	109.5	56.0
	Cut off BCL (ms)	328.6	184.3	126.6	44.9
2D	CV (mm/ms)	0.26	0.26	0.26	0.258
	Cut off S2 (ms)	320	152	95	46
	TVW (ms)	14.6	15.2	14.7	14.6
	Wavelength (mm)	81.7	38.4	20.6	5.78
	LS (s)	1.4	> 10	> 10	> 10
	DF (Hz)	3.6	7.1	9.8	16.1
	Tip meander area (cm^2)	5.25	1.10	0.58	0.32
	SVW (mm)	49.2	7.45	6.15	0.6
3D	LS (s)	4.2	>6	-	-
	DF (Hz)	3.1	8.9	-	-

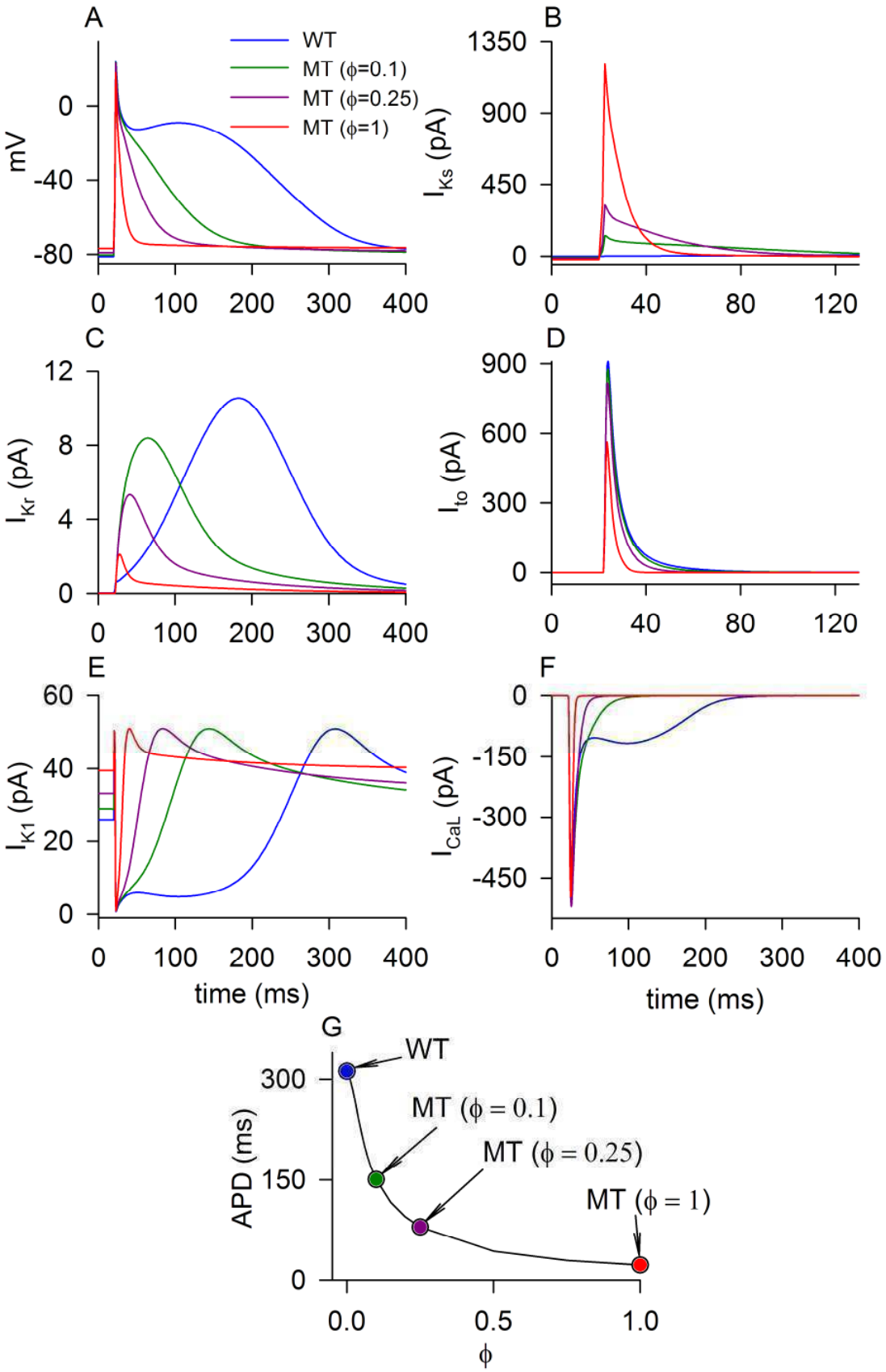

Figure 2.2. Simulated AP profiles and current traces under WT (blue line), and MT conditions where simulated data for φ = 0.1 (green line), φ = 0.25 (purple line) and φ = 1 (red line) are shown in panels A-F. A: AP profiles. B: I_{Ks} current profiles during APs. C: I_{Kr} current profiles during APs. D: I_{to} current profiles during APs. E: I_{K1} current profiles during APs. F: I_{CaL} current profiles during Ps. G: Changes in APD as the modeling parameter φ is increased from 0 (WT) to 1 (MT) condition.

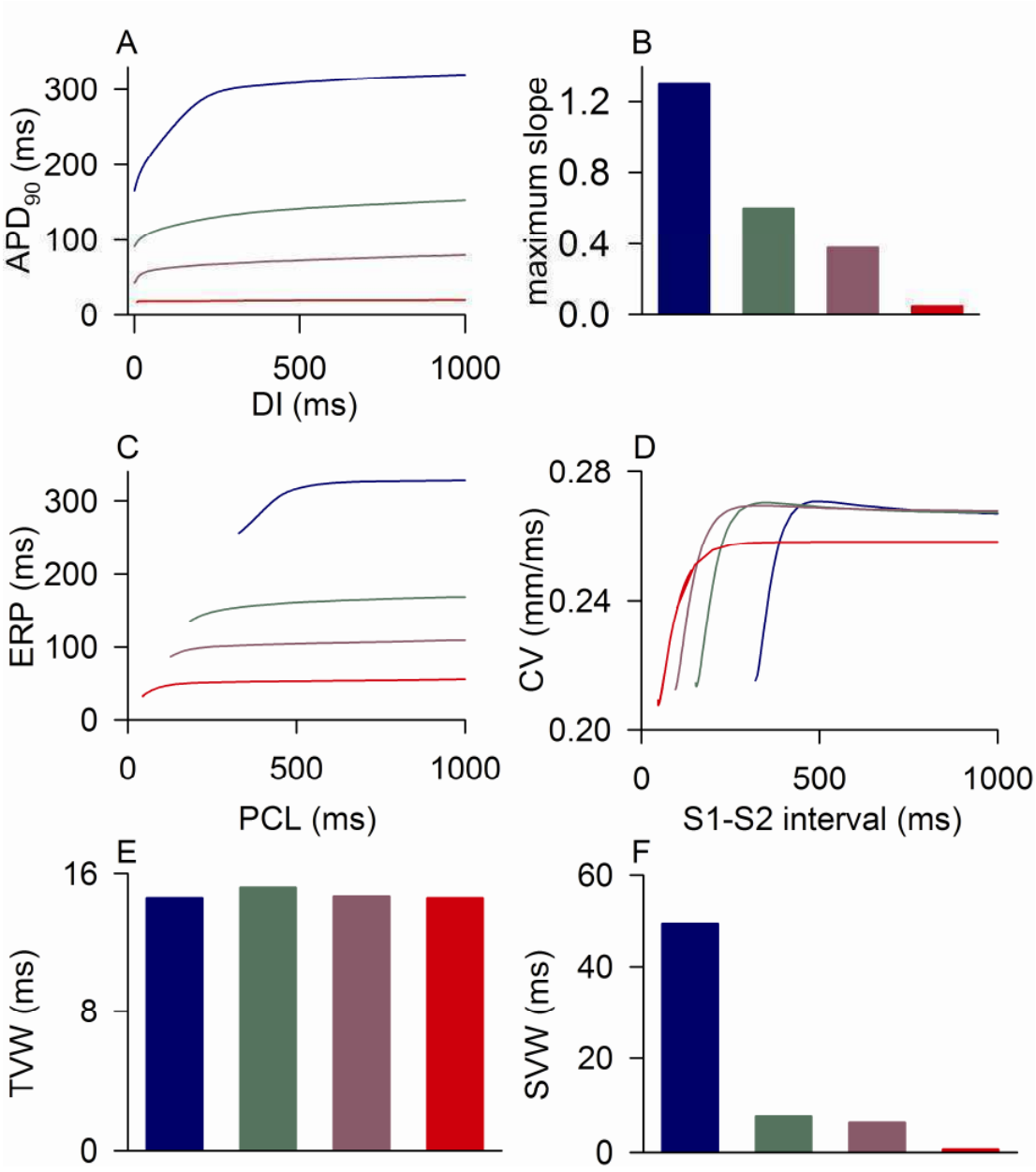

Figure 2.3 Simulated restitution profiles and temporal and spatial VW under WT (blue), and MT conditions where simulated data for φ = 0.1 (green), φ = 0.25 (purple) and φ = 1 (red) are shown in panels A-F. A: APDr, B: maximal slope of the APDr curves, C: ERPr, D: CVr, E: Temporal VW, F: spatial VW.

2.3.2 Effects of increased I_{Ks} on APD and ERP restitutions

The effects of the increased I_{Ks} due to the KCNQ1 S140G mutation on atrial APD restitution are shown in Figure 2.3A. Across the range of DI, the measured APD under the MT condition was considerably smaller than in the WT condition. MT conditions flattened the APDr curves. The measured maximal APDr slopes were 1.3 (WT), 0.6 ($\varphi = 0.1$), 0.38 ($\varphi = 0.25$), and 0.05 ($\varphi = 1$) conditions (Figure 3B). Such a mutation-induced loss in the rate-dependent adaptation of APD, indicated by flattened APDr curves, was similar to that observed in chronic AF patients (Osaka, Itoh et al. 2000; Watanabe, Masaki et al. 2002). This suggests an increase in the ability of the atrial cells to support high pacing rate electrical excitations.

The mutation induced increase in I_{Ks} reduced atrial ERP (Figure 2.3C), which decreased from 327.9 ms in the WT condition to 169.1 ms, 109.5 ms, and 56 ms under $\varphi = 0.1$, $\varphi = 0.25$, and $\varphi = 1$ conditions respectively, as computed at a PCL of 1 s. The cut-off PCL of the ERP curve under WT conditions was 328.6 ms. The mutation shifted the ERP restitution curves leftward, measuring 184.3 ms, 126.6 ms, and 44.9 ms for $\varphi = 0.1$, $\varphi = 0.25$, and $\varphi = 1$ conditions respectively, again demonstrating an increase in the ability of the atrial cells to support high rate electrical activities.

2.3.3 Effects of increased I_{Ks} on intra-atrial conduction velocity and tissue's temporal and spatial vulnerability

CVr curves are shown in Figure 2.3D. Under WT conditions the CV at a PCL of 1000 ms was measured to be 0.26 mm/ms. When $\varphi = 0.1$ and $\varphi = 0.25$ the CV remains unchanged from WT conditions. However, when $\varphi = 1$ there was a reduction in CV to 0.258. In addition to this reduction in CV, the mutation facilitated high excitation rate wave propagation. This is shown in Figure 2.3D by the leftward shift of the CVr curves. Under WT conditions the cut-off PCL was measured to be 320 ms, whereas under $\varphi = 0.1$, $\varphi = 0.25$, and $\varphi = 1$ MT conditions the cut-off PCL was 152 ms, 95 ms, and 46 ms respectively. This indicates that increasing the level of the mutation through augmenting the parameter φ increases the ability of the tissue to sustain electrical wave propagations at ever higher excitation rates.

The measured TVW are shown in Figure 2.4E. Under WT conditions the VW was measured to be 14.6 ms. For $\varphi = 0.1$, $\varphi = 0.25$, and $\varphi = 1$ the VW was measured at 15.2 ms, 14.7 ms, and 14.6 ms respectively. The alterations to VW due to the mutation were nominal.

Measured spatial vulnerability of atrial tissue in the 2D model is shown in Figure 2.3F. Under the WT condition, the measured minimal substrate size was 49.2 mm. Under the MT conditions, the measured minimal size decreased by 84.8% to 7.45 mm when φ =0.1, by 87.5% to 6.15 mm when φ =0.25, and was lower than 0.6 mm in the φ = 1 case. Thus, mutant I_{Ks} caused a marked reduction in the substrate required to induce and sustain re-entry, demonstrating a remarkable increase in the susceptibility of the tissue to arrythmogenesis.

2.3.4 Effects of increased I_{Ks} on the dynamical behavior of re-entrant excitation waves in 2D model

Figure 2.4 shows that increased I_{Ks} stabilized re-entrant spiral waves, which led to sustained re-entrant excitation in a limited atrial mass. In the WT condition, the initiated spiral wave was unstable. The tip meandered in a large area, which led to self-termination when it meandered out of the model boundaries or collided with its own repolarisation tail. Core traces, representative time traces and PSD are shown in Figure 2.5. The measured LS of spiral waves was 1.4 s under WT conditions. Power spectrum analysis of the recorded local electrical activity revealed a peak frequency of 3.6 Hz for WT. Under MT conditions (φ =0.1 and φ =0.25), re-entrant waves were stable, persistent and had limited meander throughout the 6 s simulation. Power spectrum analysis of the recorded electrical activity from the tissue revealed a peak frequency of 7.1 Hz and 9.8 Hz for φ = 0.1 and φ = 0.25 respectively. Under the homozygous MT φ = 1 condition the spiral wave was highly stable with a DF recorded as 16.1 Hz.

2.3.5 Erratic re-entrant electrical excitation waves in the 3D atria

Re-entrant excitation waves (scroll waves), representative time traces and PSD, of the 3D anatomical model of human atria are illustrated in Figure 2.6 and Figure 2.7 respectfully for the WT and MT (φ=0.1) conditions. Under the WT condition, the scroll wave broke up into multiple re-entrant wavelets, with each meandering in a large area of the tissue leading to self-termination at 4.2 s. The observed self-termination of scroll waves was independent of the initiation location. Under the MT condition, the scroll wave also broke into multiple wavelets, each propagating erratically due to interaction with the complex atrial anatomy. The re-entrant excitations persisted throughout the duration of the simulation period of 6 s. The dominant frequency in the MT case was much higher (~ 8.9 Hz at φ = 0.1) than under the WT condition (3.1 Hz).

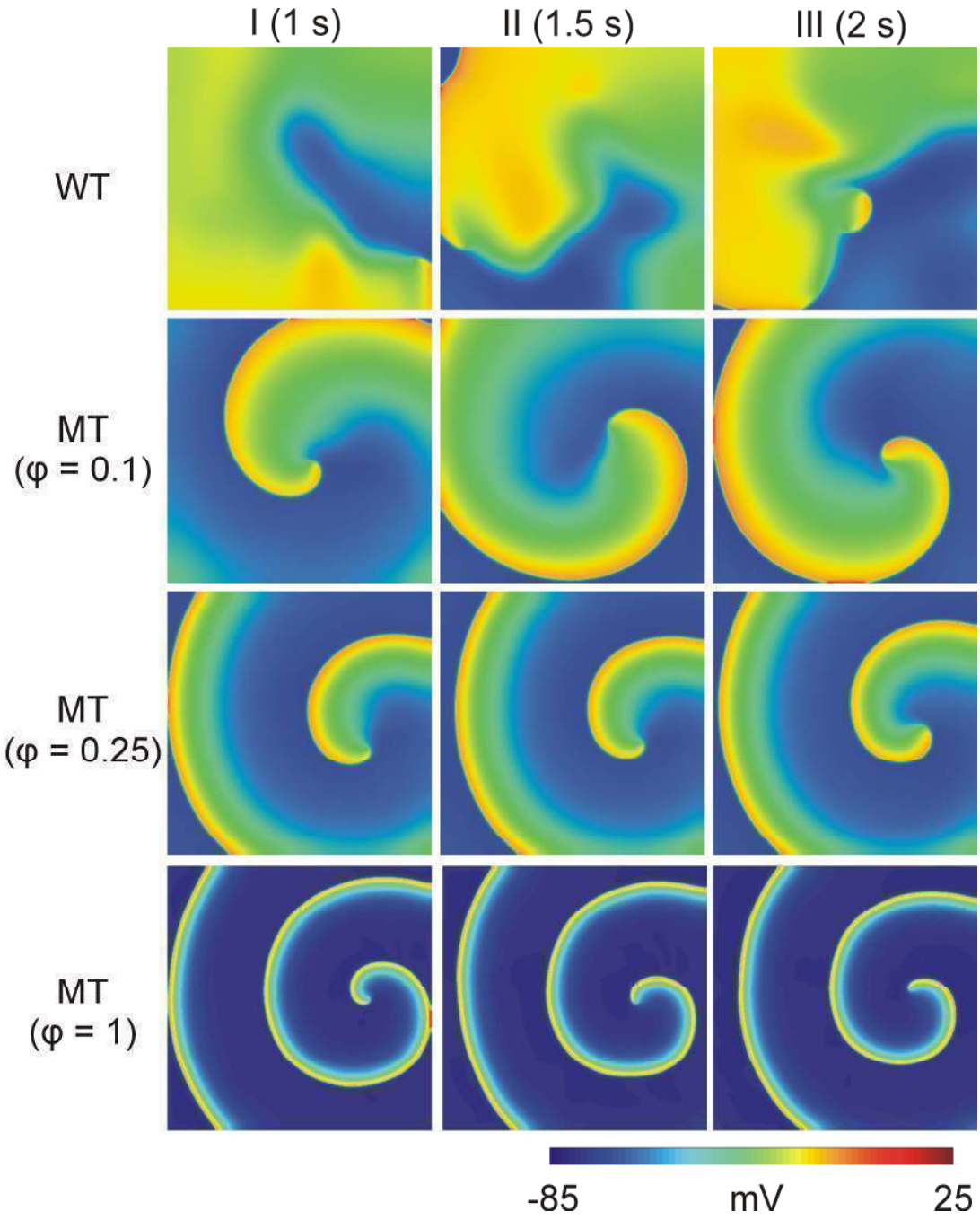

Figure 2.4 Top panels show results from 2D re-entrant wave simulation under WT condition; the second row of panels show results for φ = 0.1 conditions; the third row of panels show results for φ = 0.25 conditions and the bottom row show results for φ = 1. Frames from the 2D simulation at time t = 1 s (column I), time t = 1.5 s (column II) and time t = 2 s (column III) are shown.

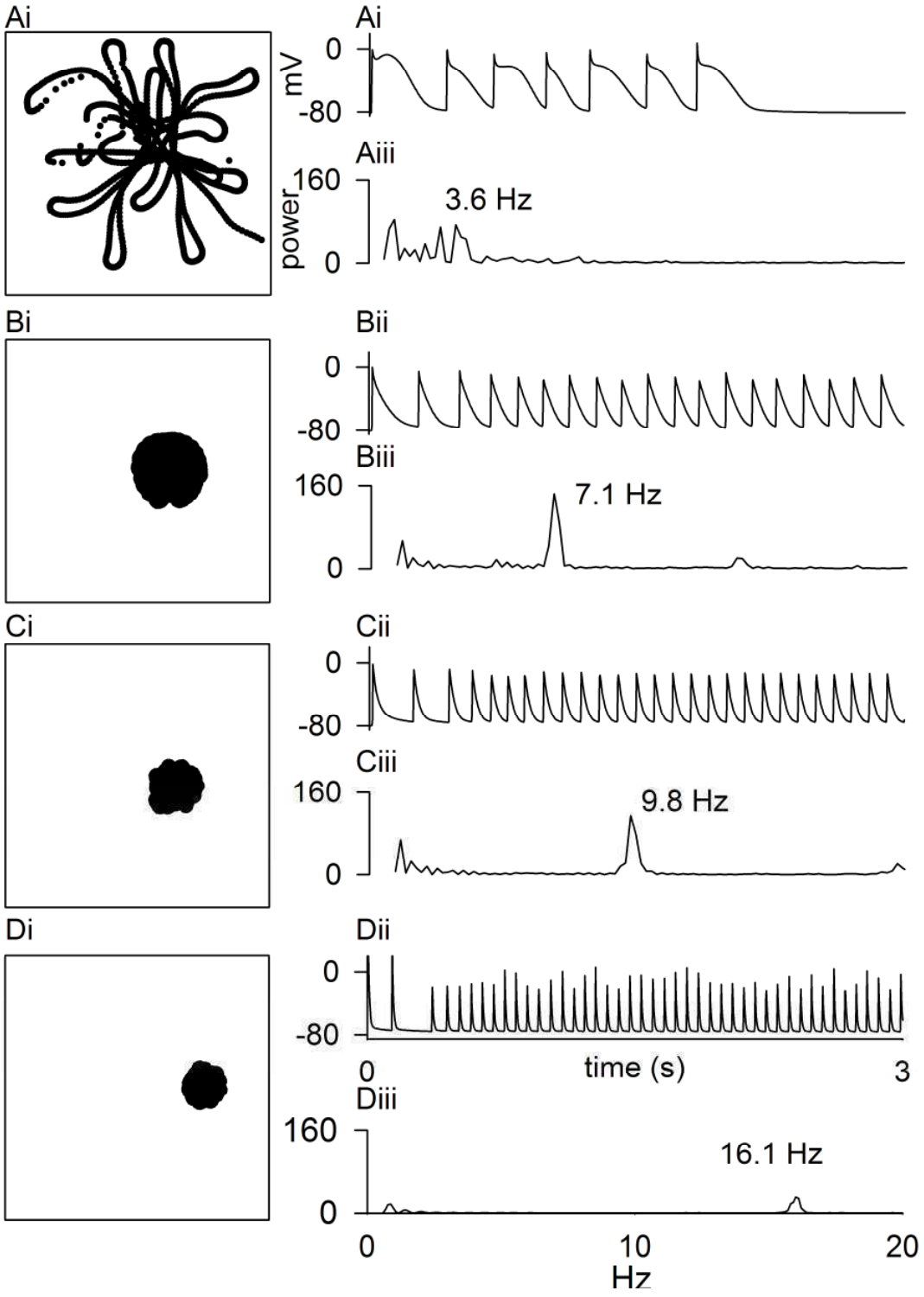

Figure 2.5 2D spiral wave tip traces (panel i), representative AP traces taken from 2D simulations (panel ii), and power spectrum density showing frequencies of maximal power (panel iii) under A: WT, B: φ = 0.1 , C: φ = 0.25, D: φ = 1 conditions.

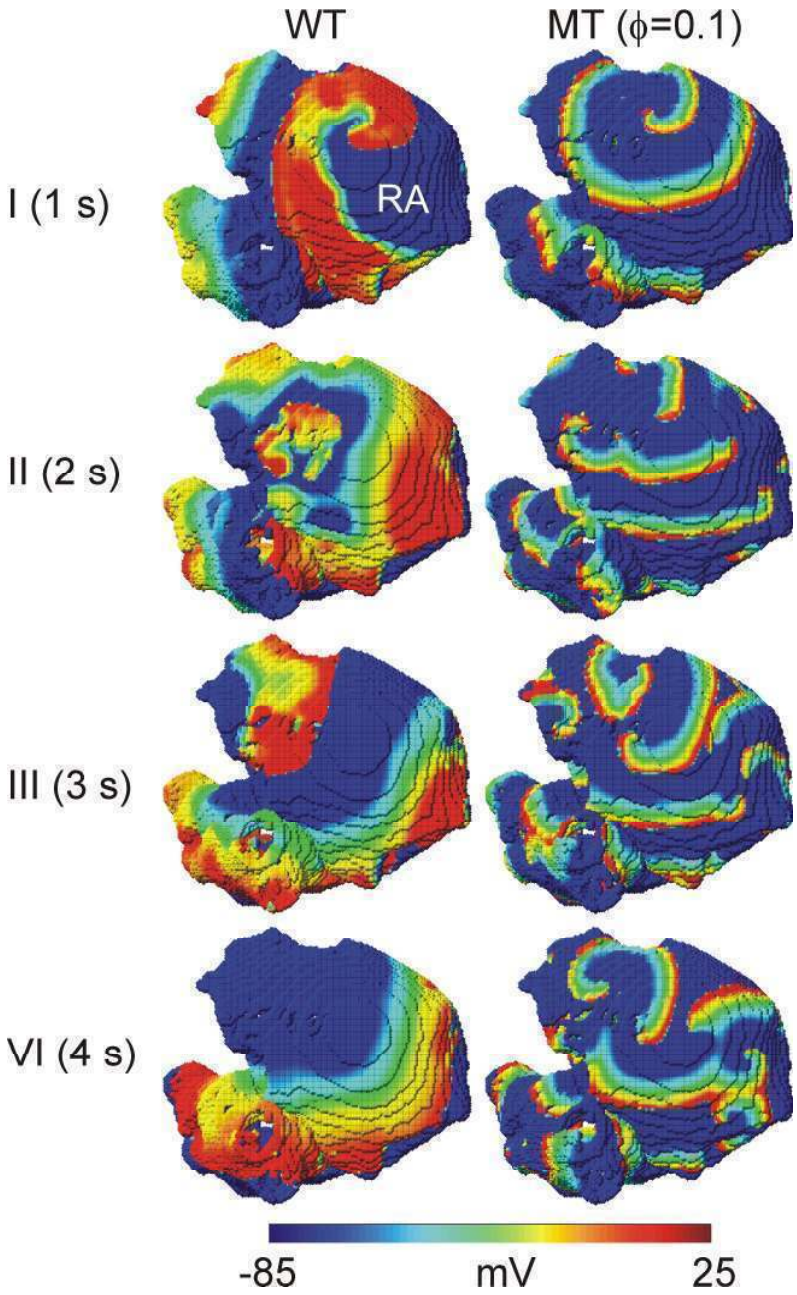

Figure 2.6 Simulation of scroll waves in the 3D virtual human atrium. Left column shows representative frames from the simulation under WT condition and right column shows frames from the simulation under MT (φ = 0.1). Row I shows frames at time t = 1 s, in Row II at time t = 2 s, Row III at time t = 3 s and Row IV at time t = 4 s.

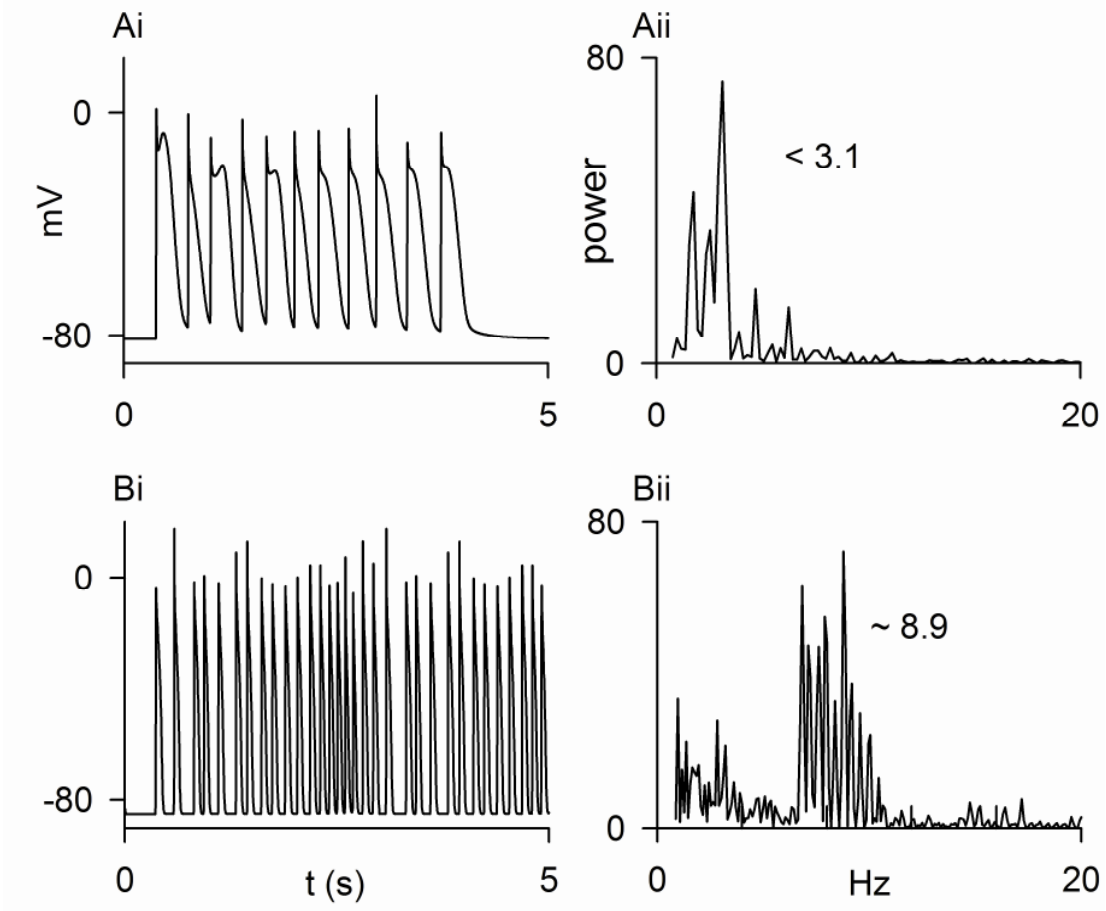

Figure 2.7 Traces taken from 3D simulations (panel i), and PSD showing frequencies of maximal power (panel ii) under A: WT, B: $\varphi = 0.1$ conditions.

2.4 Discussion and Conclusion

Due to a lack of phenotypically accurate experimental models, the mechanisms by which the KCNQ1 S140G mutation influences atrial cellular electrophysiology and AF susceptibility at the tissue level have not been investigated. In the present study, a computation model was used to gain insights into the mechanisms underlying the genesis and maintenance of AF in patients with the KCNQ1 S140G mutation. The major findings are: (i) the KCNQ1 S140G mutation increased the I_{Ks} by inducing a voltage dependent leakage component. This is similar to the constitutive leakage current of I_{Ks} arising from KCNQ1 V141M mutation responsible for atrial fibrillation and short QT syndrome (Hong, Piper et al. 2005); (ii) the mutation induced gain in I_{Ks} abbreviated and flattened APD and ERP restitutions, leading to a loss in rate dependent adaptation of APD and ERP; (iii) the changes in cellular electrophysiology modulated the tissue level atrial conduction which facilitated high rate conduction, and increased tissues' temporal and spatial vulnerability. As a consequence, the tissues' susceptibility to AF genesis and maintenance was increased; (iv) the gain in I_{Ks} stabilized re-entry, allowing more wavelets to persist and co-exist in a given volume of tissue, leading to more irregular and high frequency atrial excitation.

2.4.1 Mechanisms of pro-fibrillation of the KCNQ1 S140G mutation

Shortening of atrial ERP has been demonstrated to be pro-fibrillatory, as seen in the effects of vagal stimulation (Liu, Guo et al. 2009), acetylcholine (Voigt, Maguy et al. 2008), or adenosine (Turley, Murray et al. 2008) on initiation of AF. In the case of the KCNQ1 S140G mutation, the increased I_{Ks} abbreviated atrial APD and ERP. In turn, the shortened ERP led to reduced excitation wave wavelengths facilitating high rate intra-atrial conduction, allowing more re-entrant wavelets to persist in a limited atrial mass. In the study of Chen *et al.*, AF persisted in individual patients with the mutation once it appeared. This is consistent with our simulation that re-entry sustained the mutant condition ($\varphi > 0.07$). The genesis of AF in those patients may be attributed to the increased susceptibility of atrial tissue to re-entry. Tissue susceptibility to re-entry can be indexed by its temporal and spatial vulnerability. While temporal vulnerability is mainly determined by the repolarisation phase of APs (Shaw and Rudy 1995), spatial vulnerability is mainly determined by the wavelength of the excitation wave, defined as the product of CV and APD. In our simulations, the KCNQ1 S140G mutation increased the spatial vulnerability of the tissue by markedly decreasing the critical size of the re-entrant substrate due to abbreviated APD and ERP. Consequently, the susceptibility of the atrial tissue to maintain re-entry was increased.

2.4.2 Limitations

The CRN model was used here to simulate cellular electrical AP of human atrial myocytes and its limitations have been discussed elsewhere (Courtemanche, Ramirez et al. 1998). In the multi-cellular tissue model, homogeneous cellular electrical properties and isotropic cell-to-cell electrical coupling are assumed. However, intrinsic electrical heterogeneity in cellular electrical properties (Hong, Piper et al. 2005) and anisotropic intercellular electrical coupling play important roles in the initiation and perpetuation of re-entry. Another limitation is that AF-induced electrical re-modelling was not considered (Bosch, Zeng et al. 1999; Workman, Kane et al. 2001; Zhang, Garratt et al. 2005; Kharche and Zhang 2008) as well as gap junctional re-modelling (Jongsma and Wilders 2000; van der Velden, Ausma et al. 2000), which influences the mechanisms of AF. However, these limitations are not anticipated to influence the fundamental conclusions about the mechanisms by which the KCNQ1 S140G mutation increases arrhythmic risk.

2.4.3 Mutant I_{Ks} and cardiac arrhythmia – relevance to previous studies

Abnormality in I_{Ks} arising from KCNQ1 mutations has been identified in various cardiac diseases that include the LQT (Lundby, Ravn et al. 2007; Zhang, Kharche et al. 2008) syndrome, the SQT (Bellocq, van Ginneken et al. 2004) syndrome and atrial fibrillation (Brugada, Hong et al. 2004; Hong, Piper et al. 2005; Ellinor, Petrov-Kondratov et al. 2006; Restier, Cheng et al. 2008; Abraham, Yang et al. 2009; Das, Makino et al. 2009) . Significantly, the gain-in-function of I_{Ks} associated with KCNQ1 variants can produce overlapped phenotypes of SQT and AF (Bellocq, van Ginneken et al. 2004; Restier, Cheng et al. 2008). Patients with these augmented I_{Ks} mutations exhibit shortened atrial and ventricular refractory periods, and an increased susceptibility of atrial and ventricular fibrillation. It was hypothesized that a gain-in-function of I_{Ks} results in a shortened APD and ERP, which facilitates multiple re-entrant circuits in atrial and ventricular fibrillation. In our previous study (Zhang, Garratt et al. 2009) we have shown that an augmented I_{Ks} arising from KCNQ1 V307L mutation (SQT-2) shortened ventricular APD and ERP, increased intra-ventricular heterogeneity, led to abbreviated QT interval, and increased ventricular susceptibility to arrhythmia. The present study is the first to elucidate the functional impacts of the KCNQ1 S140G mutation in promoting AF.

There is an increasing awareness of the molecular basis underlying the mechanisms of AF. Particular emphasis has been placed on AF-induced electrical re-modelling which produces a predominant pro-fibrillatory ERP reduction (Yang, Snyders et al. 1997; Hong, Piper et al. 2005; Olson, Michels et al. 2005; Xia, Jin et al. 2005; Olson, Alekseev et al. 2006; Otway, Vandenberg et al. 2007; Ravens and Cerbai 2008; Restier, Cheng et al. 2008). Our data indicate that in the

case of the KCNQ1 S140G mutation, the resulting ERP reduction not only stabilizes re-entry, but also increases the susceptibility of human atrial tissue to the *genesis* of re-entry. Our study therefore substantiates a causative link between the KCNQ1 S140G mutation and AF.

Chapter 3

Effects of elevated Homocysteine on the electrical activity of the human atrium: A simulation study

3.1 Introduction to the Homocystein hormone

Homocystein (Hcy) is a naturally occurring amino acid present in the human body. Typical diets contain trace amounts of the amino acid and the majority of Hcy found in the body is biosynthesized as part of the 'methionine cycle', the process by which cells metabolize the essential amino acid methionine. The total concentration of Hcy within a cell is strictly regulated and any excess produced is transported into the body's plasma. The role that Hcy plays in the normal functioning of the body is complex and is still not fully understood. However, it has been clinically observed that elevated levels of Hcy are associated with coronary, cerebral, and peripheral vascular disease; renal disease, dementia neural tube defects, and other disorders (Williams and Schalinske). It has also been associated with arteriosclerosis and coronary heart disease (CHD). The first evidence that elevated levels of Hcy could be a possible risk factor for CHD was linked when Mudd identified a patient with a deficiency of the enzyme cystathionine β-synthase (CBS) with elevated levels of Hcy, a condition referred to as homocystinuria (Mudd, Finkelstein et al. 1964). Subsequently McCully identified two further patients, one suffering from CBS and the other possessing a different enzymatic abnormality also leading to homocystinuria. As both patients were identified with arterial damage, and McCully concluded that the risk factor resulting in arterial damage were a direct result of elevated levels of Hcy (McCully 1969). It has only recently been proven conclusively that elevated levels of Hcy result in an increased risk of CHD (De Bree, Verschuren et al. 2002).

Although several underlying genetic conditions are associated with elevated levels of Hcy, it has also been observed that Hcy concentration rises with age. In men, this is thought to be due to increased muscle mass due to the ageing process resulting in augmented creatine/creatinine synthesis (Andersson, Brattstrom et al. 1992). In women, increased Hcy is thought to be primarily due to hormonal imbalances due to the onset of the menopause (Wouters, Moorrees et al. 1995). Lifestyle choices have also been identified as causes of increased Hcy concentrations, including coffee, smoking, and alcohol (Nygard, Vollset et al. 1995; Nygard, Refsum et al. 1997; Halsted 2001). It is now accepted that an elevated

level of Hcy is a risk factor for athlersocsis and consequently strokes. Recent experimental studies have found that elevated levels of Hcy above normal physiological concentration (5 – 20 μmol/L) is associated with alterations in the electrophysical properties of ion channels in human atrial myocytes. Ion channels affected were identified to include the down-regulation of the ultra-rapid potassium current (I_{Kur}) and transient outward potassium current (I_{to}), and up-regulation of the inward rectifier potassium current (I_{K1}) (Cai, Gong et al. 2007). Because these potassium currents play an important role in atrial repolarisation, alterations to them produce an imbalance between the depolarization and repolarisation currents, which may produce a disturbance to atrial excitation wave conduction. Previous computational studies have shown that a decrease in the depolarizing currents or an abnormal increase in the repolarising currents can lead to erratic wave propagation in the human atria resulting in atrial fibrillation (Zhang, Garratt et al. 2005; Kharche, Garratt et al. 2008). However, the pro-arrhythmic potential of the Hcy induced electrical changes to the potassium current have not yet been substantiated

In this study, the effects of an elevated level of the Hcy hormone on atrial electrical activities are investigated. Biophysically-detailed computer models of human atria at multi-scale levels that include cellular, 1D tissue, and 3D anatomical organ models of human atria are utilized.

3.2 Modelling elevated levels of the Homocystein hormone

The biophysically detailed CRN model was implemented in the study and series of multi-scale simulations were performed as described in Chapter 1 to quantify how elevated levels of the Hcy hormone result in the onset of AF. Experimental data from Cai *et* al. (Cai, Gong et al. 2007) were incorporated into the single cell model. Hcy was observed to result in electrical alterations of several potassium ion channels. It was found that Hcy augments the inward rectifying potassium channel conductance (g_{K1}), while reducing the ultra rapid potassium channel conductance (g_{Kur}) and the transient outward potassium channel conductance (g_{to}). However, it does not affect the kinetics of these channels. Based on the experimental data (Cai, Gong et al. 2007), the dose dependent alterations to the maximum channel conductance of g_{K1}, g_{Kur} and g_{to} in the Courtemanche *et al.* model (Courtemanche, Ramirez et al. 1998) are summarized in Table 3.1. The original and modified CRN models are used to simulate of atrial action potential APs under Control and the Hcy conditions respectively.

Table 3.1
Conductance Gains for Potassium Channels due to Hcy

Model	g_{to}	g_{Kur}	g_{K1}
50μmol/L	24.8% ↓	10% ↓	10% ↑
500μmol/L	38.4% ↓	29.6% ↓	39.2% ↑

3.3 Results of multi-scale simulations of the Homocystein hormone

The simulated APs and current traces of altered ionic currents under Control, Hcy (50 μmol/L), and Hcy (500 μmol/L) conditions at a PCL of 1000 ms are show in Figure 3.1A. Elevated levels of Hcy are observed to alter the morphology of the AP substantially. These changes included an elevated plateau potential during the early stage of repolarisation and a more hyperpolarized resting potential. In addition, both APD_{90} and APD_{50} were reduced from the Control condition of 314.2 ms and 210.6 ms respectively. APD_{90} was reduced under Hcy (50 μmol/L) conditions by 8.3% (287.9 ms) and by 9.2% (261.4 ms) in the Hcy (500 μmol/L) case. APD_{50} was measured to be reduced by 5.3% (199.4 ms) in the Hcy (50 μmol/L) case and by 16.8% (196.6 ms) under Hcy (50 μmol/L) conditions. The alterations in the AP morphology can be attributable to the integrative actions of the Hcy-induced electrical remodelling of the I_{to} (Figure 3.1B), I_{K1} (Figure 3.1C) and $I_{K,ur}$ (Figure 3.1D). As Hcy decreases I_{to}, which is responsible for the early stage of repolarisation, the AP's plateau potential is elevated. Although the maximal channel conductance of $I_{K,ur}$ is reduced, $I_{K,ur}$ is actually increased in the early phase of repolarisation due to this elevated plateau potential. However, it decreases in successive repolarisation phases. Augmented I_{K1} contributes mainly to a more hyperpolarized resting potential and an abbreviated APD.

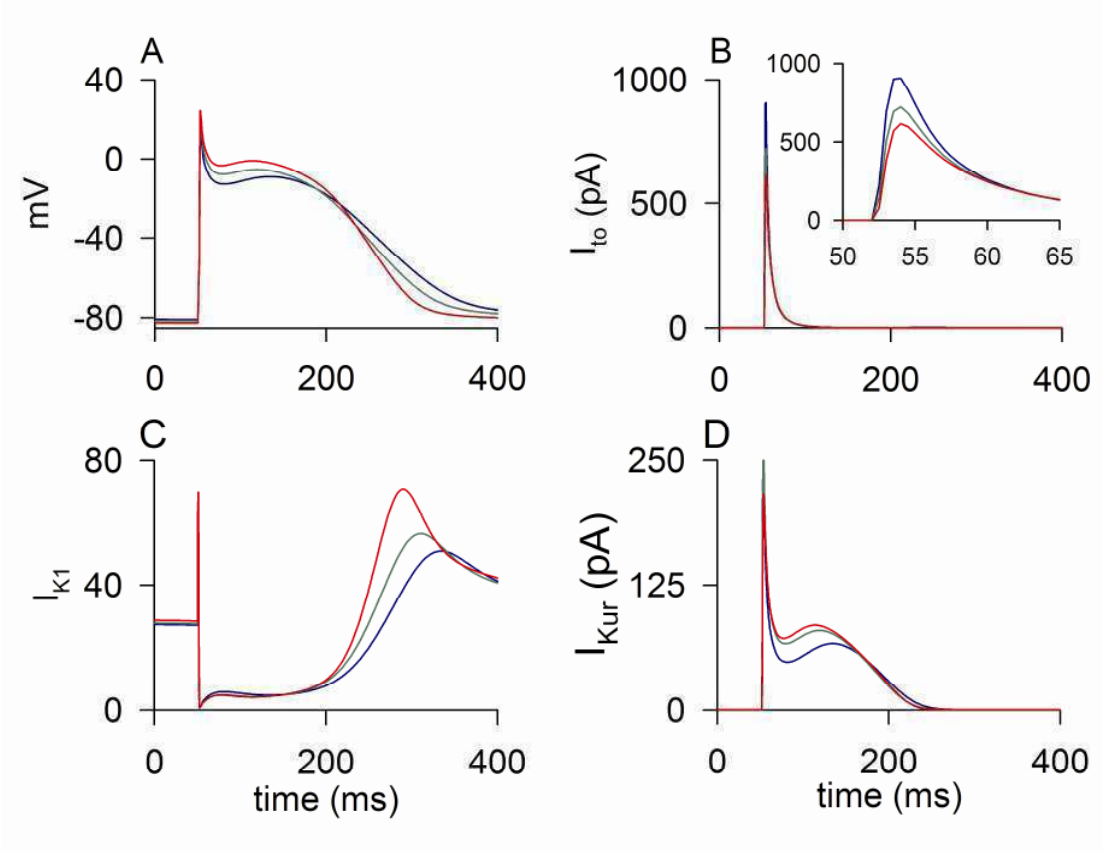

Figure 3.1. Time traces of simulates APs and some of the re-modeled ionic currents under Control (red lines), 50 µmol/L Hcy (green lines) and 500 µmol/L Hcy (blue lines) conditions. A. AP profile B. I_{to}. C. I_{K1} D. $I_{K,ur}$. Increased Hcy concentration results in APD_{50} and APD_{90} abbreviation, a hyperpolarized resting potential, and elevated plateau-potentials in the early repolarisation phase.

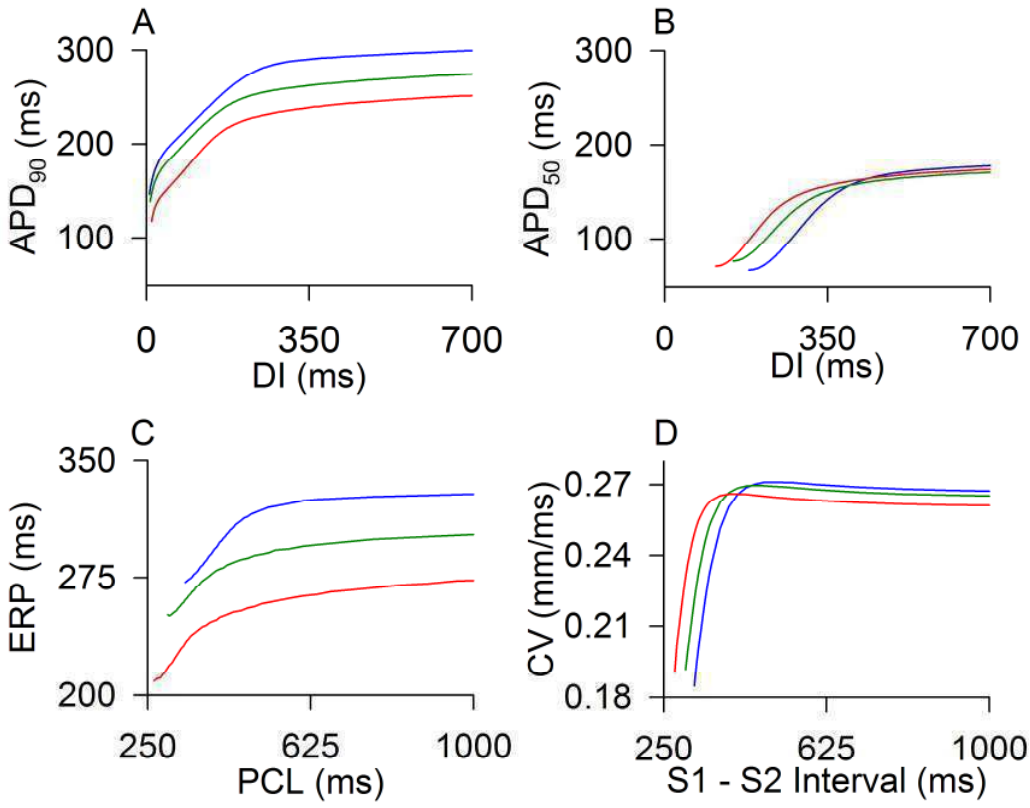

Figure 3.2. Computed APD_{90} (A), APD_{50} (B), ERP (C), and CV (D) restitution curves under Control (blue line), 50 µmol/L (green line) and 500 µmol/L (red line) conditions. APDr,50 shows that APD_{50} is shortened by Hcy at low excitation rates, but prolonged by Hcy at high excitation rates. APDr,90 shows that APD_{90} is consistently abbreviated due to elevated levels of the Hcy hormone. Shift of the ERPr curve left-ward indicates the loss of rate-dependent accommodation of ERP, which is pro-arrhythmic. Hcy reduces atrial tissue's excitability resulting in slowed intra-atrial conduction. Shift of the CVr curve left-ward indicates that Hcy facilitates atrial tissue to conduct high rate excitation waves.

The effects of the Hcy hormone on APD are rate dependent. APD_{90} (APDr,90) restitution and APD_{50} restitution (APDr,50) curves are shown in Figure 3.2A and 3.2B respectively. APDr,50 curves show at low excitation rates (large DIs), APD_{50} is shortened modestly due to elevated levels of Hcy. Conversely at high pacing (short DIs), APD_{50} is observed to increase. However, the APD_r,90 curves show that elevated levels of Hcy abbreviates APD_{90} consistently for both high and low excitation rates. For both the APDr,50 and APDr,90 curves, Hcy flattens them and shifts them left-ward, indicating the loss of rate dependent accommodation of APD, similar to the functional impacts of chronic AF-induced electrical remodelling on human atrial action potentials (Kharche and Zhang 2008). In addition, it was found that a simple estimation of maximal slopes did not necessarily predict the behavior of re-entrant waves in spatial models.

Effects of Hcy on the ERP are shown in Figure 3.2C. Under Control conditions the measured ERP was found to be 327.9 ms. Under Hcy conditions, the measured ERP decreases by 9.7% to 302.9 ms for 50 μmol/L Hcy and by 16.8% to 273.7 ms for 500 μmol/L Hcy at a PCL of 1000 ms. Hcy is observed to result in a left-ward shift and flatten the ERP restitution curves, indicating the loss of the rate dependent accommodation of ERP, similar to the observation of human atrial cells due to AF-induced electrical remodelling.

The CV restitution curves shown in figure 3.2D show that under Control conditions and at a PCL of 1000 ms the CV is measured to be 0.27 mm/ms. Elevated levels of Hcy cause a slowing of the wave propagation to 0.26 mm/ms and 0.25 mm/ms for 50 μmol/L and 500 μmol/L of Hcy respectively. The reduction of CV may be explained by the role of elevated I_{K1} currents resulting in a hyperpolarisation of the resting potential of the atrial cell. This decreases the excitability of the tissue which manifests as a reduction in the intra-atrial excitation wave conduction. The effect of Hcy hormone on intra-atrial conduction velocity is also rate-dependent. At low excitation rates (*i.e*. large PCLs), Hcy decreases CV due to reduced atrial tissue excitability as a consequence of a more hyperpolarized resting potential. As Hcy hyperpolarizes the resting potential to a more negative voltage range, it requires more stimulus current to depolarize the cell membrane potential from its resting state to the excitation threshold potential of the cell (normally determined by the activation potential of the sodium channel, ~ -65 mV), and so the tissue's excitability will decrease. However, at high excitation rate (i.e., small PCLs), Hcy increases CV due to the reduced

APD and ERP, which allows tissue to recover sooner from previous excitation. The TVW was calculated to study how Hcy alters the tissue's ability to produce uni-directional conduction block by applying a premature stimulus to the refractory tail of a previous excitation wave. Hcy moderately reduces the measured VW, which decreases from 14.6 ms under Control condition to 14.2 ms under Hcy 50μmol/L and 12.9 ms under Hcy 500μmol/L. Hcy increases the stability of reentrant excitation wave as shown in Figure 3.3, in which snapshots of the 3D simulations are shown for Control and Hcy (500 μmol/L) conditions. Under the Control condition, the scroll wave is unstable with its organization centre (*i.e.* filament) meandering in a large area of tissue. The scroll wave is non-sustainable as it self-terminates at approximately 4.2 s. This self-termination is due to a combination of factors such as longer wavelength (*i.e.* larger ERP and higher CV) and the fact that they are non-stationary, meaning they do not allow the atria to accommodate the re-entrant excitation wave. However, under the Hcy condition (500 μmol/L), the simulated scroll wave sustains through the whole period of simulation (6 s). The increased persistence of reentrant excitation wave under Hcy condition is attributable to the shortened wavelength of excitation waves, as a result of abbreviated ERP and reduced CV.

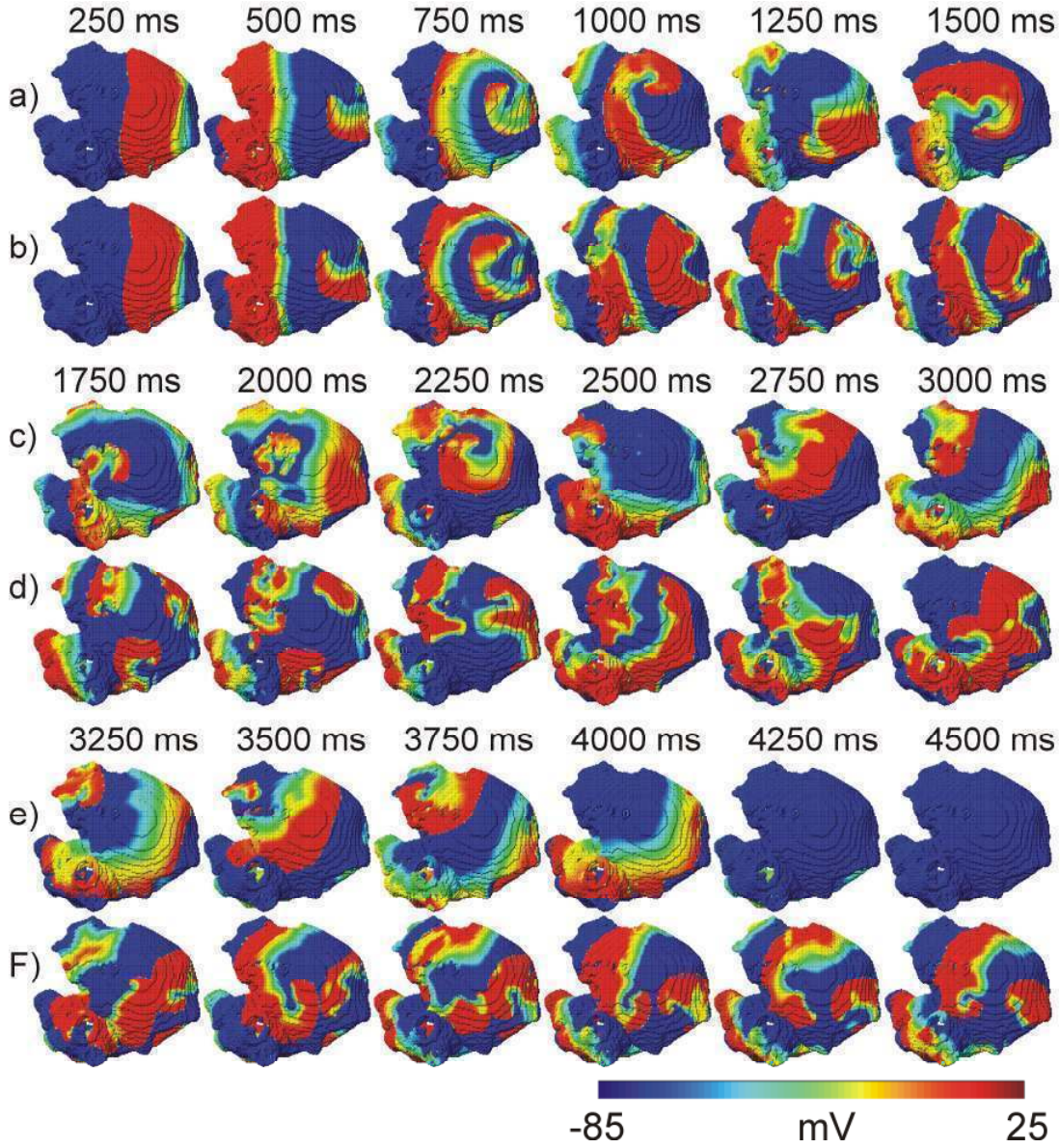

Figure. 3.3. Snapshots of re-entrant waves in a 3D anatomical model of human atria under Control (rows a, c, and e) and Hcy 500µmol/L (rows b, d, and f) (ii). Under Control conditions, scroll wave self-terminates at 4.1 s and in the presence of Hey the scroll wave persists for the full period of the simulation (6 s).

Table 3.2 Summary of quantitative results for Control, 50 μmol/L, and 500 μmol/L conditions

Model	Quantity	Control	50 μmol/L	500 μmol/L
Cell	Resting potential (mV)	-80.80	-80.4	-82.5
	APD_{50} (ms)	210.6	199.4	196.6
	APD_{90} (ms)	314.2	287.9	261.4
	dV/dt_{max} (mV/ms)	217.10	218.2	202.6
	APDr maximal slope	1.3	1.38	1.45
	ERP (ms) (stimulus interval ~ 1 s)	327.9	302.9	273.7
1D	CV (mm/ms)	0.27	0.26	0.25
	VW (ms)	14.6	14.2	12.9
	Wavelength (mm)	81.7	74.9	65.4
3D	LS (s)	4.2	N/A	>6

3.4 Conclusions and discussion of the effects of the Homocystein hormone

The study into the underlying mechanisms which result in the onset and maintenance of AF has been attributed to numerous risk factors which include ageing, heart disease-induced electrical and structural remodelling, and gene mutations. While these have been extensively studied clinically and experimentally, little knowledge has been obtained about the role of abnormal secretion of hormones. In this chapter, the functional role of elevated Hcy on atrial excitation was investigated using biophysically detailed computer models and multi-scale simulations were performed to evaluate the effects of Hcy-induced changes in potassium currents on the electrical activity of human atrium at single cell, 1D strand of tissue, and 3D anatomical models.

3.4.1 Main findings

Simulations show that the Hcy-induced electrical remodelling of I_{to}, I_{Kur} and I_{K1} currents have marked effects on the electrical activities of human atrial cells thereby affecting excitation wave propagation. The pro-arrythmogenic effects of an elevated Hcy are obvious with the reduction in action potential duration, effective refractory period and intra-atrial conduction velocity, and the loss of their rate dependency. The integrative action of these cellular and tissue properties reduces the wavelength of atrial excitation waves allowing atria to sustain high rate re-entrant excitation waves. This pro-arrhythmic mechanism is similar to that of AF-induced electrical remodelling on some ion channels (Workman, Kane et al. 2001; Zhang, Garratt et al. 2005; Kharche, Seemann et al. 2007) and gain-in-function of I_{K1} arising from KCNJ2 gene mutation. This study substantiates the link between an elevated Hcy concentration and incidence of AF in some patients.

3.4.2 Limitations of the study

While simulations performed on the 3D anatomical structure indicated that elevated levels of the Hcy hormone resulted in re-entry, 2D simulations failed to initiate a stable spiral wave despite several single cell simulations measurements indicating increased risk of AF genesis. This suggests that the 3D structure of atria is an important factor in the genesis of AF. The 3D simulations assume that the atria consist of a single cell type. In reality the atria is constructed of multiple cell types with differing electrophysiological properties which may hinder or exacerbate the genesis of AF (Seemann, Hoper et al. 2006).

More recent experimental studies have identified that elevated levels of Hcy alter the electrophysiological properties of the sodium channel I_{Na}, which is primarily responsible for the depolarization of the cardiac myocytes (Cai, Shan et al. 2009). Alterations to the ionic current conductance and kinetics of this channel are likely to have a significant impact on CV. This may in turn alter the wavelength of which the tissue can sustain re-entrant waves. The combined effects of this re-modelling in conjunction with the alterations to the potassium currents require further simulation.

Chapter 4

A computational evaluation of the arrhythmogenic effects of Serotonin in the human atria

4.1 Introduction to serotonin

Previous chapters of this thesis have shown studies into how genetic defects and hormonal imbalances can result in an alteration of ion channel properties causing a change to the overall electrophysical behaviour of the cell, thereby increasing the susceptibility of the tissue to the genesis and maintenance of AF. However, understanding the mechanisms by which different hormones alter the electrophysiology of atrial myocytes may provide valuable insight into possible drug development strategies which may aid clinical treatment of AF.

Elevated levels of 5-hydroxytryptamine (5HT), more commonly known as Serotonin, has long been observed to produce strange electrical properties in the atrium (Hollander, Michelson *et al.* 1957; Lemessurier, Schwartz *et al.* 1959). However, as 5HT receptors have been identified in multiple systems which regulate the heart rate it has not yet been conclusively identified how elevated levels of 5HT effect the arrhythmogenic properties of atrial cells. The 5HT receptor 5-HT_4 was identified in the right atrium (Yusuf, Al-Saady *et al.* 2003) which provides the mechanism by which 5HT could bind to the ion channel protein responsible for the I_{CaL} current and alter the electrophysiology of the cell directly. Interestingly, this receptor is found in the atrium, but is absent in the ventricles (Yusuf, Al-Saady et al. 2003). This selectivity of the 5HT hormone to act on the atria could provide a novel mechanism by which medication could be used to specifically target the atria.

This chapter studies how changes in the L-type calcium current (I_{CaL}) resulting from non-physiological levels of the hormone 5HT affects the tissues' susceptibility to AF. The effects of 5HT on I_{CaL} current densities have been quantified experimentally (Pau, Workman et al. 2007). These results are incorporated into a detailed electrophysiological model of the human atrium. Theses simulated cells are investigated at single cell, 1D strand, 2D sheet and full 3D anatomical geometry, and the results are used to quantify the arrhythmogenic effects of 5HT.

4.2 Methods

This section outlines the development of four cell types: sinus-rhythm (SR), elevated levels of 5HT in a cell under normal SR (5HT), cells with reduced I_{CaL} current density due to AFER (AF), and AF cells with elevated levels 5HT (AF+5HT). The multi-scale simulations as describe in Chapter One are implemented to quantify the arrhythmogenic effects of alterations to the current density of $I_{CaL.}$

4.2.1 Simulating the effects of 5HT

A CRN biophysically detailed 21-variable cell model for simulating the human atrial AP was implemented in this study (Courtemanche, Ramirez *et al.* 1998). The I_{CaL} current responsible for the flow of Ca^{2+} ions across the cell membrane was observed experimentally to be increased by elevated levels of the 5HT hormone and AFER (Workman, Kane et al. 2001; Pau, Workman et al. 2007). The mathematical interpretation of the I_{CaL} ion-channel is described by the following Hodgkin-Huxley formulation in the CRN model:

$$I_{Ca,L} = g_{Ca,L} d \times f \times f_{Ca} (V - E_{CaL}) \tag{4.1}$$

where g_{CaL} is the current conductance (0.1238 nS/pF), E_{CaL} is the reversal potential of I_{CaL} (-65 mV), d is the activation gate, f is the inactivation gate, and f_{Ca} in the $[Ca^{2+}]_i$ dependent inactivation gate.

Alterations due to elevated 5HT and AFER are modelled as an alteration in the conductance g_{CaL} and are based on Workman *et al.* (Pau, Workman et al. 2007) where experiments were performed on isolated atrial cells. The study concluded that the alterations to g_{CaL} under 5HT conditions result in a 288.7% increase, AF in a 43.8 % reduction, and AF+5HT in a 20.2% increase. These alterations are also outlined in Table 4.1.

Table 4.1 Conductance Alterations to I_{CaL} Channels due to 5HT and 4F

Model	g_{CaL}
5HT	288.7% ↑
AF	43.8% ↓
AF+5HY	20.2% ↑

4.3 Results

The aforementioned methods were implemented to quantify the arrhythmogenic effects of 5HT, AF, and AF+5HT on the cellular, 1D, 2D, and anatomical 3D level. A summary of the measured quantities are listed in Table 4.2.

4.3.1 Effects of 5HT, AF, AF+5HT on single atrial myocyte

Simulated AP profiles and I_{CaL} current a trace at PCLs of 1000 ms, 430 ms and 330 ms under SR, 5HT, AF, and AF+5HT conditions are shown in Figure 4.1. At a PCL of 1000 ms the APD_{90} of the SR case is measured to be 314.2 ms. When 5HT is present I_{CaL} current is augmented substantially and the APD_{90} is increased by 19.7% to 376.7 ms. Under AF conditions I_{CaL} current is reduced causing a shortening of APD_{90} by 16.0% to 263.9 ms. In the AF+5HT case I_{CaL} is augmented from SR conditions, resulting in an increased APD_{90} of 7.8% to 338.8 ms. At a PCL of 430 ms the SR case has and APD_{90} of 274.9 ms. Under 5HT conditions the APD_{90} is increased by 10% to 302.6 ms, where in the AF case APD_{90} is reduced by 17.3% to 227.1 ms. In the AF+5HT case the APD_{90} is reduced by 6.2% to 257.9 ms. At a PCL of 340 ms the SR case has an APD_{90} of 237.7 ms. Under 5HT conditions the APD_{90} is increased by 16.6% to 277.2 ms, where in the AF case the APD_{90} is reduced by 10.2% to 213.3 ms. In the AF+5HT case the APD_{90} is reduced by 18.4% to 193.9 ms. Interestingly at lower PCLs 5HT had the effect of increasing APD_{90} from SR conditions and decreasing APD_{90} from SR conditions at high PCLs. This indicates that the cardio-protective effects of the 5HT hormone are limited to low pacing rates and at high pacing 5HT results in an increased risk of AF. Upstroke velocity in the SR case was measured at 217.1 mV/ms. The 5HT case resulted in a reduction of 2.5% to 211.8 mV/ms. Under AF conditions the upstroke velocity is increased moderately by 0.5% to 218.3 mV/ms. In the AF+5HT case the maximal upstroke velocity was reduced from the AF case but was still 0.05% lower than the SR case, with an upstroke velocity of 216.1 mV/ms. As I_{CaL} current is nominal in the upstroke part of the AP the alterations in maximal slope are likely a result of the alteration to the RP.

4.3.2 The effects of HT5 on APR, ERP, and CV restitution curves

The APDr,90 curves in Figure 4.2A shows that in the 5HT and AF cases there was a marked increase and decrease respectfully in APD_{90} in comparison to SR over the full range of DIs. The AF+5HT restitution curve showed some interesting characteristics: at long DI the APD_{90} remained approximately 25 ms longer than the SR case. However, as DI is reduced to less than 235 ms the difference in APD_{90} between the SR and AF+5HT case begins to reduce until at very short DI (~20 ms) they are equal to the SR case. This indicated that any possible anti-arrhythmogenic effects of 5HT are reduced in a high pacing regime. The APDr,50 curves were also constructed and are shown in Figure 4.2B and shows similar structural characteristics to the APDr,90 curves.

Table 4.2 Summary of quantitative results for SR, 5-HT, AF and AF+5HT conditions

Model	Quantity	SR	5HT	AF	AF+5HT
Cell	Resting potential (mV)	-80.8	-79.2	-81.3	-80.5
	APD_{90} (ms)	314.2	376.7	263.9	338.8
	Overshoot (mV)	24.7	25.4	24.6	24.8
	dV/dt_{max} (mV/ms)	217.1	211.8	218.3	216.1
	APDr maximal slope	1.3	1.75	0.93	1.51
	ERP (ms) (stimulus interval ~ 1 s)	327.9	396.2	275.3	354.5
	Cut off BCL (ms)	328.7	360.4	298.7	339.0
	CV (mm/ms)	0.26	0.27	0.25	0.26
	Cut off S2 (ms)	320	380	315	345
	VW (ms)	14.6	9.3	17.9	10.1
	Wavelength (mm)	81.7	101.7	66.0	87.8
2D	LS (s)	1.4	1.1	1.8	0.9
	DF (Hz)	3.6	1.5	5.2	0.6
	MS (mm)	49.2	72.0	17.4	58.0
3D	LS (s)	4.2	< 1	> 6	4.5
	DF (Hz)	3.1	N/A	4.2	2.7

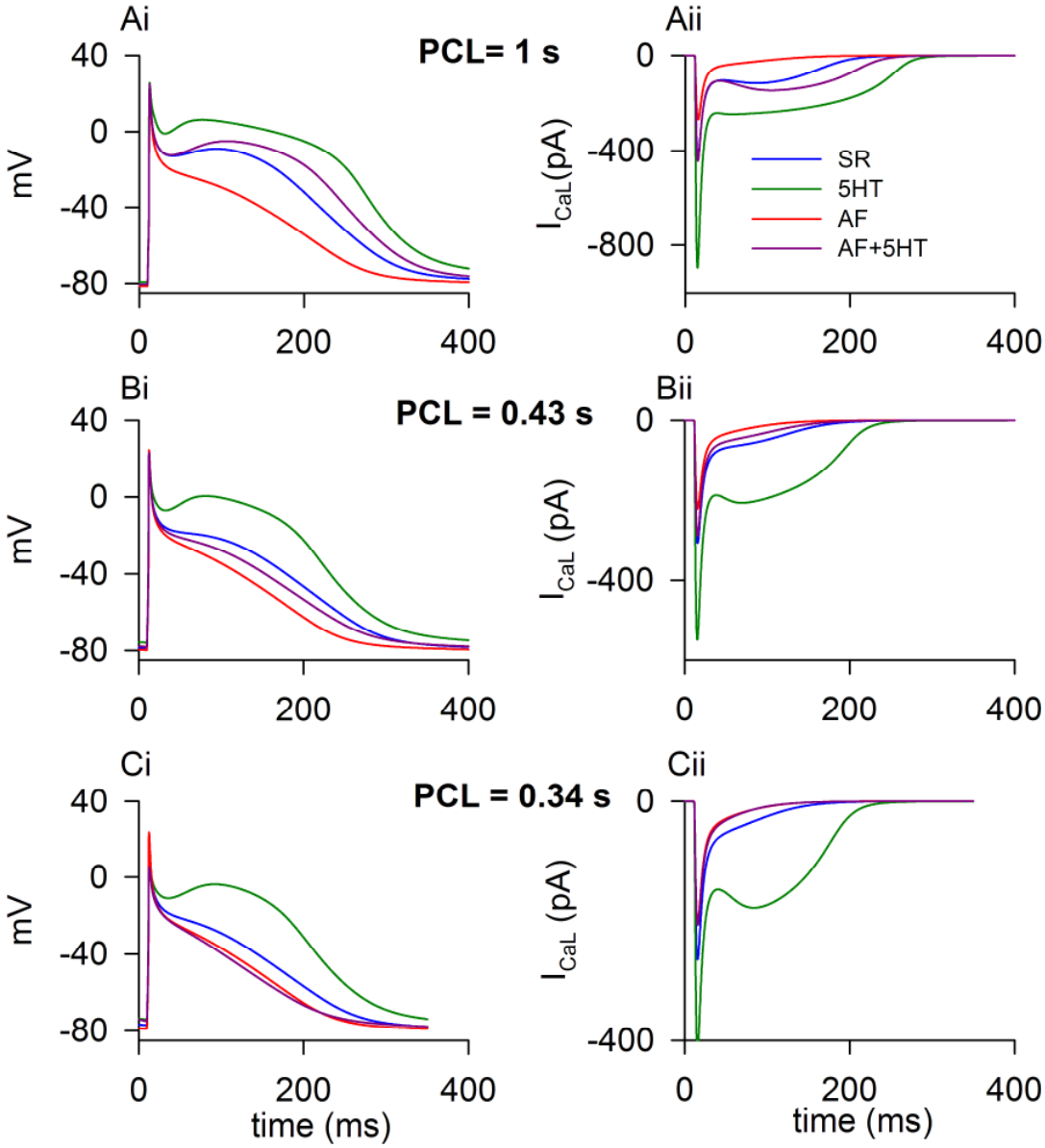

Figure 4.1 Simulated AP profiles (left column) and I_{CaL} current traces (right column) using the CRN model models under SR (blue lines), 5HT (green lines), AF (red lines), and AF+5HT (purple lines) conditions at PCLs of. A: 1000 ms. B: 430 ms. C: 340 ms.

The ERPr curves given in Figure 4.2C show that at a PCL of 1000 ms under SR conditions the ERP is measured to be 327.9 ms. Under 5HT conditions the ERP is increased substantially by 20.8% to 396.2 ms and in contrast AF reduces ERP by 16% to 275.3 ms. Under AF+5HT conditions the ERP is measured to increase moderately by 8.1% to 354.5 ms. These results indicate that at low pacing rates AF reduces ERP resulting in an increased susceptibility to arrhythmogenesis whereas in the AF+5HT case ERP is restored to values modestly higher than the SR case indicating possible arrhythmogenic effects of 5HT. It is also observed that in a high pacing regime under 5HT and AF conditions the ERPr curves are flattened, indicating a loss of rate dependant adaptation. In the AF+5HT case the ERP, which is consistently higher than SR at low pacing rates, has a dramatic increase in slope at high pacing rates, reducing ERP to values lower than SR. The cut-off PCL under SR conditions was recorded to be 328.7 ms, and under 5HT conditions this increased by 9.63% to 360.4 ms. For AF conditions the cut-off PCL is reduced by 8.79% to 298.7 ms and for AF+5HT conditions the cut-off PCL is 339.0 ms, which is 3.16% higher than the SR case. This further indicates the restorative effects of the 5HT hormone, while AF results in a negative shift, demonstrating an increased ability of atrial cells to sustain high-rate electrical excitation rates.

The CVr curves are shown in Figure 3D. At a PCL of 1000 ms the measured CV under SR conditions was 0.26 mm/ms. In the 5HT case the CV is increased modestly to 0.27 mm/ms, and the AF case results in a modest reduction to 0.25 mm/ms. Measured CV under AF+5HT conditions was restored to 0.26 mm/ms. These results again indicate the restorative effects of 5HT in a low pacing regime. The cut-off PCL for the SR case was measured to be 320 ms. Under 5HT conditions there is a shift in the positive direction, with a cut-off PCL of 380 ms. In contrast, AF results in a negative shift of the restitution curve with a measured cut-off PCL of 315 ms. The AF+5HT case causes a positive shift from SR conditions, with a measured cut-off PCL of 345 ms. A positive shift in the CVr curve indicates a loss of propagation in a high pacing regime whereas, for example, the AF case there was a negative shift which indicates successful wave propagation is possible in a high pacing regime. It is observed that in the AF+5HT case the restitution curve is shifted back to a position which is more similar to that of SR conditions, indicating that the hormone 5HT counteracts the arrhythmogenic effects of AF.

The wavelength at which the tissue can sustain re-entry is calculated as the product of the CV and APD_{90}. Under SR conditions the wavelength is calculated to be 81.7 mm, and for 5HT conditions the wavelength is increased to 101.7 mm. In the AF case there is a

significant reduction to 66.0 mm. This is restored to 87.8 mm in the AF+5HT case showing the possible anti-arrhythmogenic effects of 5HT.

4.3.3 Effects of 5HT on the temporal and spatial vulnerability window

The TVW was calculated using the 1D strand of tissue and is shown in Figure 4.2F. Under SR conditions the TVW was measured to be 14.6 ms, whereas under 5HT conditions the VW was reduced by 36.3% to 9.3 ms. In the AF case the TVW is increased by 22% to 17.9 ms and in the AF+5HT case the TVW is reduced by 30.8% to 10.1 ms. The 5HT hormone has the effect of dramatically reducing the TVW resulting in a cardio-protective effect.

The SVW was calculated by applying a stimulus to an idealised 2D homogenous sheet is shown in Figure 4.2F. In the SR case the SVW required to initiate re-entry was measured to be 49.2 mm. Under 5HT conditions the SVW required is increased by 42% to 72.0 mm. Under AF conditions the SVW is reduced dramatically by 64.6% to 17.4 mm. In the AF+5HT case the SVW is measured at 58.0 mm, which is 17.8% longer than under SR conditions. These results again indicate that the effects of 5HT are cardio-protective in cells which have undergone AF.

4.3.4 Simulation re-entry in a homogenous 2D sheet of atrial tissue.

2D simulations of re-entry in a homogenous sheet of atrial tissue are shown in Figure 4.3 and an accompanying core trace of the spiral tip, a representative time-voltage plot of a single atrial cell, and power spectrum density plot are shown in Figure 4.4. In SR conditions the LS of the resultant spiral wave is 1.4 s with a DF of 3.6 Hz. In the 5HT case the LS is reduced substantially due to the increased APD and ERPr. AF conditions result in a moderately prolonged LS of 1.8 s and a increase in DF to 5.2 Hz. The AF+5HT case causes a shortening of LS to 0.9 and a dramatic reduction of DF to 0.6 Hz.

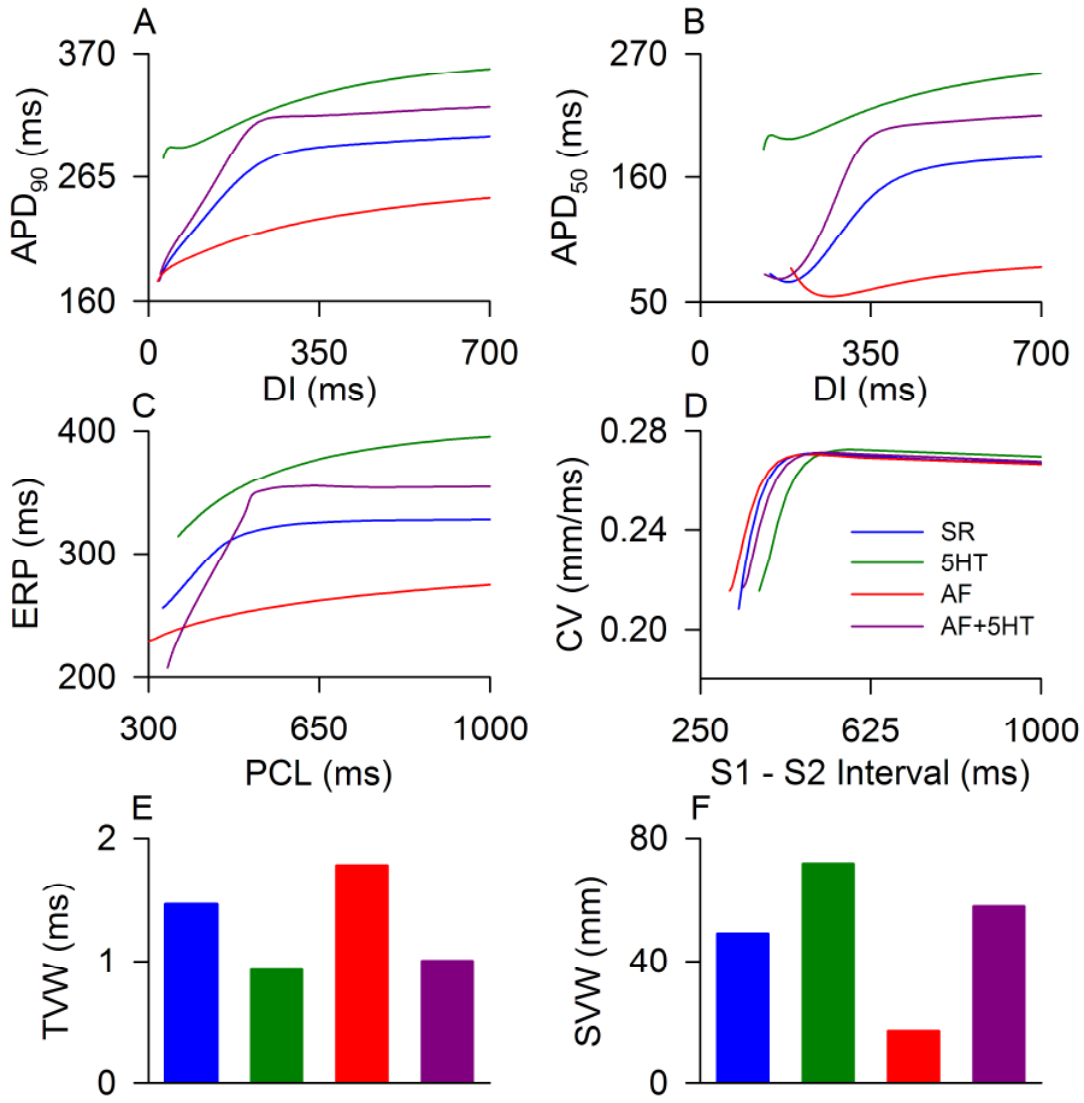

Figure 4.2 Simulated APDr,90, APDr,50 , ERPr, CVr, Temporal VW, and Spatial VW calculated using the CRN model under SR (blue), 5HT (green), AF (red), and AF+5HT (purple) conditions. A: APDr,90 curves. Bi: APDr,50 curves. Ci: ERPr curves. D: CVr curves. E: Temporal VW. F: Minimal substrate.

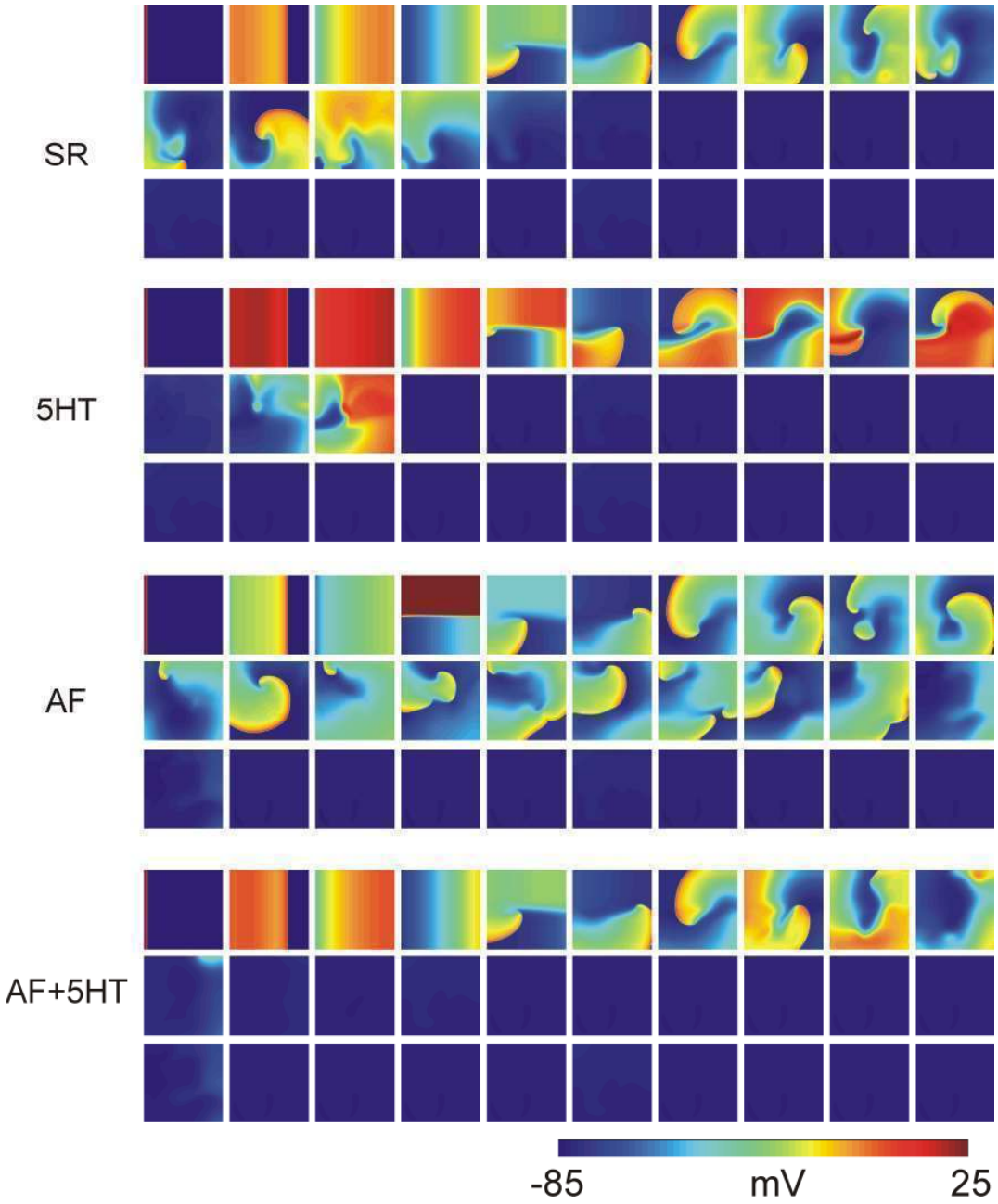

Figure 4.3 Simulation of 2D re-entry in an idealized sheet of virtual atrial tissue under SR, 5HT, AF, and AF+5HT conditions. Panels show 3 s of simulation starting from 0 ms in the top left panel progressing in 100 ms intervals horizontally from left to right until the bottom right panel.

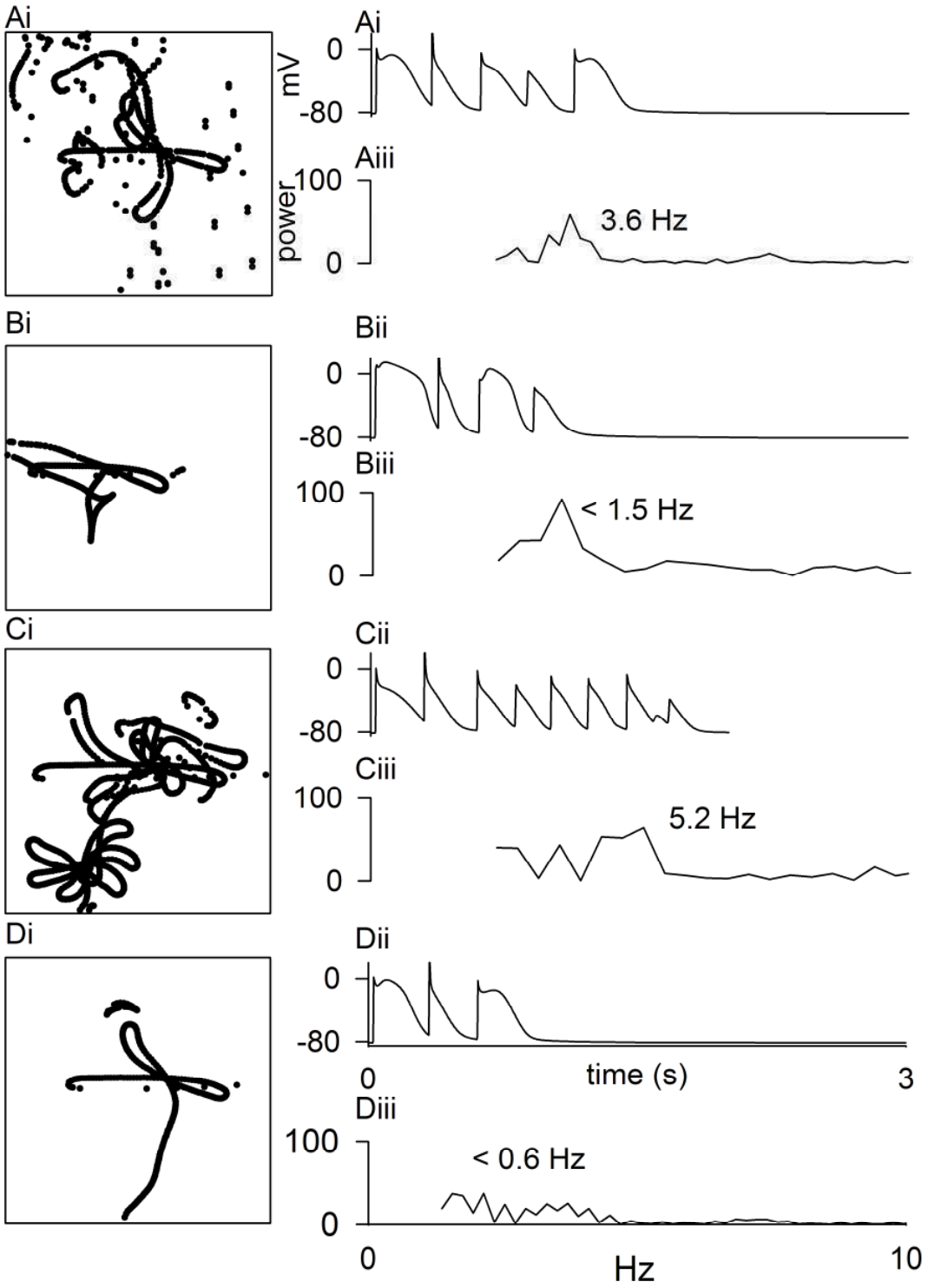

Figure 4.4 2D spiral wave tip traces (panel i), representative AP traces taken from 2D simulations (panel ii), and power spectrum density showing frequencies of maximal power (panel iii) under SR (A), 5HT (B), AF (C), AF+5HT (D) conditions.

4.3.5 3D Simulation of a detailed anatomical correct construct of the atria

The simulation of spiral wave behaviour in a realistic 3D geometry is show in Figure 4.5 and a representative time-series plot of a selected node in the atrial wall along with a power spectrum density plot to indicate the dominant frequency is shown in Figure 4.6. Under SR conditions the re-entrant wave behaviour dies after 4.2 s and has a DF of 3.1 Hz. In the 5HT case, due to the long APD_{90} and an increase in ERP, the 3D construction is unable to maintain a persistent spiral wave. In the AF case a persistent stable spiral rotor is born for the duration of the simulation. The DF of the waves is measured to be 4.2 Hz. Under AF+5HT conditions the re-entry persists for only 0.3 ms longer than in SR conditions and the DF is reduced to below SR conditions to 2.7 Hz. The fact that oscillations persisted in the 3D case and not in the 2D simulation is an indication that anatomical structure is important in the onset of AF.

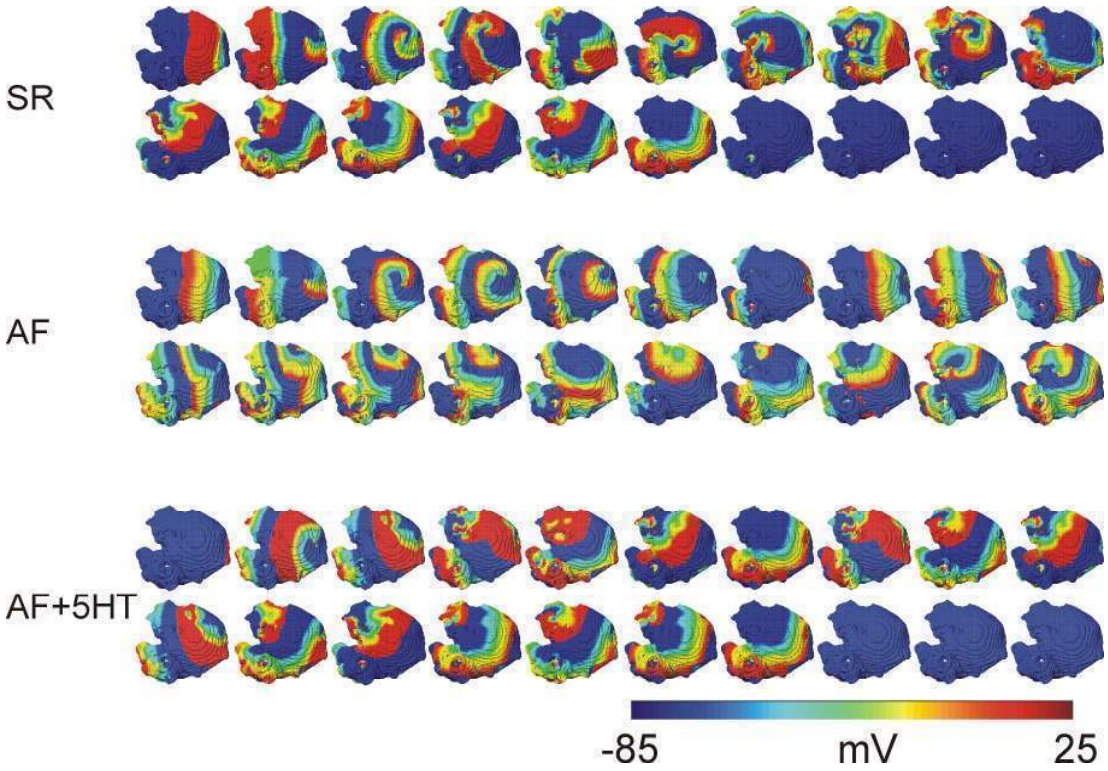

Figure 4.5 Simulation of re-entry in a 3D geometry of the human atria under SR, AF, and AF+5HT conditions. Panels show 4s of simulation starting from 0 ms in the top left panel progressing at 200 ms from left to right in 200 ms intervals until bottom right panel

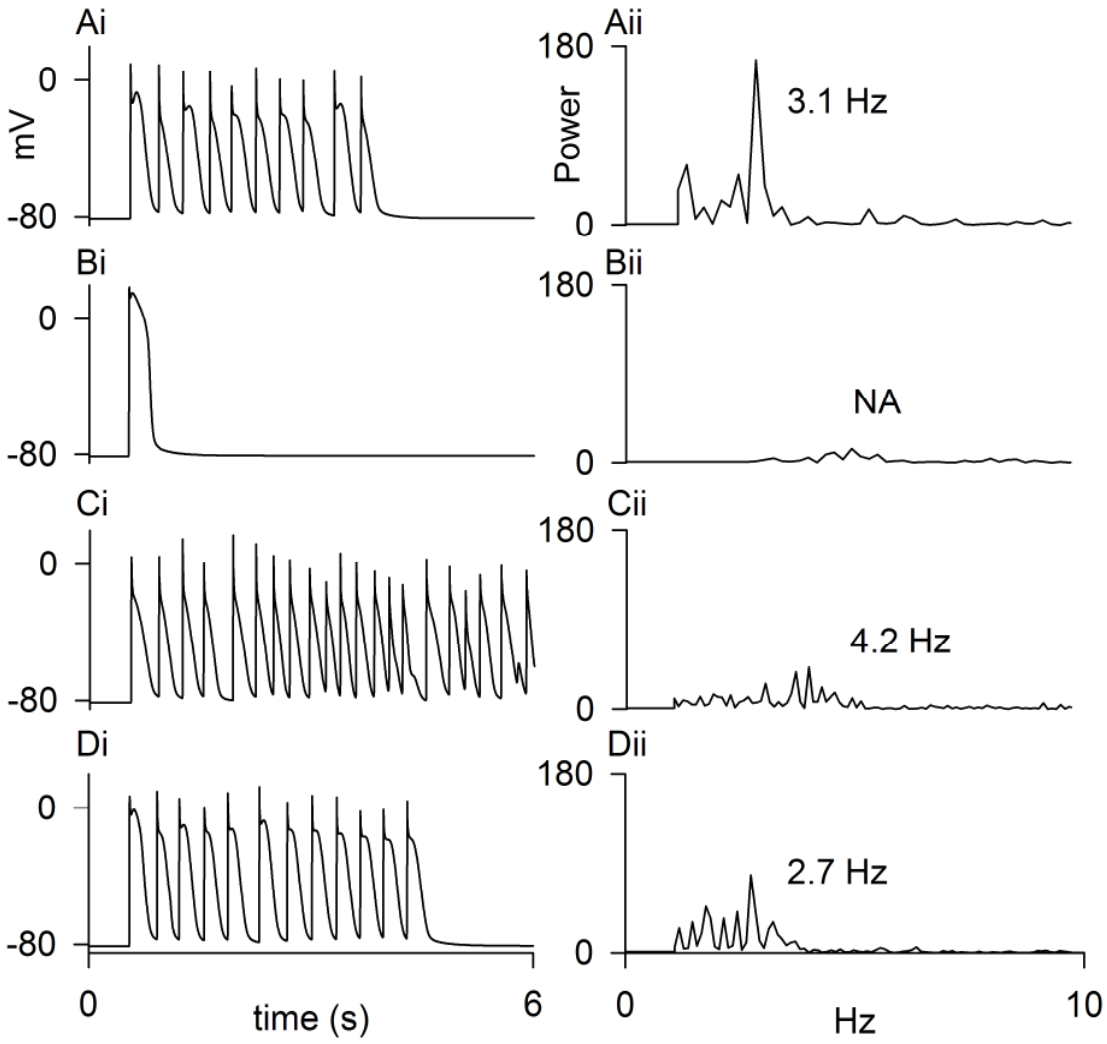

Figure 4.6 AP traces taken from 3D simulations (panel i), and power spectrum density showing frequencies of maximal power (panel ii) under SR (A), 5HT (B), AF (C), AF+5HT (D) conditions.

4.4. Conclusions and discussion

This section outlines the main findings of this chapter. There is also a discussion into the limitations of the study, in particular the modelling methods for simulating AFER and the simulation of the I_{CaL} current in the CRN model. The results are also compared to that of previous simulation studies and the possible implications in the clinical setting are discussed.

4.4.1 Main findings

It has been known for some time that elevated levels of 5HT is linked to an increase in susceptibility to AF, primarily by increasing the atrial myocytes' susceptibility to exhibiting EADs and DADs (Kaumann and Levy 2006). Clinical evidence indicates that 5HT directly alters the conductance of I_{CaL} (Pau, Workman *et al.* 2003). However, the possible anti-fibrillatory effect of 5HT when applied to tissue which has undergone AFER has not been studied. The main focus of this chapter was therefore to investigate the arrhythmogenic effects of 5HT. We employed computational techniques to simulate the effects of this hormone by incorporating experimental data into a biophysically detailed model and studying the effects of the hormone on multi-scalar tissue levels. AFER was simulated in this study as a reduction in the $I_{CaL,}$ which when incorporated into single cell model simulations resulted in a substantially reduced APD and ERP. Simulations in an idealised 2D sheet indicated that the reduction to I_{CaL} was insufficient to allow the tissue to maintain re-entry. However, in the 3D construct of the atria the reduction in ERP was sufficient to allow the initiation and maintenance of stable spiral waves. The increase in I_{CaL} due to elevations in 5HT is observed to limit the effects of AFER via the restoration of I_{CaL} current density to values more comparable to those observed under SR conditions. In fact, APD and ERP are seen to be slightly augmented in comparison to SR conditions and as a result the 3D atrial tissue simulations are no longer able to sustain re-entrant behaviour. Our principal findings were therefore that the 5HT hormone augmented the I_{CaL} current sufficiently in tissue which had undergone AFER to provide a cardio protective effect. Therefore it can be concluded that targeting the 5-HT_4 receptors in tissue which has undergone AFER may provide a possible target for the development of drug treatments.

4.4.2 Limitations of the study

The potential limitations of the model used in this study have been discussed previously (Courtemanche, Ramirez et al. 1998; Cherry and Evans 2008). A limitation of our 3D simulations is the absence of heterogeneity in the structure of the atria, both electrically as the structure only consists of atrial cell types while it is known that cells in different regions of the atria have different electro-physical properties (Seemann, Hoper *et al.* 2006). The model also neglects spatial heterogeneity due to fibers within the atria.

Our simulations show that elevated levels of 5HT were found to have a cardio protective effect when applied in conjunction with cells that have undergone AFER as a result of prolonged periods of rapid pacing due to AF. However, elevated 5HT levels under normal SR produced an AP which has an abnormally large dome in phase III of the repolarisation , substantially prolonged APD_{90}, which is not consistent with experimental data. In the CRN model this resulted in a substantially extended simulated ERP which severely limited the tissues' susceptibility to sustain re-entrant waves, resulting in rapid break up of any re-entrant behaviour in our simulations. In clinical reality it is observed that elevated levels of 5HT under normal SR results in spontaneous DADs and EADs. However, no such phenomena were observed. The absence of this phenomenon is thought to be due to the underlying biology on which the CRN model is based. In fact currently no atrial cell model had been observed to produce them. However, it is possible to artificially test the tissues' susceptibility to eliciting a spontaneous depolarization by artificially incorporating a sudden release of Ca^{2+} from the SR (Priebe and Beuckelmann 1998).

In addition to the simulations failing to successfully reproduce DADs and EADs, the methods used to simulate the effects of AFER were simplistically modeled as a reduction in I_{CaL} current density. This neglects the several other ion-channels know to be remodeled during AFER. In addition alteration in the time kinetics in I_{CaL}, which are know be altered by elevated levels of 5HT, are neglected. It is observed that modelling the effects of AFER using this method was sufficient to induce re-entry in a 3D geometry. However, experimental evidence has shown that multiple ion-channels are observed to be remodeled as a result of prolonged rapid pacing. Figure 4.7Ai and 4.7Aii show simulated APs which incorporate more detailed physiological changes to ion channels as described by Workman *et al*. (Workman, Kane *et al.* 2001). In addition to this we also tested the tissues' ability to initiate a spontaneous depolariastion as described by Priebe *et. al*. (Priebe and Beuckelmann 1998), which can be seen in Figure 4.7Bi and 4.7Bii. In this method an

injection of Ca^{+} ions are placed into the cell 1 s after the previous excitation. This may initiate a release of Ca^{+} from the SR causing an AP to be elicited. It is observed that under normal SR conditions the tissue is unable to elicit a sudden depolarisation. However, under SR+5HT conditions, a sudden depolarisation is possible. This result confers well with experimental observations where healthy extracted atrial cells exhibit EADs and DADs when subjected to increased concentrations of 5HT (Pau, Workman et al. 2007). In addition, experimental evidence shows that atrial cells from patients who are suffering from persistent AF show no spontaneous depolarisations even if there are elevated levels of 5HT.

4.4.3 Clinical significance and comparison to previous studies

In healthy tissue extracted from a patient in SR the hormone 5HT augments I_{CaL} resulting in EADs and DADs which are extremely dangerous as resultant ectopic beats act as focal points for the initiation of arrhythmias. However, in patients who have undergone AFER due to persistent AF the effects of the hormone is to increase the I_{CaL} which results in an increase in APD and ERP providing a possible cardio-protective effect. Current pharmacological treatment methods are based on the management of AF by rate and rhythm control However, the success rates of commonly used drugs have been disappointing with high rates of reoccurrence of the underlying arrhythmia (Lally, Gnall *et al.* 2007). The naturally occurring 5HT hormone acts as an agonist for the $5HT_4$ receptor which is located only in the atrial tissue, therefore providing an attractive target for drug development. It has recently been shown that a specific antagonist, RS-10032, suppressed AF in a porcine model. A second $5HT_4$ receptor antagonist, piboserod was also in clinical development but was halted for unspecified reasons (Rahme, Cotter *et al.* 1999; Page and Roden 2005).

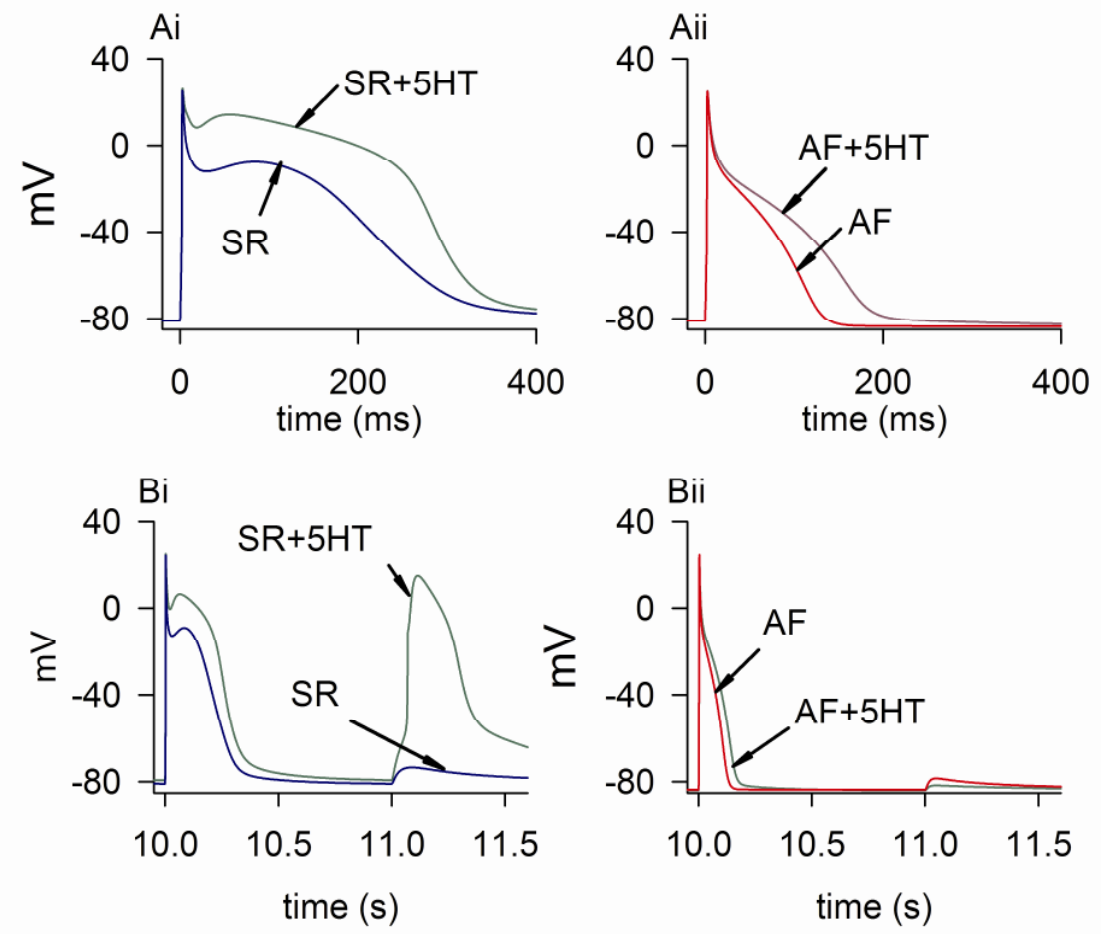

Figure 4.7 A: Simulated APs and B: Simulated AP initiated at 10 s followed by an artificially induced spontaneous depolarisation via the injection of Ca^{+} into the cell at 11 s. The CRN model was used for simulations and cases, SR (blue lines), 5HT (green lines), AF (red lines), and AF+5HT (purple lines) are shown.

Chapter 5

Computational evaluation of electrophysiological effects of Beta-Blockers on chronic atrial fibrillation

5.1. Introduction to Beta-Blockers

Cardiac modelling can provide valuable insights into how alterations in the properties of ion-channels as a result of various medical conditions can manifest themselves as the genesis and maintenance of AF. However, these models can also be utilised to simulate the effectiveness of current pharmacological treatment methods. These methods are favored by clinicians in the management of AF as they are non-invasive and far simpler to administer than surgical counterparts. The emphasis on anti-arrhythmic drugs is reflected in recent experimental and clinical studies (Workman, Kane *et al.* 2003; Wettwer, Hala *et al.* 2004; Ehrlich, Nattel *et al.* 2007; Shamiss, Khaykin *et al.* 2009; Viswanathan and Page 2009; Workman 2009). The underlying mechanism by which these drug actions are effective is the modification of the electrophysiological properties the atrial myocyte that are anti-arrhythmogenic. Despite the significant advances in ablation and cardioversion techniques (Schouchoff 2007; Buch and Shivkumar 2009; Callahan, Di Biase *et al.* 2009; Saltman and Gillinov 2009; Smelley and Knight 2009; Weerasooriya, Jais *et al.* 2009), anti-arrhythmic drugs remain the first course of action for management of AF (Wijffels and Crijns 2004; Amani and Smith 2005; Olshansky 2005; Roy, Talajic *et al.* 2008; Kalus 2009). Various pharmacological agents have been used traditionally and have been improved considerably in their function (Viswanathan and Page 2009).

A large proportion of pharmacological intervention relies on atrial-specific ion channel augmentation, or blocking drugs (Burashnikov and Antzelevitch 2009), and are commonly used for reducing aberrant atrial electrical activity. In particular, members of the class of drugs called beta-blockers (BBs), also called beta-adrenergic antagonists, are used as a preventative treatment for elevated blood pressure. The effectiveness of BBs was recognized in the early 1960s and BBs were judged to satisfactorily control atrial arrhythmias (Fitzgerald 1975). The effects of some BBs extend to atrial cells and may facilitate sinus rhythm in AF patients (Singh 2009). The effectiveness of individual members of this class of drugs has been studied in expansive clinical trials (Steeds, Birchall *et al.* 1999; Kuhlkamp, Schirdewan *et al.* 2000; Plewan, Lehmann *et al.* 2001). BBs target the catecholamine secreting cardiac adrenergic system, over activity of which

initiates and maintains AF (Bettoni and Zimmermann 2002; Gould, Yii *et al.* 2006). The antiarrhythmic effects of these agents are generally attributed to the reversal of beta-adrenergic stimulation of cardiac cells. In addition to the adrenergic system, BBs also affect dysfunctional atrial ion channels and attempt to restore atrial AP and ERP, in view of rhythm control (Wijffels and Crijns 2004; Kalus 2009) and to educe the incidence of persistent re-entrant circuits atypical of AF in the atria.

Recent experimental studies by Workman *et al.* (Workman, Kane et al. 2001; Workman, Kane et al. 2003; Workman 2009) quantified the BB-induced ion channel alterations in human atrial myocytes isolated from human patients in sinus rhythm (SR, Control) and AFER. However, an experimental evaluation of the isolated effects of BBs on organ level re-entrant circuits proved difficult. This study therefore adopts a multi-scale computer modelling approach with the aim of quantifying the anti-fibrillatory consequences of BBs on atrial conduction propagation behaviour in atrial cell and tissue models. This study quantifies the cardio-protective nature of BBs under Control (*i.e.* sinus rhythm, SR) conditions, and also quantifies the degree of restorative effectiveness under AF conditions. To address these aims, simulations in cell, 1D, 2D and 3D anatomical models were performed under SR, BB, AF, and BB treated AF (AFBB) conditions.

5.2. Methods

This section outlines the techniques used to simulate the effects of BBs and AFER on human atrial cells. The alterations to ion-channel dynamics were incorporated into the NYG and CRN model, which are two commonly used atrial cell models. A series of simulations as descried in Chapter One are performed to quantify the arrhythmogenic effects of cells under these conditions.

5.2.1 Cellular excitation models

The CRN (Courtemanche, Ramirez *et al.* 1998) and N*YG.* (Nygren, Fiset *et al.* 1998) (hereafter referred to as NYG) models were used in this study. Although based on similar experimental data, the spike-and-dome AP produced by the CRN model and the triangular AP produced by the NYG model are strongly regulated by the respective ionic currents and biophysical properties considered in the two models. Intracellular ion dynamics are also different between the two models, with the NYG model incorporating a cleft space. With detailed mathematical descriptions of ionic currents and intracellular ion dynamics, the CRN model consists of a 24 variable non-linear coupled ODE system and has been used

widely in computational studies (Zhang, Garratt *et al.* 2005; Seemann, Hoper *et al.* 2006; Kharche, Garratt *et al.* 2008). The 29 variable ODE NYG model, based on the previous LMCG model (Lindblad, Murphey *et al.* 1996), also consists of biophysically-detailed descriptions of cell membrane ion currents and intracellular ion dynamics. The NYG model is parametrically tuned for stable APs at a pacing frequency of 1 Hz under basal (SR) conditions. It has been used in previous computational studies, and has been shown by others to be functionally similar to the CRN model (Zhang, Garratt *et al.* 2005). Conductance parameters in the CRN model can be manipulated to reproduce the NYG model AP (Syed, Vigmond *et al.* 2005). However, prolonged pacing of the NYG model, even at low pacing rates, gave rise to errant spontaneous APs. The pacing protocols in simulations using both models were therefore altered to avoid such modelling defects.

Table 5.1 Ion channel conductance for major currents under SR conditions and their percentage changes under AF, BB, and AF+BB conditions.

	g_{K1}	g_{CaL}	g_{to}	g_{Kur}	I_{NaK}
SR	0.09 nS/pF	0.1238 nS/pF	0.1652 nS/pF	g_{Kur}	0.6 nS/pF
AF	90% ↑	64% ↓	65% ↓	12% ↑	12% ↓
BB	8% ↓	16% ↑	29% ↓	14% ↑	-
AFBB	74.8% ↑	58% ↓	75% ↓	18% ↑	12% ↓

5.2.2 Ionic current alterations due to BB and AF on atrial cell APs

The effects of BBs on human atrial-isolated myocytes were taken from an experimental study by Workman *et al.* (Workman, Kane *et al.* 2003). The experimental data are based on voltage clamp studies of enzymatically isolated human atrial cells from atrial appendages of a total of 40 patients in SR. BBs were seen to reduce the inward rectifier potassium current (I_{K1}) by 8%, with an increase in the L-type calcium current (I_{CaL}) of 16%, a reduction in the transient outward current (I_{to}) of 29%, and an increase in the sustained outward potassium current (I_{Ksus}) of 14%. AF induced ion channel remodelling has been quantified in a previous experimental study *(Workman, Kane et al.* 2001) and was studied in depth in our previous computer modelling simulations (Zhang, Garratt *et al.* 2005; Kharche, Garratt *et al.* 2008). In brief, ion current alterations due to AF were found to be a 90% increase of the I_{K1}, a 64% reduction of $I_{Ca,L}$, a 65% reduction of I_{to}, a 12% increase of I_{Ksus}, and a 12% reduction of the sodium potassium pump ($I_{Na,K}$). The effects of BB on AF affected cell models (AFBB) were simulated as a combination of the ion current

remodelling as described for AFER and BB above. The alteration of ion currents to simulate AF and BB are listed in Table 5.1. Cell level ion channel remodelling due to BB and AF was incorporated into the CRN and NYG cell models.

5.3. Results

The effects of BB, AF and AFBB affected cells and tissues were quantified as described above, using cellular, 1D, 2D and 3D models. The multi-scale quantitative cell, 1D, 2D and anatomical 3D results are summarised in Table 5.2 for the CRN and NYG models. Please note that as previously outlined in Chapter One the 4th AP is taken for measurement in the NYG simulations to ensure the stability of the simulations. For consistency the 4th AP is also measured in the CRN model, this explains the slight difference in values from the standard results outlined in Table 1.1.

5.3.1 Effects of AF, BB and AFBB on single cell atrial APs

The simulated atrial cells APs, as well as some major currents, under the SR, BB, AF, and AFBB conditions are shown in Figure 5.1. In the CRN case under the SR condition, the measured APD_{90} is 312.9 ms, with BB prolonging APD_{90} to 317.4 ms, a modest increase of 1.4%. AF dramatically abbreviated APD_{90} by 53.8% to 147.6 ms. The combined effect of AF and BB (*i.e.* the AFBB case) gave an APD_{90} of 161.0 ms, a 9.1% increase in comparison to the AF case. AF reduced the upstroke dV/dt_{max} as compared to SR (a reduction of 5%).

The effects on NYG model APs were qualitatively similar to that of the CRN model, with the APD under the SR being 221.3 ms, and 242.6 ms under BB conditions (an increase of 9.6%). AF dramatically reduced APD to 110.4 ms (a 50.1% reduction). The AFBB case resulted in an AP of 121.8 ms (a 10.3 % increase compared to the AF condition). The upstroke velocity was measured to be 217.1 mV/ms and 141.7 mV/ms for the CRN and NYG models respectfully. The application of BB has conflicting results between the two models. In the CRN model BB is observed to reduce upstroke velocity modestly by 0.8% to 215.3 mV/ms. In contrast, in the NYG model it is increased by 5.7% to 149.8 mV/ms. In the AF case upstroke velocity is reduced in both the CRN and NYG models to 205.6 mV/ms and 139.3 mV/ms respectfully. This indicated that AF results in a possible reduction in CV for both models. The application of BB to the AF case (AFBB) results in no significant change in the CRN model. However, in the NYG model there is a modest

increase of 7.0% to 149.1 mV/ms in comparison to the AF case. This indicates a possible restorative effect due to application on BBs

AF results in the reduction of I_{CaL} and augmentation of I_{K1} which have a significant effect on the morphology of the simulated APs. These changes have also been observed experimentally by Workman *et al.* (Workman, Kane *et al.* 2001) validating the simulations. The application of BB results in a minor augmentation of I_{CaL} and a reduction in I_{K1} alleviating the effects of AF modestly and therefore providing an anti-arrhythmogenic effect. The effects of AF on cellular AP have also been quantified in previous simulation studies (Zhang, Garratt *et al.* 2005; Kharche, Seemann *et al.* 2007; Kharche and Zhang 2008). The effects of BB on SR atrial cells have also been studied by Workman *et al.* (Workman, Kane *et al.* 2003) and our simulations also agree well with this data.

Table 5.2 Summary of multi-scale simulations using the CRN and Nygren models. The NYG model was found to be unsuitable for prolonged simulations and therefore was not used in the 2D and 3D simulations.

Model	Quantity	SR (CRN/ Nygren)	BB (CRN/ Nygren)	AF (CRN/ Nygren)	AF+BB (CRN/ Nygren)
Cell	Resting potential (mV)	-81.2 / -73.7	-80.5 / -72.9	-83.9 / -77.8	-83.7 / -77.3
	APD_{90} (ms)	312.9 / 221.3	317.4 / 242.6	147.6 / 110.4	161 / 121.8
	dV/dt_{max} (mV/ms)	217.1 / 141.7	215.3 / 149.8	205.6 / 139.3	205.1 / 149.1
	APDr maximal slope	1.3 / 0.64	0.95 / 0.7	1.6 / 0.49	1.53 / 0.53
	ERP (ms) (stimulus interval ~ 1 s)	327.9 / 216	338.2 / 289	165.3 / 154	179.8 / 173
	Cut off BCL (ms)	325 / 200	330 / 225	142 / 125	119 / 125
1D	CV (mm/ms)	0.2666 / 0.2719	0.2686 / 0.2666	0.2553 / 0.2722	0.2567 / 0.2681
	Cut off S2 (ms)	304 / 213	308 / 250	186 / 130	198 / 136
	TVW (ms)	14.6 / 12.1	15.7 / 11.8	13.6 / 8.0	13.2 / 9.1
	Wavelength (mm)	83.4 / 60.2	85.3 / 64.7	37.7 / 30.1	41.3 / 32.65
2D	LS (s)	1.4	3.4	> 10	> 10
	DF (Hz)	3..6	< 3	7.6, 16	7.3, 14.2
	Tip meander area (cm^2)	5.25	2.04	6.01	1.87
	MS (mm)	49.1 / 27.5	60 / 33.5	17.4 / 15	27.5 / 16
3D	LS (s)	4.2	3.3	> 6	> 6
	DF (Hz)	3.1	2.8	7.1	6.5

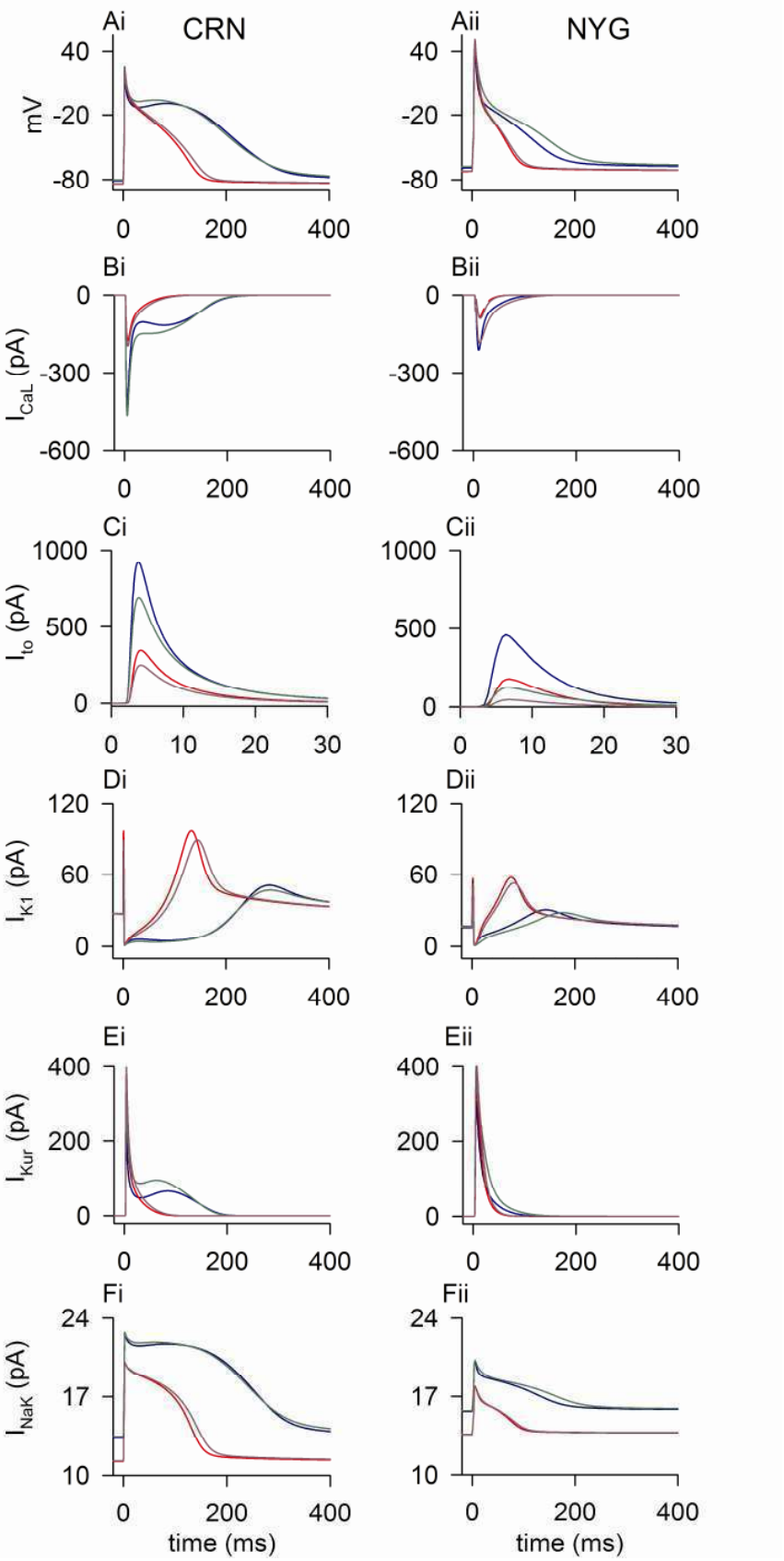

Figure 5.1 Simulated AP profiles and major current traces using the CRN (left column) and NYG (right column) models under SR (blue lines), BB (green lines), AF (red lines), and AFBB (purple lines) conditions. Ai, Aii: AP profiles. Bi, Bii: I_{CaL} current traces. Ci, Cii: I_{to} current traces. Di, Dii: I_{Kur} current traces. Ei, Eii: I_{NaK} current traces. Fi, Fii: I_{Kr} current traces.

5.3.2 APD and ERP restitutions under SR, BB, AF, and AFBB conditions

APDr using the CRN and NYG models are shown in Figure 5.2, Ai and Aii respectfully. APDr were studied in a wide DI range to allow the study of rate dependent pacing at high and low rates. Both models gave a consistently higher APD across the range of pacing rates under BB conditions as compared to the SR case. The AF case, on the other hand, gave consistently lower APD than SR across the range of pacing rates. The effects of BB on SR and AF affected cell models was to augment APD marginally across the range of pacing rates.

The APDr maximal slopes gave different results in the two models (Figure 5.2, Ci and Cii). Under SR conditions, the maximal slopes of APDr using CRN model was 1.3 whilst that using the NYG model was 0.64. The maximal slope of APDr under BB conditions was reduced in the CRN model by 26% and increased in the NYG model by 9.4%. Under AF conditions, the CRN model gave an increased APDr maximal slope (by 23.5%) whilst the NYG model gave a reduced slope (by 23.4%). Under AFBB conditions, APDr maximal slope was augmented in the CRN model by 17.6% and reduced in the NYG model 17.1%.

The alterations in maximal APDr slope under ion current remodelled conditions using the CRN model are due to the large changes in the repolarising and depolarising currents and depends on the quantitative change in the functional role of these currents during APs. Such alterations in APDr maximal slopes have been seen in our previous computational studies (Zhang, Garratt *et al.* 2005; Kharche, Seemann *et al.* 2007; Kharche, Garratt *et al.* 2008; Kharche, Seemann *et al.* 2008; Zhang, Garratt *et al.* 2009). The NYG model is, however, fine tuned for reproducing human atrial AP at 1 Hz and may not be as robust as the CRN model after a few excitations at any pacing rate. The underlying ionic mechanisms regulating the APs in the CRN and NYG models are different, which accounts for the difference in APDr properties of the two models under similar alterations of ionic channels (Jacquemet 2007; Cherry and Evans 2008).

Single cell ERPr curves using the CRN and NYG models are shown in Figure 5.3, Ai and Aii. ERP under CRN SR at a PCL of 1 s for SR was seen to be 327.9 ms, under BB to be 338.2 ms (a 3.1% increase). And under AF was seen to be 165.3 ms (a 50% reduction from

SR). The AFBB case gave an ERP of 179.3 ms (a 8.4% increase compared to AF). In the NYG model, the SR ERP at 1 s PCL was seen to be 216 ms, which increased to 286 ms under BB conditions (a 32% increase). Under AF conditions ERP was reduced to 154 ms (a 29.6% reduction), whilst AFBB gave an ERP of 173 ms (a 13% increase over the AF case). In both models, BB shifted ERPr rightwards, indicating the reduced ability of atrial cells to sustain AP excitations at high rates of pacing. BB shifted both ERPr leftwards, indicating the increased ability of atrial cells to sustain AP excitations at high rates of pacing. The effects of AFBB were to compensate this leftward shift due to AF, but had limited restorative effects in bringing the AF affected cellular ERPr closer to the SR ERPr.

5.3.3 Alterations to CV due to AF and BBs

CVr under SR, BB, AF and AFBB conditions were computed using 1D homogeneous strands of CRN and NYG virtual atrial tissue models as described in the methods section and are shown in Figure 5.3, Bi and Bii. Under SR conditions, the CV of solitary waves, *i.e.* at PCL exceeding 1 s, was 0.2666 mm/ms (CRN) and 0.2717 mm/ms (NYG). BB had no significant effect on the SR CVr. At low rates of pacing, AF was seen to reduce solitary wave CV from 0.27 mm/ms to 0.26 mm/ms, whilst dramatically increasing the rate at which electrical conduction was sustained as compared to SR conditions. The effect of BB on AF, *i.e.* the AFBB case, did not alter the AF CVr significantly and retained the tissues' ability to sustain high pacing rate electrical conduction. Quantitative results are given in Table 5.2.

5.3.4 Effects of AF and BB on the temporal VW

TVW was computed using 1D homogeneous strands of atrial tissue based on the CRN and NYG models results of which are shown in Figure 5.4, Ai and Aii. Under SR conditions, VW was found to be 14.6 ms (CRN) and 12.1 ms (NYG). Under BB conditions the VW increased in the 1D strands based on the CRN model (15.7 ms), but reduced based on the NYG model (11.8 ms). AF conditions reduced VW (CRN: VW = 13.6 ms; NYG: VW = 8 ms), largely due to the drastic increase of I_{K1} (Kharche, Garratt *et al.* 2008). However, when BB was applied to the AF affected strands, *i.e.* under AFBB conditions, the VW remained unaltered (CRN: VW = 13.2 ms) or increased (NYG: VW = 9.1 ms) as compared to the AF case. Overall, BB, AF and AFBB conditions gave a reduced VW as compared to SR conditions (Figure 5.4, Ai and Aii). Quantitative results are given in Table 5.2.

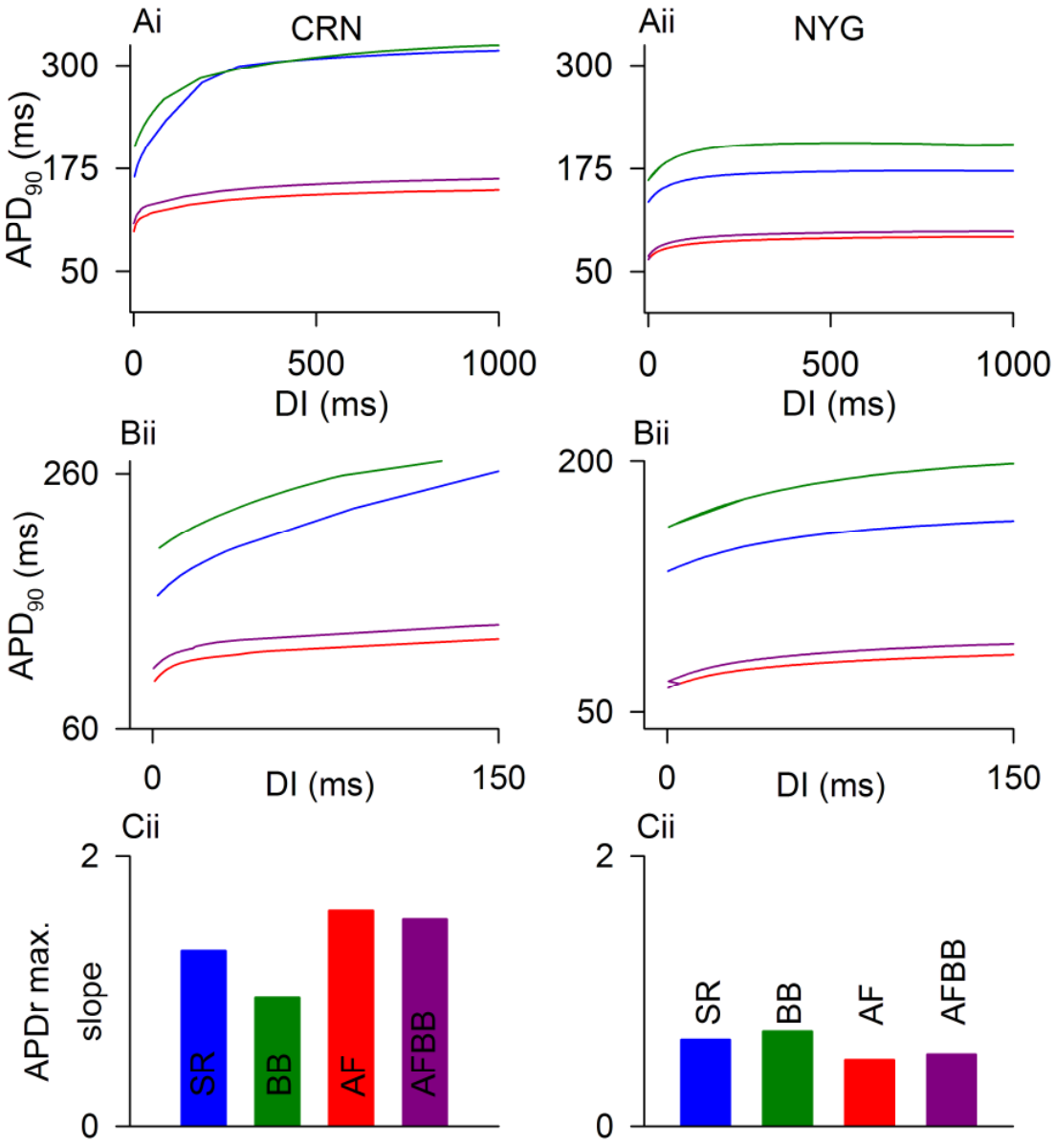

Figure 5.2 Simulated APD restitution curves and APDr maximal slopes for CRN (left column) and NYG (right column) models under Control (blue), BB (green), AF (red), and AFBB (purple) conditions. Ai, Aii: APDr curves. Bi, Bii: Expanded APDr curves as shown in Ai, and Aii at low DI (i.e. high pacing rates). Ci, Cii: Maximum slopes of APDr curves shown in Ai and Aii.

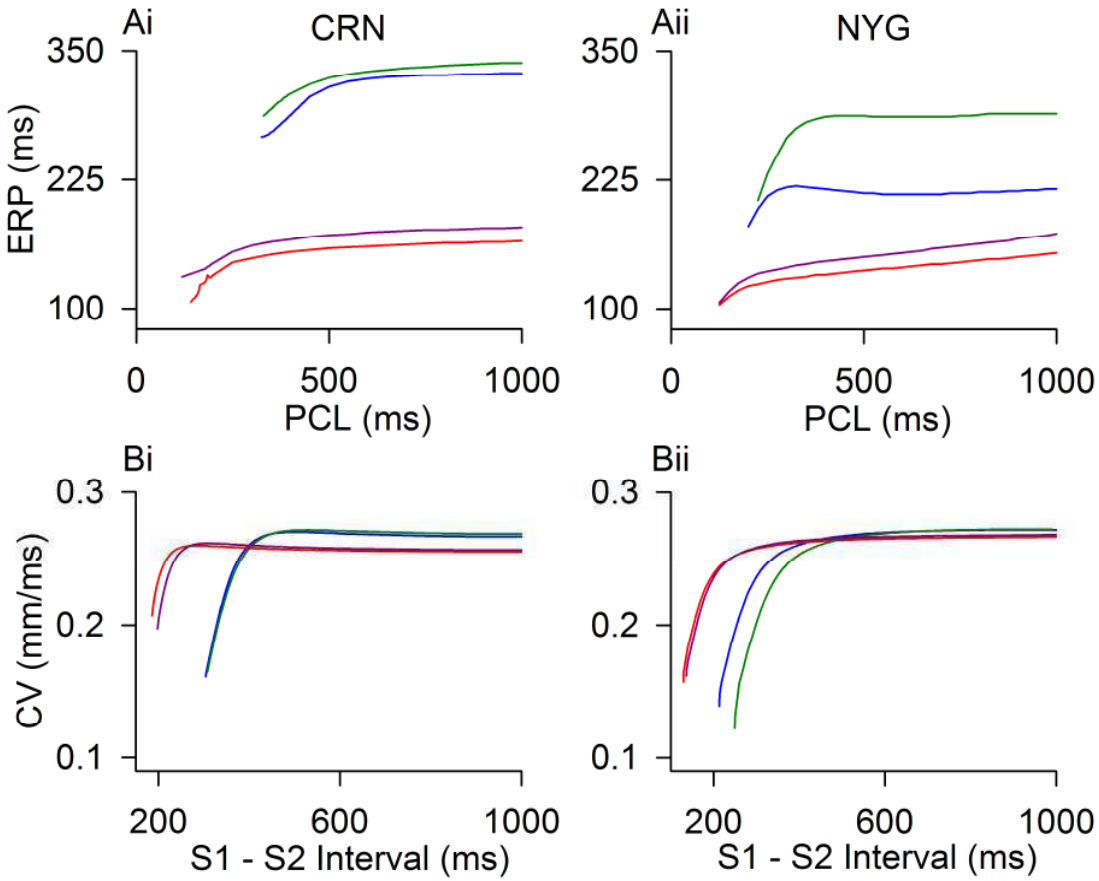

Figure 5.3 Simulated ERP and CV restitution curves for CRN (left column) and NYG (right column) models under SR (blue lines), BB (green lines), AF (red lines), and AFBB (purple lines) conditions. Ai, Aii: ERPr curves. Bi, Bii: CVr .

5.3.5 Effect of AF and BBs on spatial VW

The vulnerability of atrial tissue to spatially extended ectopic events was quantified by computing the critical length required to induce sustained re-entrant waves. The results are shown in Figure 5.4, Bi and Bii. The critical length under SR conditions was found to be more than 49.1 mm, which is much larger than the human atrial size of approximately 40 mm. This indicates that under SR conditions, human atrial tissue does not sustain re-entrant activity induced due to premature stimuli. It also indicates that the length of atrial obstacles required to induce erratic propagations is much larger than human atrial sizes. In contrast, the critical length under AF conditions was found to be 17.4 mm, a much smaller value compared to SR. Under BB conditions, the critical length was longer than SR at 60 mm. Under BB upon AF conditions (AFBB), the critical length was computed to be 27.5 mm. This is modestly extended from the AF conditions but is still substantially shorter than in the SR case. These results indicate that BB has some limited protective effects when applied to tissue which has undergone AFER. The NYG simulations yielded similar quantative results which can be seen in Table 5.2.

5.3.6 Re-entry in 2D homogeneous sheet models

The NYG model was found to be unsuitable for prolonged simulations showing abnormal pace making activity due to intracellular ion accumulation, and due to its optimal operating pacing rate being 1 Hz. 2D and 3D simulations of re-entry and scroll waves were therefore carried out using the CRN model.

The 2D simulations of re-entrant waves under various patho-physiological conditions is illustrated in Figure 5.5 and the associated spiral wave tip trace, representative time traces, and PSD are shown in Figure 5.6. Under SR conditions, the re-entrant waves in the 2D homogeneous sheet of atrial tissue meandered over a large area. It self-terminated within 1.4 s due to localised excitation wave fronts colliding with repolarisation tails of previous excitations. The rate of excitation of localised tissue was low, as revealed by a simple power spectrum density analysis of representative AP profiles (3.6 Hz). Under BB conditions, the behaviour of re-entry is similar to SR conditions. On the other hand, AF had a dramatically stabilising effect on re-entrant waves in a 2D idealised sheet of atrial tissue. Due to the large abbreviation of propagation wavelength, re-entrant waves under AF were highly stable with a very small area of meander. The re-entry persisted for more than the total simulated electrical activity of 6 s and caused a high rate of excitation of atrial tissue (~ 7.6 Hz, 16 Hz). In the AFBB case, the re-entry was considerably more stable than

in the SR case and persisted for the duration of simulated atrial activity (6 s). The power spectrum of AP profiles also gave higher localised pacing rates (~ 7.3 Hz, 14 Hz). Thus BB reduced the risk of persistent re-entry under SR conditions, although it may not be able to alleviate re-entry in patients with chronic AF.

5.3.7 Scroll wave propagation in 3D organ model

Figure 5.7 shows re-enrty simulation in a 3D atria. Under SR conditions, the re-entrant waves self-terminated within 4.2 s, irrespective of the location of the initiated scroll wave. Interactions between the arm of the scroll wave and anatomical obstacles did not cause the genesis of persistent erratic propagations. Localised atrial excitation was at low pacing rates (3.1 Hz) as demonstrated by the DF in the power spectrum of AP profiles. Scroll waves had a similar behaviour under BB conditions with self-termination at around 3.3 s. Again, the lifespan of the scroll wave did not depend upon the location of birth. Under AF conditions, however, the scroll wave was highly localised and stable. Eventually, interactions between the arm of scroll wave and anatomical obstacles caused persistent erratic propagations. The erratic electrical activity persisted for the whole 6 s duration of the simulation. Localised atrial excitation was at high pacing rates (7.6, 16 Hz). In the AFBB case, the scroll waves were stable and BB on chronic AF did not cause scroll waves to self-terminate, and persisted for the period of the simulations (6 s).

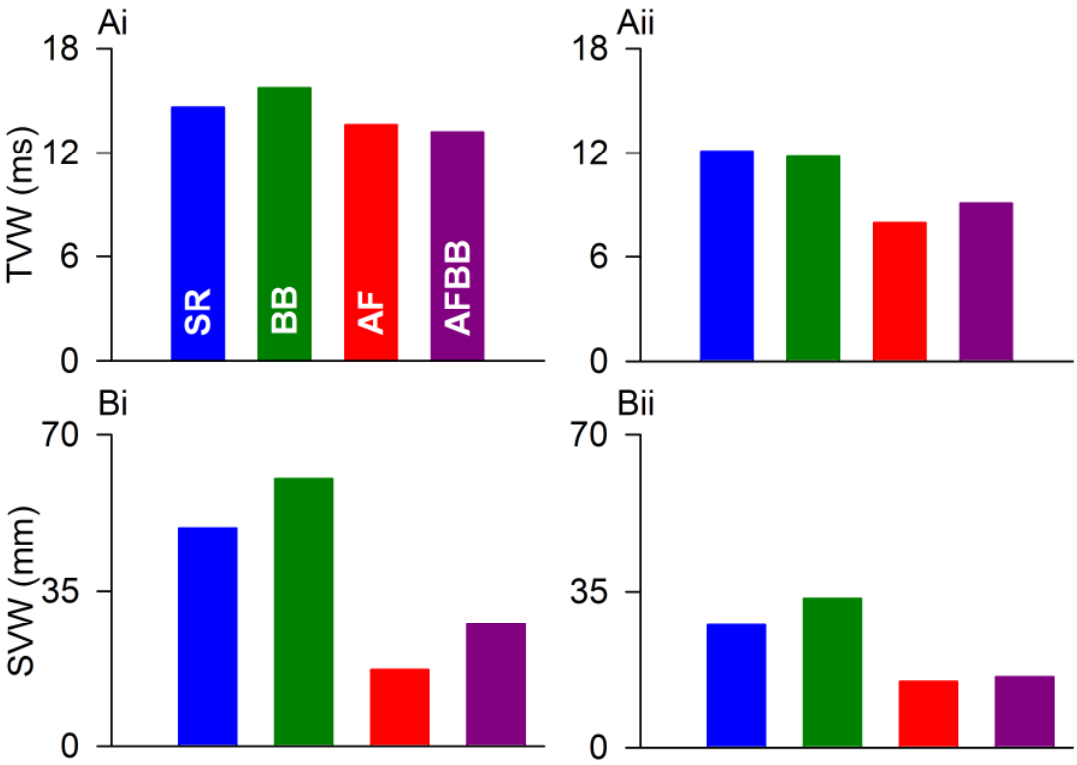

Figure 5.4 Temporal VW and Spatial VW simulation results for CRN (left column) and NYG (right column) models under Control (blue), BB (green), AF (red), and AFBB (purple) conditions. Ai, Aii: VW. Bi, Bii: MS.

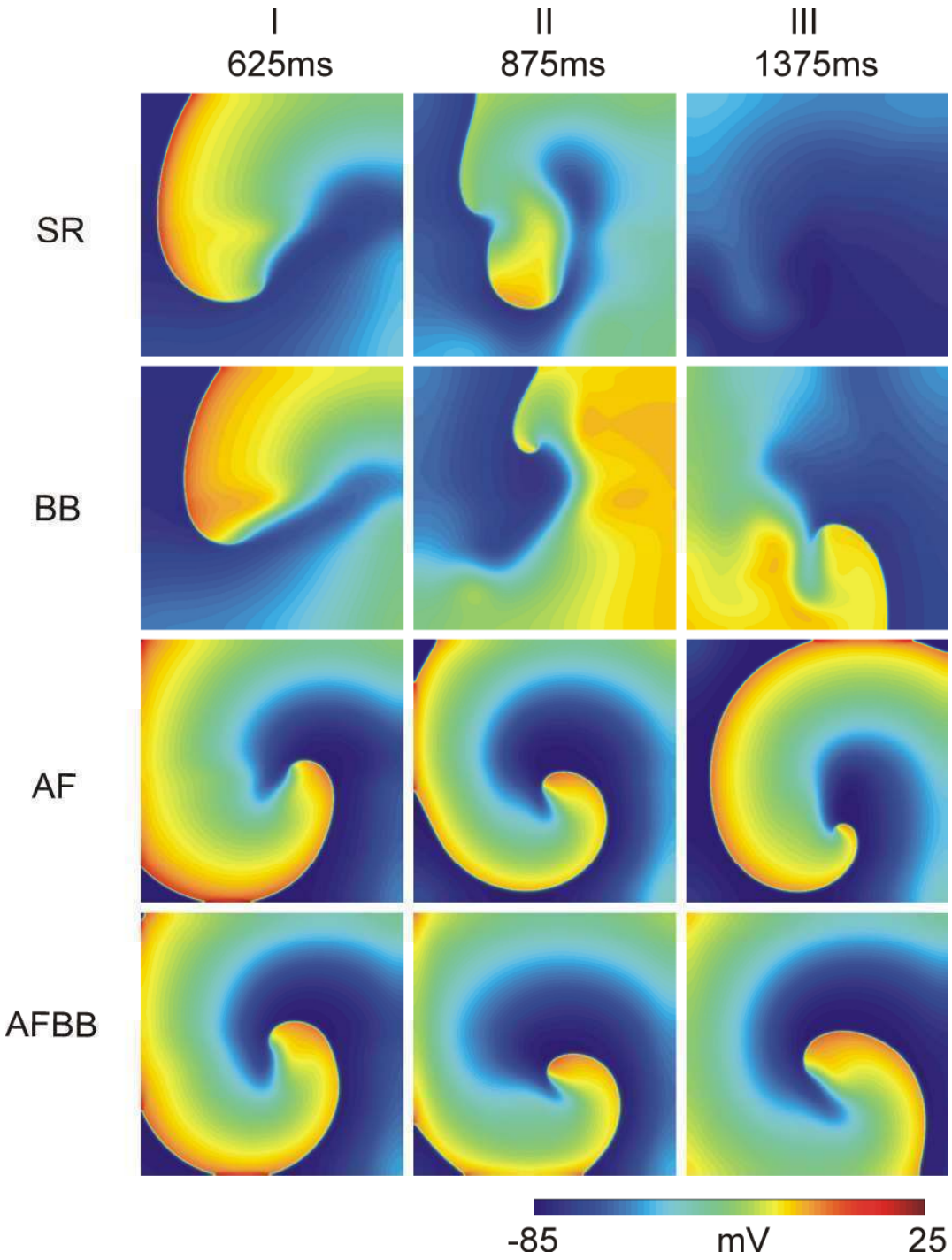

Figure 5.5 Simulation of re-entry in 2D idealised sheets of virtual atrial tissue. Top panels show representative frames from the SR simulation, second row from BB, third row for AF and bottom row of panels show data for AFBB. Columns I-III show representative frames from the simulations at 325 ms, 875 ms and 1375 ms respectively.

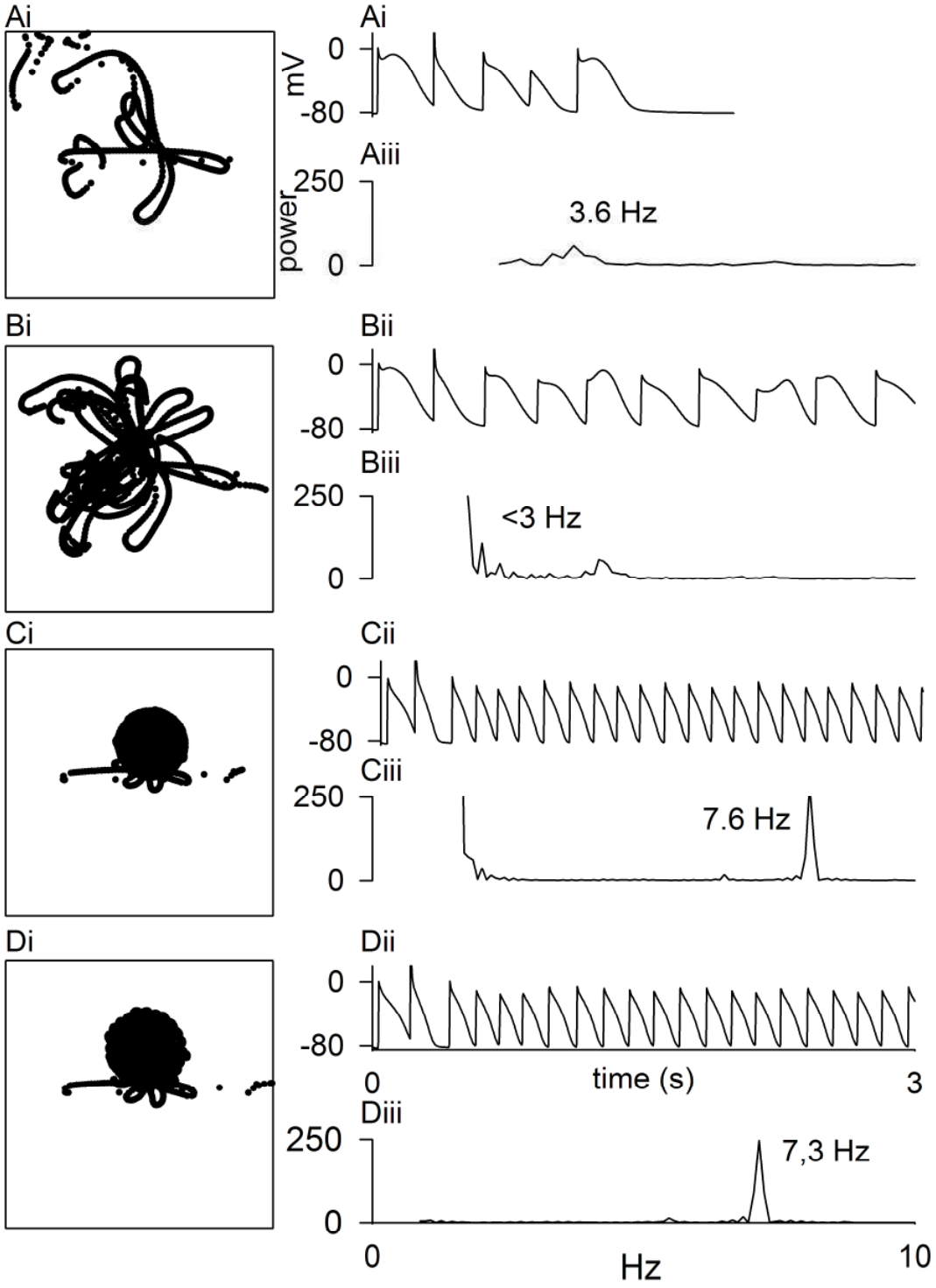

Figure 5.6 2D spiral wave tip traces (panel i), representative AP traces taken from 2D simulations (panel ii), and power spectrum density showing frequencies of maximal power (panel iii) under SR (A), BB (B), AF (C), AFBB (D) conditions.

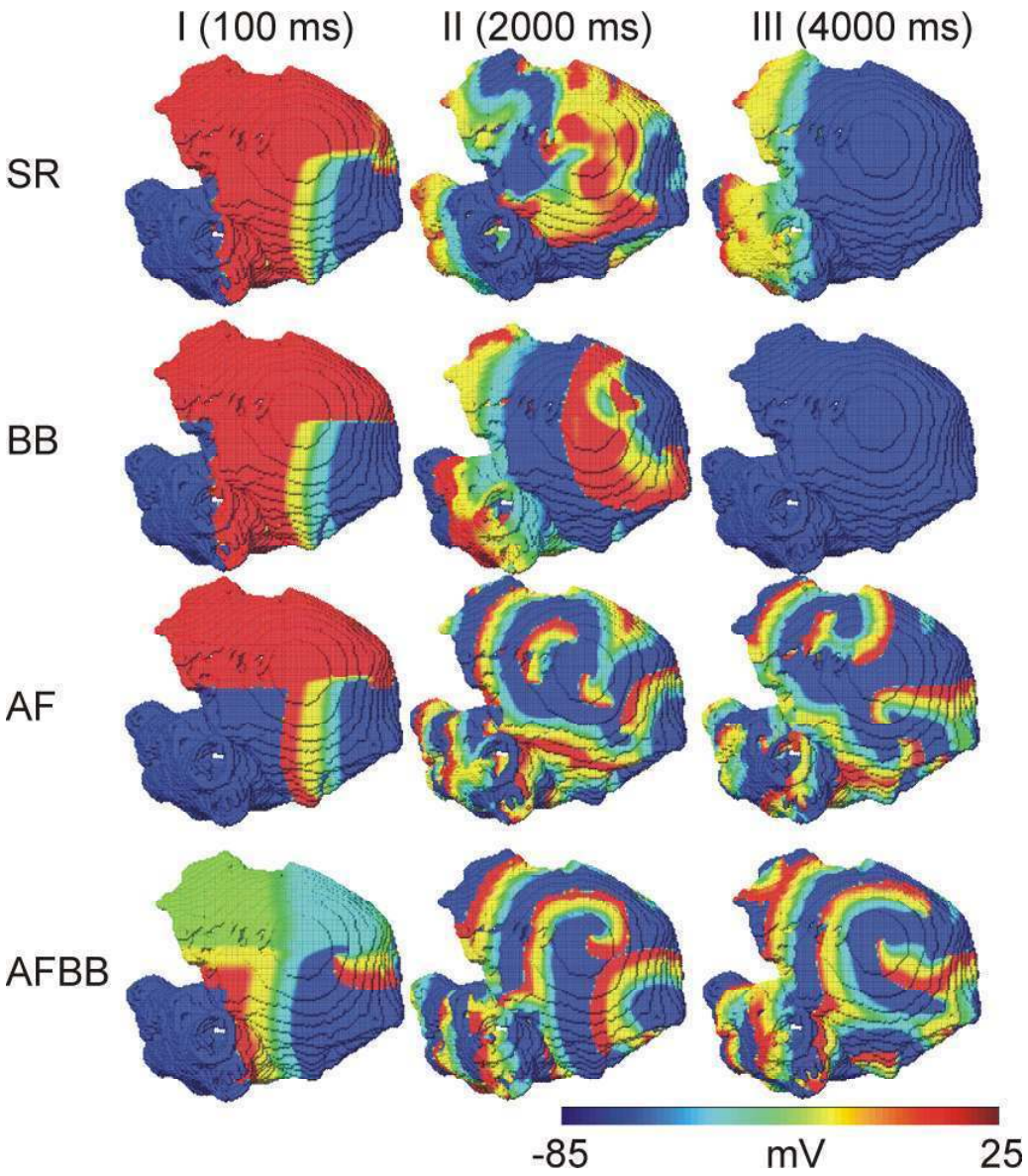

Figure 5.7 3D scroll wave simulation results. Top panels show data for Control, second row for BB, third row for AF and bottom panels show data for AFBB. Columns I, II, and III show panels from the 3D re-entry simulations at 100 ms, 2000 ms, and 4000 ms respectively.

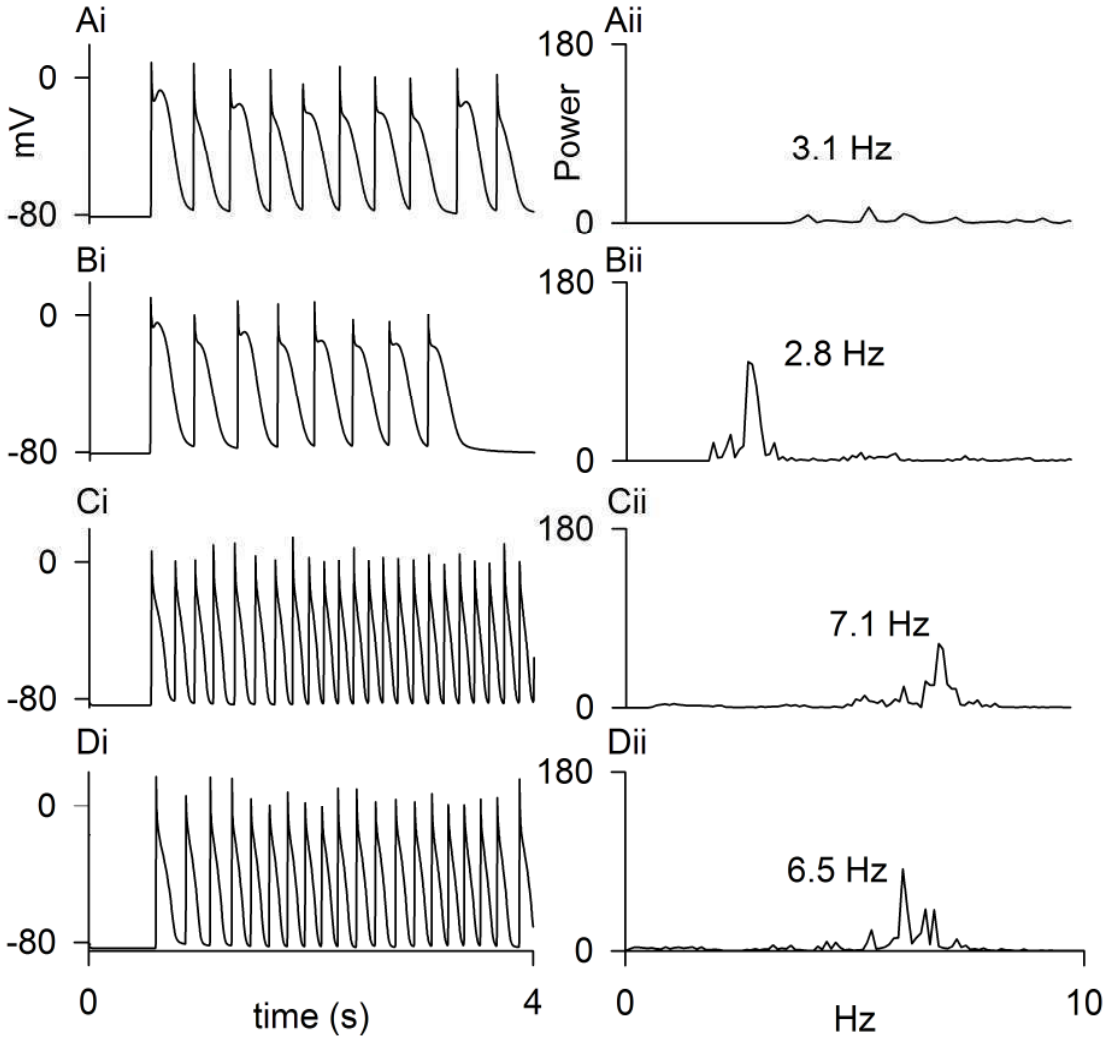

Figure 5.8 Representative AP traces taken from 3D simulations (panel i), and power spectrum density showing frequencies of maximal power (panel ii) under SR (A), BB (B), AF (C), AFBB (D) conditions.

5.4. Conclusions and discussion

5.4.1 Main findings

BB target ion channel function in the atria and are routinely prescribed due to their recognised cardio-protective properties (Ishiguro, Ikeda *et al.* 2008) with varying rates of success. The anti-fibrillatory effects of BB on atrial tissue conduction, and on organ level conduction behaviour, have not been studied to date. In this study, a computational approach was adopted to gain insights into the cardio-protective and anti-fibrillatory effects of beta-blockers at tissue and organ levels. The principal findings were that the effects of BB on normal (SR) electrical behaviour was to prolong APD, moderately reduce susceptibility to ectopic activity (increased MS) and reduce lifespan of re-entrant waves at 2D and scroll waves at organ levels. The effects of BB on AF affected cells was to modestly prolong APD and MS. BB however did not restore atrial excitation behaviour to SR conditions and re-entrant waves in 2D and scroll waves in organ level simulations were persistent.

In conclusion, it was found that BBs have a cardio-protective effect of human atrial AP and electrical conduction behaviour, but cannot restore electrical properties of AF affected atrial tissue to SR conditions and therefore have limited applicability in the diseased stages.

5.4.2 Limitations of the study

The CRN and NYG models were used in this simulation study. The potential limitations and suitability of these models have been discussed elsewhere (Courtemanche, Ramirez *et al.* 1998; Nygren, Fiset *et al.* 1998; Cherry and Evans 2008). The NYG model, in particular, is parametrically fine tuned to reproduce human atrial APs at a pacing rate of 1 Hz. Upon pacing at higher rates, it readily shows intracellular ion accumulation and depletion making it unsuitable for prolonged simulations. A limitation in our multi-cellular models was the presumption of electrical and spatial homogeneity, whilst it is known that human atria are electrically and spatially heterogeneous (Seemann, Hoper *et al.* 2006). In the simulations of the effects of AF and BB, ion current remodelling of several currents has been incorporated. However, it is known that AF also affects intracellular gap junctions (van der Velden and Jongsma 2002; Chaldoupi, Loh *et al.* 2009). Over and above AF

affecting them, beta-blockers and anti-arrhythmic drug therapies target gap junctions (Burashnikov and Antzelevitch 2009) as well as ion channels. Thirdly, the effects of AF and BB on intracellular ion dynamics has not been considered, as these could potentially be the basis for persistent AF (Liang, Xie *et al.* 2008) and also be drug therapy targets (Dobrev and Nattel 2008).

Having identified the limitations in this computer modelling study, the fundamental conclusions of this study are unaffected. The structural effects of AF and BB on the human atria should not affect the electrophysiological functional effects demonstrated in this study.

5.4.3 Clinical significance and comparison to previous studies

Alterations in a plethora of atrial ion channels have been implicated in AF (Bosch, Zeng *et al.* 1999; Workman, Kane *et al.* 2001; Wettwer, Hala *et al.* 2004). Because age-related AF is connected to such AF induced electrical remodelling, several hereditary genetic defects have also been conclusively associated with AF (Abraham, Yang *et al.*; Chen, Xu *et al.* 2003; Xia, Jin *et al.* 2005; Das, Makino *et al.* 2009; Watanabe, Darbar *et al.* 2009; Yang, Li *et al.* 2009). These experimental and clinical studies and our multi-scale computer modelling studies have shown that electrophysiological alterations in the biophysical properties of human atrial ion channels lead to the genesis and sustaining of AF (Zhang, Garratt *et al.* 2005; Kharche, Seemann *et al.* 2007; Kharche, Garratt *et al.* 2008; Kharche, Seemann *et al.* 2008; Kharche 2009; Zhang, Garratt *et al.* 2009). It is not surprising that these AF affected ion channels are drug therapeutic targets, and are being investigated extensively (Wijffels and Crijns 2003; Antzelevitch and Burashnikov 2009; Hundal and Garg 2009; Kemeny-Suss, Kasneci *et al.* 2009; Kozlowski, Budrejko *et al.* 2009; Nanda, Siddique *et al.* 2009). In particular, the anti-arrhythmogenic effects of beta-blockers have long been identified (Lambert 1972; Levi and Proto 1972) and beta-blockers have been known to reduce mortality by 25% (Yusuf, Peto *et al.* 1985). Beta-blockers are routinely prescribed in the clinic, but in recent times their effectiveness has been seen primarily in alleviating post-operative discomfort (Cheng and Nayar 2009; Sinha, Schwartz *et al.* 2009) rather than as an absolute pharmacological solution to AF, which is primarily a degenerative disorder. In fact, several anti-arrhythmic drugs used in the treatment of AF have been shown to result in ventricular proarrhythmia and extra-cardiac toxicity (Burashnikov and Antzelevitch). Atrial selective drugs at effective dosage have also been

shown to demonstrate adverse effects (Burashnikov and Antzelevitch 2008; Burashnikov, Di Diego *et al.* 2008; Ford and Milnes 2008).

Clinical practice aside, the mechanisms by which beta-blockers may alleviate the risk of re-infarction in AF patients remains under investigated. In a recent experimental study on human atrial cells (Workman, Kane *et al.* 2003), beta-blockers have been shown to have a moderate effect on major electrical ion channels. The restorative effect on the major ion channels affected by AF was at most mild. The incorporation of the effects of AF into mathematical models showed the expected reduction of APD, ERP along with genesis of erratic wave propagations in an organ model. Upon simulation of treatment with beta-blockers, the effects of AF were not alleviated and erratic propagations persisted. The therapeutic effects of beta-blockers on alleviating electrophysiological atrial arrhythmias due to re-entry are therefore limited. However, the effects of BB on limiting non-re-entrant cannot be ignored and therefore this area required further study.

Chapter 6

Computational evaluation of the anti-arrhythmogenic effects of an I_{Kur} channel blocking agent

6.1 Introduction

The clinical management of AF is often via rhythm control, which is primarily achieved with the administration of Class I and Class III drugs. However, while interventions with these classes of drugs are common practice, their medium to long term effectiveness in maintaining sinus-rhythm (SR) is limited (Fuster, Ryden *et al.* 2001; de Denus, Sanoski *et al.* 2005). Pharmacological agents aim to prevent the onset of AF by blocking key ion-channels responsible for the repolarisation of a cardiac myocyte, thereby lengthening APD and ERP. Increased ERP lengthens the wavelength at which the excitable tissue of the myocardium can sustain a re-entrant circuit. This limits the tissues' susceptibility to re-entry, allowing the normal propagation of an excitation wave to be maintained. However, the proteins responsible for the ion-channels are actively transcribed in the ventricles as well as the atria, and therefore it is not possible to alter ion-channel properties with drug therapy in the atria without also changing the electro-physical properties of ventricular cells. In fact, alterations to ion-channels which are anti-arrhythmogenic in the atria can lead to potentially life threatening side effects such as a ventricular pro-arrhythmia. Current drug development therefore focuses on developing pharmacological agents which are atrial specific so as to limit the risk of adverse side effects (Tamargo, Caballero et al. 2009).

Possible therapeutic benefits of blocking I_{Kur} are well known and in recent years a number of pharmaceutical companies have attempted to develop an I_{Kur} specific channel blocking agent with the aim to produce a more robust method for the prevention and treatment of AF (Brendel and Peukert 2003; Ford and Milnes 2008). Current efforts to develop such a drug have resulted in the synthesis of agents which inhibit other potassium channels along with the calcium and sodium channels. However, it has been observed that at low micro-molar concentrations (10–50 μmol/L),4-aminopyridine (4-AP) successfully blocks I_{Kur} without altering the properties of other ionic currents (Nattel, Matthews et al. 2000). Experimental work conducted by Wettwer *et al.* has extracted atrial myocyte cells from patients who exhibit normal sinus rhythm (SR) and patients who have been suffering from

persistent AF. Wetter *et al.* reported that applying low concentrations of 4-AP to an atrial myocyte under SR conditions, thereby blocking the I_{Kur} ion-channel, resulted in a shortening of APD. In contrast, the application of 4-AP to a cell which has undergone AFER resulted in a modest increase in APD.

While previous experimental and simulation studies have identified that the blocking of I_{Kur} results in a shortneting of APD and ERP in healthy cells, and conversely a lengthening of APD and ERP in cells which have undergone AFER, the full effects have not been studied in detail at a multi-scale level. This chapter focuses on implementing single cell, 1D, 2D, and 3D simulation protocols to investigate and quantify the underlying arrhythmogenic effects of blocking the I_{Kur}. Two cell types, an atrial myocyte under SR conditions, and an atrial myocyte which has undergone AFER. The simulated cells are incorporated into the standard multi-scale techniques outlined in Chapter One to investigate and quantify how alterations of I_{Kur} result in changes to tissue susceptibility to AF.

6.2 Methods

This section outlines the methodology behind the development of four cell types: sinus-rhythm (SR), SR with the application of the blocking agent 4-AP (SR+B), AFER cell (AF), and AFER with the application of the blocking agent 4-AP (AF+B) by modifying the CRN (Courtemanche, Ramirez et al. 1998) model. This CRN model was implemented as it has been extensively used in previous simulation studies and is numerically stable under normal physiological conditions (Seemann, Hoper et al. 2006; Kharche, Seemann et al. 2007; Kharche, Seemann et al. 2008; Kharche and Zhang 2008). All multi-scale techniques for quantising the onset of AF which are outlines in Chapter One are implemented. Additionally a simulation into how augmentation and the blocking of the major ionic current alters APD_{90} is performed.

6.2.1 Development cell type model

Experimental data from Wettwer *et al.* and Workman *et al.* indicated how the major currents are reduced or augmented under various conditions (Workman, Kane et al. 2001; Wettwer, Hala et al. 2004). This data is used to construct the four cell types by incorporating this scaling factor into the value of the individual ion-channel conductance's. Under normal SR conditions the cell was considered to be the standard CRN model.

Wettwer *et al.* described the effect of adding 4-AP to SR cells as a reduction in the I_{Kur} current density of 78%. The SR+B cell was created by reducing the g_{Kur} parameter by a scaling factor of 78%. Workman *et al.* also describes ionic changes to the cell due to AFER (Workman, Kane et al. 2001). The changes due to AFER are a 90% increase in the inward rectifying potassium current (I_{K1}), a 65% reduction in the transient outward current (I_{to}), a 64% reduction in the in the late calcium current (I_{CaL}), a 12% increase in the I_{Kur} current, and a 12% reduction in the sodium-potassioum exchanger pump (I_{NaK}). These are used when creating the AF cell by scaling the relevant conductance parameters associated with each current. The AF+B cell was simulated by applying a further reduction of the I_{Kur} current by 78% in addition to the ionic changes in the AF cell. A summary of the alterations of all cell types is given in Table 6.1.

Table 6.1
Conductance Alterations of Channels due to AFER and 4-AP

Model	g_{K1}	g_{to}	g_{CaL}	g_{Kur}	g_{NaK}
SR+B	-	-	-	78% ↓	-
AF	90% ↑	65% ↓	64% ↓	12% ↑	12% ↓
AF+B	90% ↑	65% ↓	64% ↓	75% ↓	12% ↓

6.2.2 Simulating alteration to APD resulting from blocking and augmenting of conductances of the major ionic currents

Recent studies, both experimental and simulated, have shown that under normal SR conditions the blocking of I_{Kur} results in an abbreviation of $APD_{90.}$ In contrast the blocking of I_{Kur} upon a cell which has undergone AFER results in a modest lengthening of $APD_{90.}$ Therefore it is of interest to investigate how alterations in the current density of individual ionic currents manifest themselves as changes in APD. The two cells, SR and AF were used to simulate an AP using the standard protocol as described in Chapter One. The major ionic currents $I_{Kur,}$ I_{k1}, I_{CaL}, and I_{to} were scaled through the range from 0% (total block) to 200% (doubling the current density) to study the effects that the channel conductance has on the APD of the two cell types.

Table 6.2 Summary of cell properties for AFER and 4-AP cells

Model	Quantity	SR	SR+B	AF	AF+B
Cell	Resting potential (mV)	-80.8	-80.4	-83.9	-83.7
	APD_{90} (ms)	314.2	299.2	155.5	180.6
	Overshoot (mV)	24.7	24.9	24.7	24.8
	dV/dt_{max} (mV/ms)	217.1	216.2	205.5	205.4
	APDr maximal slope	1.3	1.3	0.7	0.7
	ERP (ms) (stimulus interval ~ 1 s)	327.9	319.8	167.7	193.5
	Cut off BCL (ms)	328.6	417.7	312.0	265.0
1D	CV (mm/ms)	0.26	0.26	0.25	0.25
	Cut off S2 (ms)	320	313	198	217
	VW (ms)	14.6	14.7	15.6	14.3
	Wavelength (mm)	81.7	77.8	38.8	45.1
2D	LS (s)	1.4	1.0	> 6	> 6
	DF (Hz)	3.6	4.7	8.1	8.0
	Tip meander area (cm^2)	5.25	0.9	4.0	1.5
	MS (mm)	49.2	77.8	17.4	45.1
3D	LS (s)	4.2	4.1	> 6	> 6
	DF (Hz)	3.1	2.6	7.5	6.9

6.3 Results of multi-scale simulations

This section details the results of the simulations implemented to quantify the electrical behaviour at single cell, 1D strand, 2D sheet, and an anatomically correct 3D geometry. The results of the simulations are described along with relevant measurements which quantify the onset of AF, which are summarised in Table 6.2.

6.3.1 Effects of AF and 4-Aminopyridine on single atrial myocyte AP

AP profiles and associated major ionic currents can be seen in Figure 6.1. Under SR conditions the APD_{90} is measured to be 314.2 ms. In the SR+B cell the addition of 4-AP resulted in a modest abbreviation of APD_{90} by 4.8% to 299.2 ms. In AF cells APD_{90} is measured to be 155.5 ms, a dramatic abbreviation of 51.0% from the SR case. For the AF+B cell, where 4-AP is added to the AF cell, the APD_{90} is 52.5% shorter then in the SR cell at 180.6 ms but it is augmented by 16% in comparison to the AF cell. Typically an augmentation of APD_{90} results in an increase in ERP which is anti-arrhythmogenic, whereas a reduction in APD_{90} shortens ERP which is pro-arrhythmogenic. These simulation results show that the application of the blocking agent 4-AP to SR cells results in a shortening of APD_{90} and is pro-arrhythmogenic while conversely the application of 4-AP to the AF cells results in a lengthening of APD_{90} which is anti-arrhythmogenic.

The reduction of APD_{90} in the SR+B cell in comparison to the SR cell is due to an increased activation of I_{CaL} due to the blocking of I_{Kur}. This increase of I_{CaL} results in the plateau of the AP being shifted into the positive, causing several K^+ currents to activate causing rapid repolarisation in the mid to late AP. This results in a modest overall shortening of APD_{90}. However, in AF cells there is substantial reduction in the I_{CaL} current density due to AFER which dramatically reduces the APD_{90}. Thus a reduction of I_{Kur} now increases the potential where the activation of other K^+ repolarisation currents is less pronounced and so the result is a lengthening of APD_{90}.

Resting potential RP under SR conditions was measured to be -80.8 mV. Under SR+B this was elevated moderately to -80.40 mV indicating possible pro-arrhythmic effects of the application of 4-AP to a cell under SR conditions by increasing the excitability of the tissue. Under both AF and AF+B conditions the RP remains hyperpolarised at -83.9 mV and -83.7 mV respectfully, showing that the blocking of I_{Kur} had a nominal effect when applied to cells which have undergone AFER. The hyperpolarised RP is explained by the

augmentation of I_{k1} which is primarily responsible for the resting potential. These results indicate that AFER reduces the excitability of the atrial cell and the blocking of I_{Kur} has a limited effect.

The maximal upstroke velocity in the SR case was measured to be 217.1 mV/ms. Under AF conditions this was reduced by 5.3% to 205.5 mV/ms. Under SR+B conditions the maximal slope was reduced modestly by 0.4% to 216.2 mV/ms. However in the AF+B case there is no significant change in the value of the upstroke velocity.

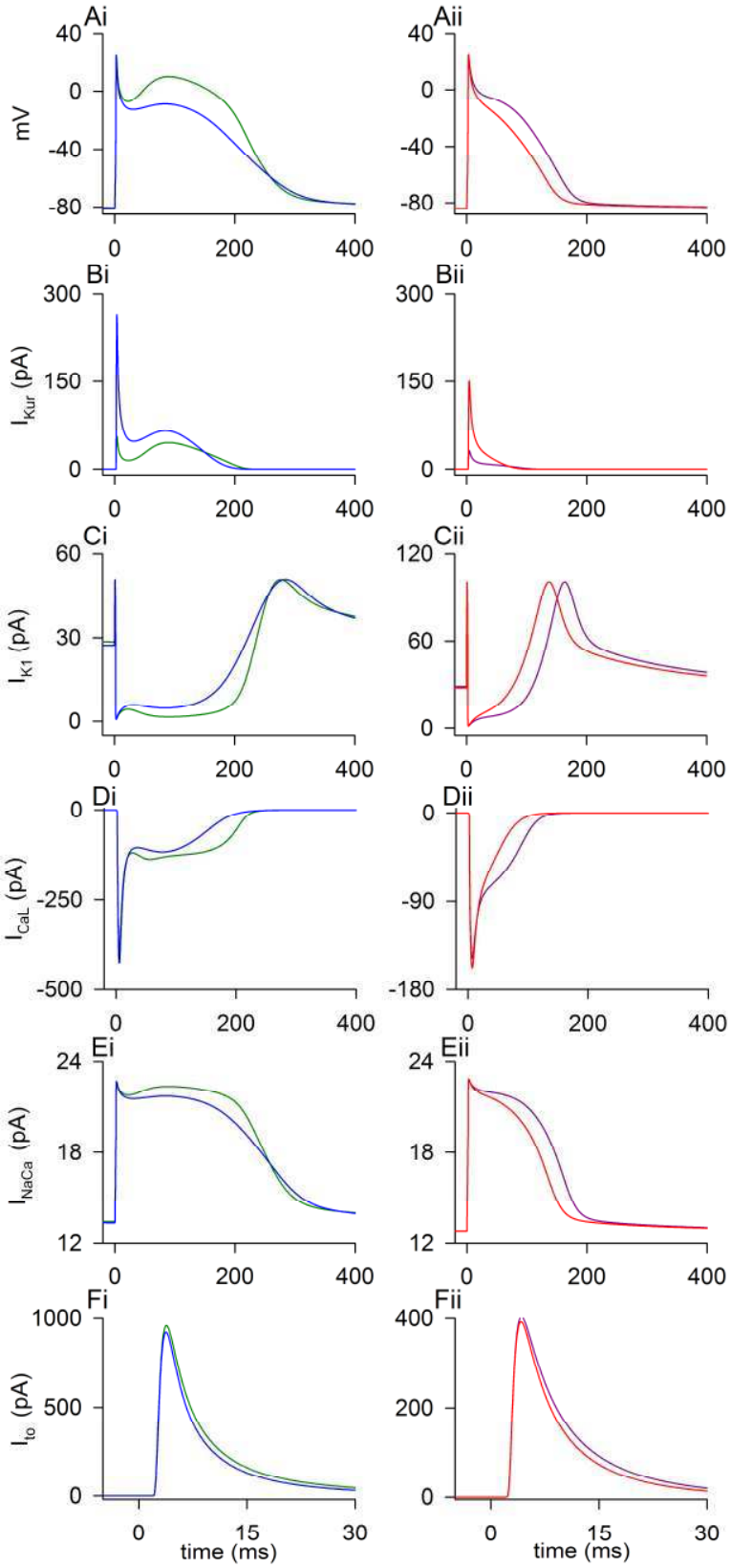

Figure 6.1 Simulated AP profiles and major ionic currents traces for no SR (blue lines), SR+B block (green lines), AF (red lines), and AF+B (purple lines) conditions where Ai, Aii: shows the AP. Bi, Bii: I_{Kur}. Ci, Cii: I_{k1}. Di, Dii: I_{CaL}. Ei, Eii: I_{NaCa}. Fi, Fii: I_{to}.hyperpolarized RP, and elevated plateau-potentials in the early repolarisation phase.

6.3.2 Alterations of APD due to reduction and augmentation of ion-channel conductance

Alterations due to the augmentation and blocking of the major ionic currents under AF and SR conditions can be seen in Figure 6.2. Under SR and AF conditions the measured APD_{90} was 314.2 ms and 155.5 ms respectively. Figure 6.2A shows that the blocking of I_{Kur} up to 70% under SR conditions results in a shortening of APD_{90} by 4.9% to 299 ms. Increasing I_{Kur} by 30% is observed to result in an slight lengthening of APD by 0.6% to 316.2 ms. It is noted that augmenting and blocking I_{Kur} under SR conditions results in minimal alterations in APD_{90} overall. Conversely, under AF conditions the blocking of I_{Kur} results in an augmentation of APD_{90}, where APD_{90} increases until full channel block is achieved. Here the APD_{90} is simulated to be increased by 21.8% from AF conditions to 189.4 ms. The overall effect of modifying I_{Kur} on APD_{90} is therefore much greater than under SR conditions.

Alterations in I_{to} under SR and AF are shown in Figure 6.2B. Under normal SR the augmentation of I_{to} up to 180% results in a lengthening of APD_{90} to a maximum of 381 ms. An increase in I_{to} current density of 180% results in a shortening of APD_{90}. The blocking of I_{to} results in a consistent shortening of APD_{90} until full block is achieved, where the APD_{90} is found to be 276 ms. Under AF conditions a reduction of the current causes a modest lengthening of APD_{90} before reaching a plateau at full block where the APD_{90} is measured to be 158 ms. However, augmentation of I_{to} in the AF case results in a modest but sustained shortening of APD_{90}.

Figure 6.2C show alterations to APD_{90} resulting from alterations to the I_{K1} current. In both cases, SR and AF, an increase in conductance results in a reduction of APD_{90}. However, the blocking of I_{K1} in both cases results in a large increase in the APD_{90}. Blocking of 60% in the SR case results in an APD_{90} of 437.9 ms and blocking on 80% under AF conditions resulted in an APD_{90} of 508.9 ms.

Figure 6.2D show alterations to APD_{90} due to changes in the I_{CaL} conductance. In both SR and AF cases increasing and reducing channel conductance results in a lengthening and shortening of APD_{90} respectfully.

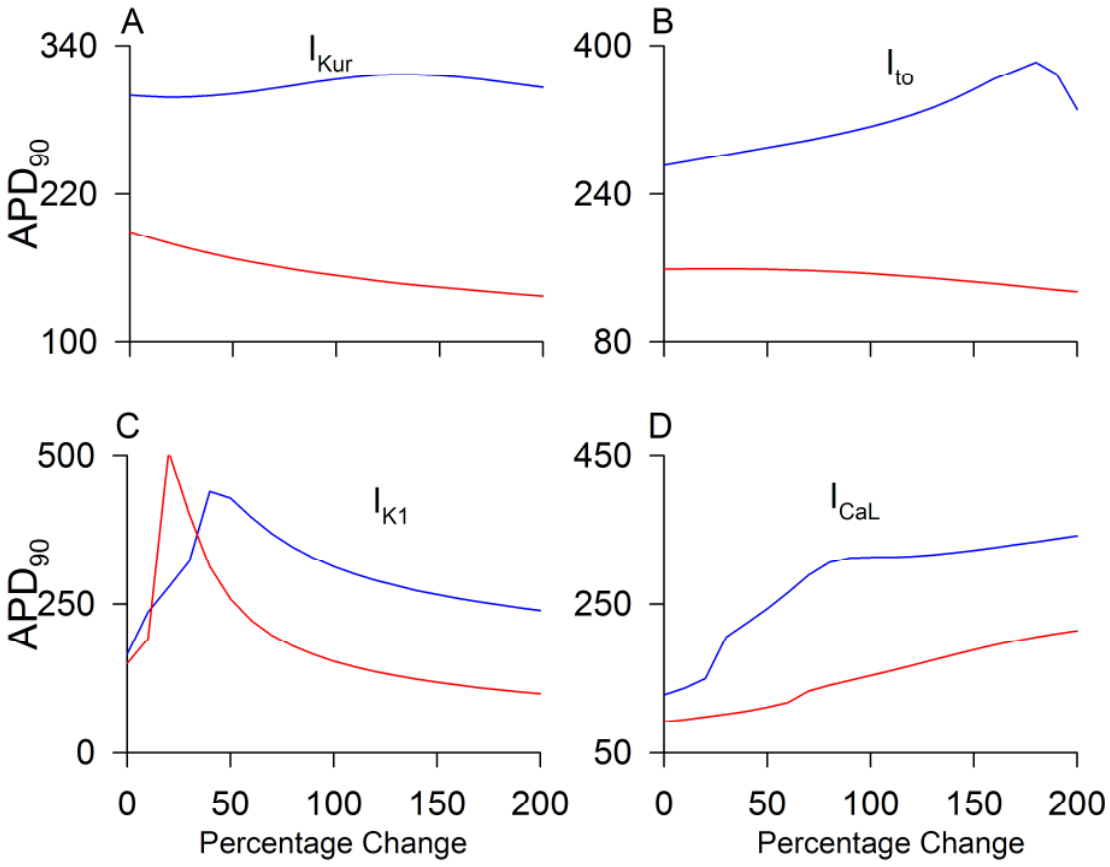

Figure 6.2 Alterations to APD_{90} due to augmentation and blocking of major ionic currents under SR (blue lines) and AF (red lines) cells for A: I_{Kur}, B: I_{to}, C: I_{k1}, and D: I_{CaL}.

6.3.3 The effects of AF and 4-Aminopyridine on APD, ERP, and CV restitution curves

The rate dependant nature of APDr curves can be seen in Figure 6.3A. It is observed that under SR+B conditions at DIs greater then 200 ms the APD_{90} is consistently higher than under SR conditions by approximately 15 ms. At DI shorter than 200 ms the APD_{90} difference between SR and SR+B increases indicating that possible arrhythmogenic effects due to SR+B become more pronounced at high pacing regimes. Under AF conditions the APD_{90} is observed to be significantly shortened from the SR case over the full spectrum of DIs. AF+B conditions result in a consistent lengthening of APD_{90} over all DI in comparison to AF. The lengthening of APD_{90} indicates the anti-arrhythmic effects of the block remain, even in a high pacing regime. The measured maximal slope of the restitution curves are shown in Figure 6.3B.

The rate dependence of the ERP is shown in Figure 6.3C. Under SR conditions the ERP at a PCL of 1000 ms was measured to be 327.9 ms with a cut off PCL of 328.6 ms. Under SR+B conditions the ERP was reduced by 2.5% to 319.8 ms indicating that the addition of the blocking agent increases the susceptibility to AF. However, it is observed that at high PCLs there is a sudden dramatic reduction in ERP and the cut off PCL is measured to be 417.7 ms, 27.1% higher than under SR conditions. This indicates that blocking I_{Kur} under SR conditions provides a possible anti-arrhythmogenic mechanism by limiting the cells' ability to initiate a successful AP in a high pacing regime. Under AF conditions the ERP is reduced to 167.7 ms which is 48.8% shorter than the SR case and the cut off BCL was measured to be 312.0 ms, a 5.1% reduction from the SR case. In the AF+B case the ERP was found to be reduced by 41.0% measuring 193.5 ms and the cut-off BCL was found to be reduced by 19.4% to 265.0 ms. This indicates that the addition of 4-AP under AF conditions reduces the excitability of the tissue by increasing ERP from AF conditions. However, it also increases the cut-off BCL meaning that excitability remains possible in a high pacing regime.

The CVr curves can be seen in Figure 6.3D. At a PCL of 1000 ms the CV under SR and SR+B were measured to be 0.26 mm/ms and CV in the cases of AF and AF+B were measured to be 0.25 mm/ms, indicating that the addition of the block did little to alter the CV at long PCLs. However, the restitution curves in Figure 6.4D illustrate that SR+B results in a shift of the restitution curve in the negative direction, which is an indication of

sustained wave propagation at high pacing rates. This contrasts with the AF+B results that show a shift of the CVr curve in the positive direction from the AF case indicating a loss of excitation at high pacing lengths, suggesting that under AF conditions the blocking of I_{Kur} has an anti-arrhythmogenic effect.

6.3.4 Effects of block on the temporal and spatial vulnerability window

The TVW was calculated using the 1D strand of tissue and is shown in Figure 6.4E. Under SR conditions the VW was measured to be 14.6 ms. Under SR+B conditions the TVW is increased marginally to 14.7 ms. In the AF case the VW is increased by 6.85% to 15.6 ms. However, under AF+B conditions the VW is returned to a slightly reduced value than under SR conditions measuring 14.3 ms. This is an indication that the blocking agent 4-AP is anti-arrhythmogenic when applied under AF conditions.

The SVW as calculated by applying a stimulus to an idealised 2D homogenous sheet is shown in Figure 6.3F. In the SR case the MS required to initiate re-entry was measured to be 49.2 mm. Under SR+B conditions the MS required for re-entry is increased substantially by 58.2% to 77.8 mm. In the AF case the MS is reduced by 22.2% to 17.4 mm. Under AF+B conditions the MS is measured at 45.1 mm, this is still 9% shorter than under SR conditions but is 259% longer than under AF conditions. This indicated that the blocking agent 4-AP is anti-arrhythmogenic when applied to both SR and AF cells. However, the application of 4-AP under AF conditions provides a restorative effect increasing MS to a value closer to SR conditions.

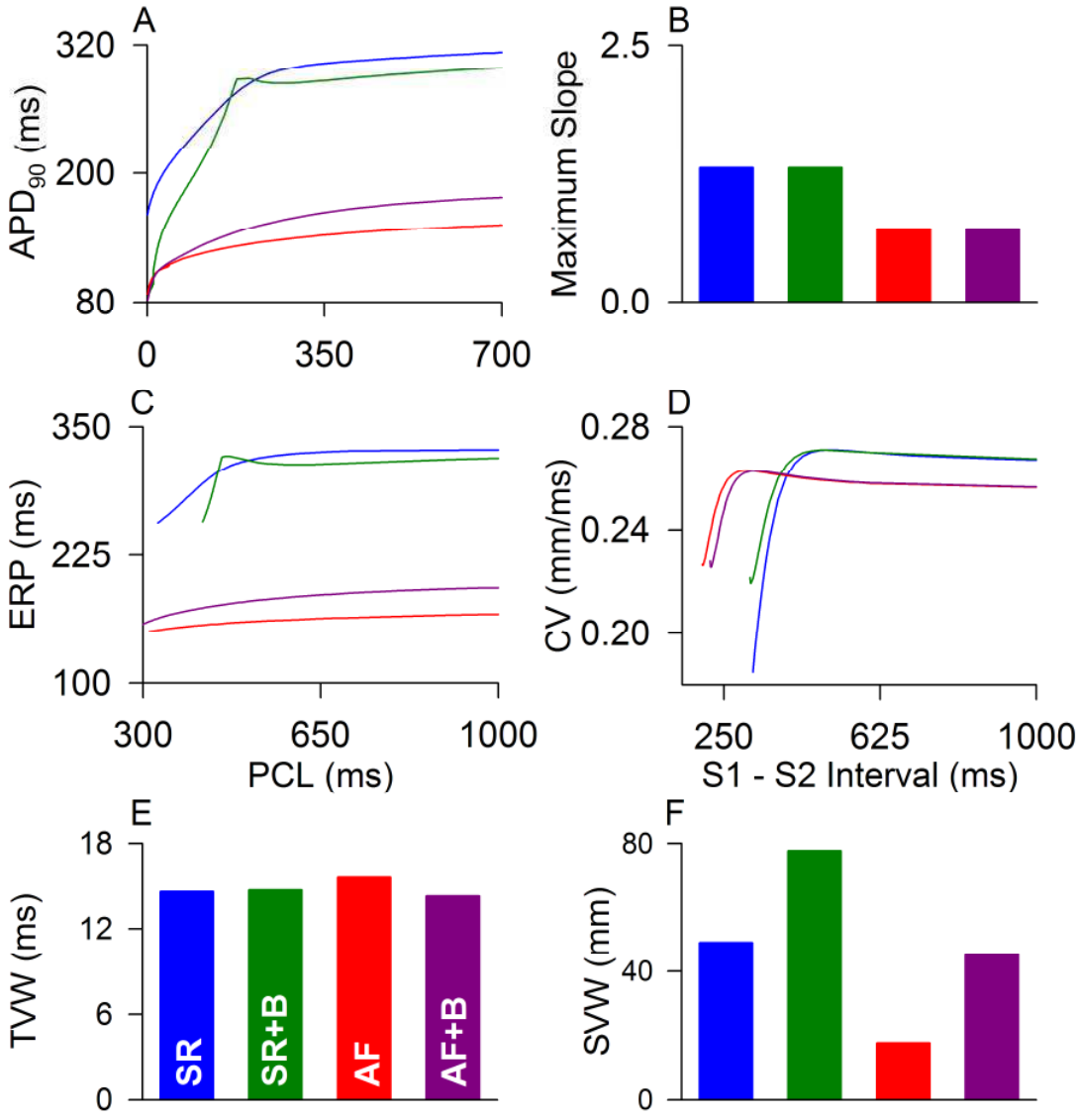

Figure 6.3 Simulated APDr (A), maximal slope (B), ERPr (C), CVr (D), Temporal VW (E), and spatial VW (F) under SR (blue), SR+B (green), AF (red), and AF+B (purple) conditions.

6.3.5 Simulated re-entry in a homogenous 2D sheet of atrial tissue

2D re-entry simulations are shown in Figure 6.4, while spiral tip traces, time-traces, and power density spectrum are shown in Figure 6.5. Under SR conditions the lifespan of the initiated spiral waves is measured to be 1.4 s before the tip of the spiral wave meanders off the 2D sheet. The DF was measured at 3.6 Hz and the tip meander area was 5.25 cm^2. Under SR+B conditions there is a dramatic shortening of lifespan of the spiral wave to 1.0 s and the measured dominant frequency was recorded to be 4.7 Hz. However, the tip meander area is reduced substantially due to the application of the blocking agent 4-AP under SR conditions, although it is important to note that measurements of the tip meander area and DF may be misleading due to the short lifespan of the re-entrant wave. In the AF case the initiated spiral wave persists for the lifetime of the simulation, the dominant frequency increases to 8.1 Hz, and the tip meander area is reduced to 4 cm^2. Under AF+B conditions the addition of 4-AP is observed to result in a failure to breakup the spiral wave in the period of the simulation as it is seen to persist over the lifetime of the simulation. However, the tip meander area is reduced to 1.5 cm^2 which may have important consequences when used in conjunction with surgical intervention in that the ablation area required may be smaller.

6.3.6 3D Simulation of a detailed anatomical correct construct of the atria

3D simulations are shown in Figure 6.6 and corresponding time traces DF are shown in Figure 6.7. Under SR conditions it is observed that the re-entrant waves terminate after 4.2 s and the dominant frequency is measures to be 3.1 Hz. Under SR+B conditions the addition of the blocking agent results in a moderate reduction of LS and DF from SR conditions to 4.1 s and 2.6 Hz respectively. In the AF case the stable spiral wave is born which persists for the lifetime of the simulation and has a dominant frequency of 7.5 Hz. In the case of AF+B the re-entrant wave persists for the period of the simulation and the dominant frequency is also reduced moderately from AF conditions to 6.9 Hz. The anti-arrhythmic property that the addition of the blocking agent has is observed in a reduction of the power of the re-entrant wave.

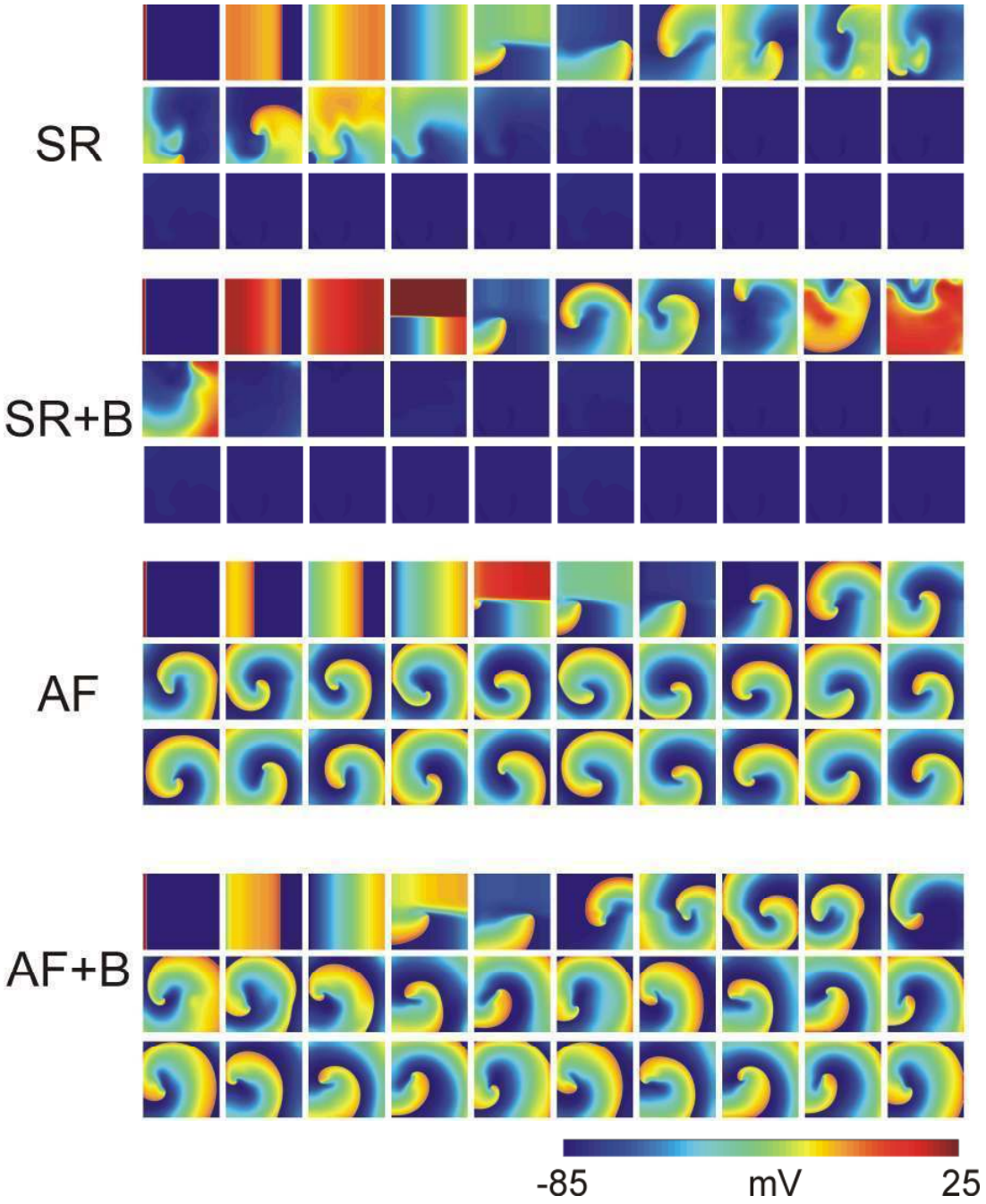

Figure 6.4 Simulation of 2D re-entry in an idealized sheets of virtual atrial tissue under SR, SR+B, AF, and AF+B conditions. Panels show 3 s of simulation starting from 0 ms in the top left panel progressing in 100 ms intervals horizontally from left to right until the bottom right panel.

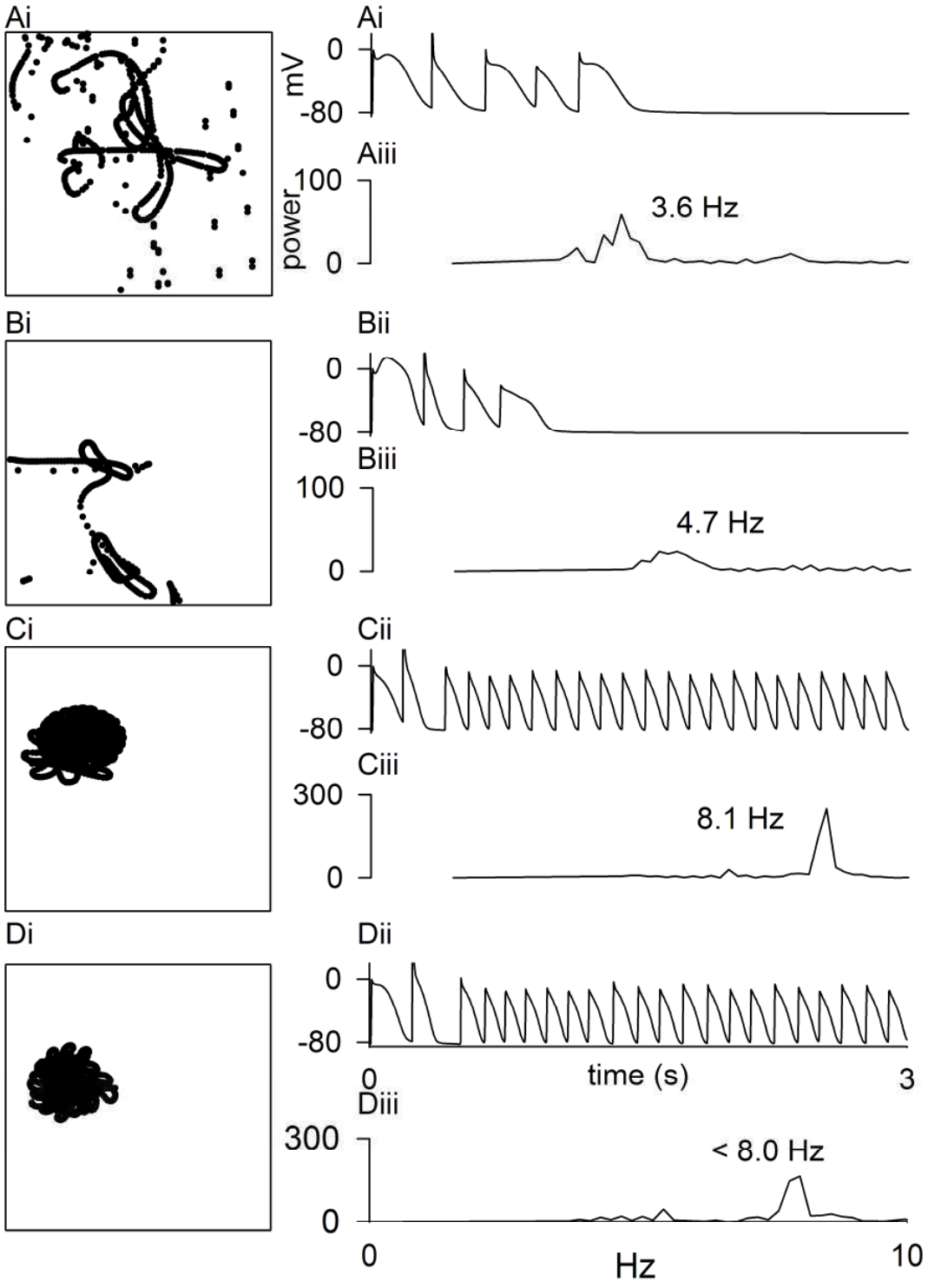

Figure 6.5 2D spiral wave tip traces (panel i), representative AP traces taken from 2D simulations (panel ii), and power spectrum density showing frequencies of maximal power (panel iii) under SR (A), SR+B (B), AF (C), AF+B (D) conditions.

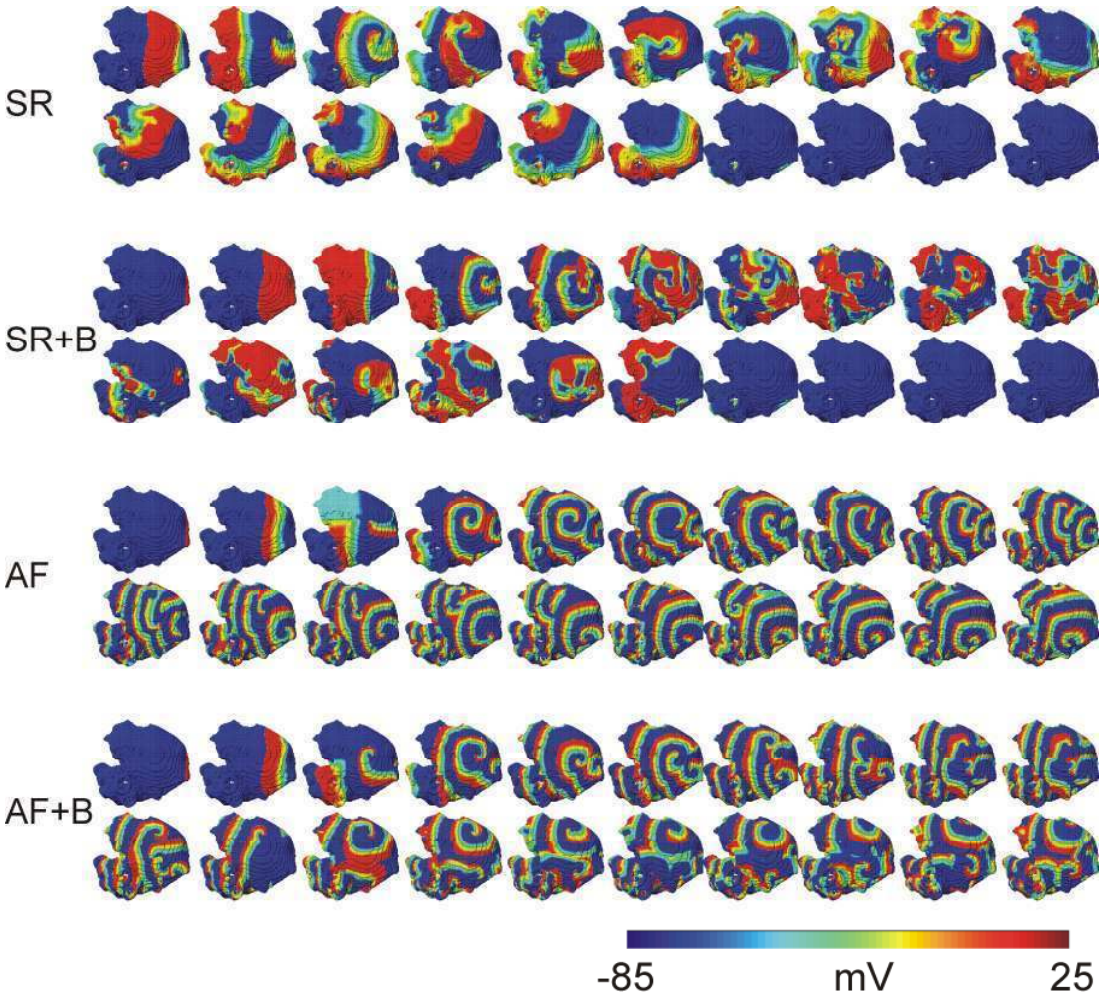

Figure 6.6 Simulation of re-entry in a 3D geometry of the human atria under SR, SR+B, AF, and AF+B conditions. Panels show 6 s of simulation starting from 0 ms in the top left panel progressing at 300 ms from left to right until bottom right panel.

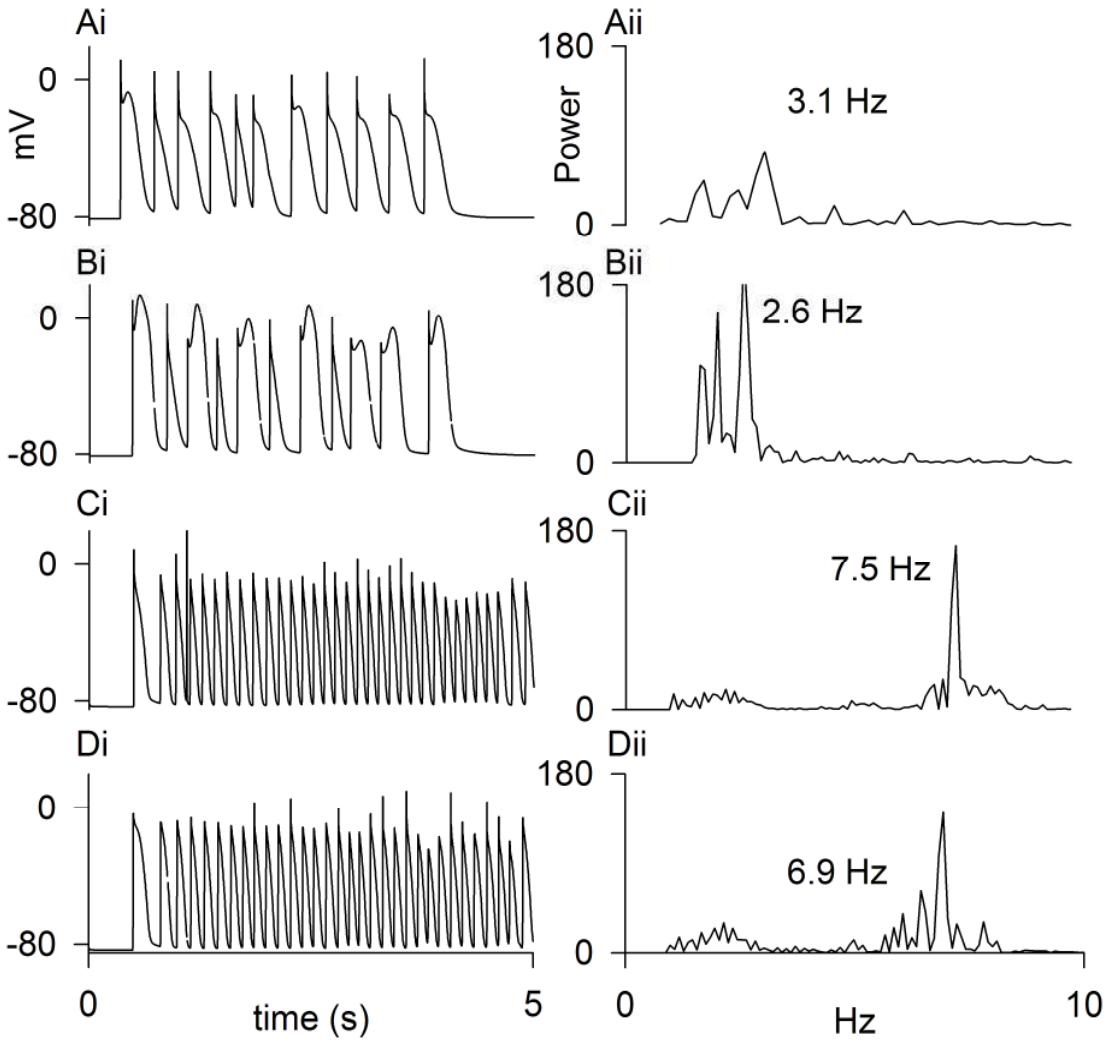

Figure 6.7 AP traces taken from 3D simulations (panel i), and power spectrum density showing frequencies of maximal power (panel ii) under SR (A), SR+B (B), AF (C), AF+B (D) conditions.

6.4 Conclusions and discussion

6.4.1 Main findings

This simulation study indicates that the blocking of the I_{Kur} channel under normal SR conditions results in a reduction of APD and ERP which may enhance the arrhythmogenic effects. However, the blockage of I_{Kur} under AF conditions results in a prolongation of AP causing an increase in ERP. While simulations in the single cell indicate the anti-arrhythmic effects of blocking the I_{Kur} current, the 2D and 3D simulations show that blocking I_{Kur} does not aid in the break-up of re-entrant spiral waves. Blocking I_{Kur} does, however, result in a reduction of the power of the re-entrant waves in both the 2D and 3D simulations. Moreover, in the 2D simulation the tip meander area is reduced substantially. This suggests that the blocking of the I_{Kur} channel via drug intervention alone may not be effective in alleviating the onset of AF, meaning that drug administration in conjunction with surgical intervention may be what is required to increase the probability of a successful treatment.

6.4.2 Limitations of the study

The potential limitations of the Courtemanche *et al.* model used in this study have been discussed previously (Courtemanche, Ramirez *et al.* 1998; Cherry and Evans 2008). A limitation of the 3D simulations is the absence of heterogeneity in the structure of the atria, as the structure only consists of atrial cell types while it is known that cells in different regions of the atria have different electro-physical properties (Seemann, Hoper et al. 2006). Spatial heterogeneities due to fiber orientation are also neglected in the simulations as a uniform diffusion tensor has been implemented.

6.4.3 Clinical significance and comparison to previous studies

Atrial selective drugs which target ion-channels only present in the atria, such as $I_{Kur,}$ provide an attractive target for drug therapy in the treatment of AF without adversely affecting the electrophysiological functions of the ventricles. However, while blocking of the I_{Kur} channel has been shown both experimentally and with simulations to prolong APD in cardiac myocytes which have undergone AFER, current pharmacological agents which

block I_{Kur}, such as Vernakalant and AZD7009, also block the sodium current (I_{Na}).Another agent, AVE0118, also blocks the transient outward current (I_{to}). These result in long term complications if administered for extended periods of time. Our simulations confirm that the blockage of I_{Kur} for patients who have undergone electrical remodelling may limit the occurrence of AF and aid in rhythm control, although this is not effective once a spiral wave has been initiated.

Chapter 7

Simulation of AF in a 2D caricature of a human heterogeneous Atrium

7.1 Introduction

Previous chapters of this thesis have studied how remodelling of ionic currents due to various external factors reduces atrial ERP, thereby increasing the tissues susceptibility to the genesis and maintenance of AF. This was observed in the multi scale simulations as the existence of stable spiral rotors in the homogenous 2D sheet and the detailed 3D anatomical representation of the atria. However, in these simulations the tissue was assumed to be homogenous, both electrically, in term on uniform cell properties, and structurally, in terms of the absence of fibre orientation. In reality the myocardium of the atria consists of multiple regions of differing tissue types each possessing their own distinct electrophysiological properties. In addition to electrical heterogeneities the presence of fibre orientation results in non uniform diffusion of electrical excitation waves, which is manifested as anisotropic wave propagation in the atria. Previously studies have identified that heterogeneities between different cell types in the in atrial tissue are an important factor in re-entrant activity (Coronel, Wilms-Schopman *et al.* 1992; Kumagai, Khrestian et al. 1997; Bernus, Zemlin *et al.* 2005). As heterogeneities within the atria have been ignored previously in this thesis this chapter aims to study their effects on re-entry by performing simulations on a simplified 2D model of the RA.

A 2D atrial sheet was constructed from an image of the RA where regions of differing cell types were identified and simulated by modifying an atrial cell model in accordance with available physiological data. Simple fibre orientation was simulated via the incorporation of a non-uniform diffusion tensor into the 2D diffusion equation (Panfilov and Keener). In addition to studying the effects that electrical and structural heterogeneities play in a healthy heart experimental data on ion channel remodelling due to AFER was incorporated into the cell models allowing for an investigation on the role that heterogeneities play in tissue which has been electrically remodelled due to AF (Bosch, Zeng et al. 1999; Workman, Kane et al. 2001).

7.2 Methods

In this methods section alterations to an atrial cell model to simulate the electrophysiology of the multiple cell types found in the atria and the ionic changes as a result of AFER based on experimental data from Workman *et al.* and Bosch *et al.* are also described. In addition, the construction of an electrically and spatially homogenous 2D atrial geometry, which was developed in our lab, is also outlined.

7.2.1 Construction of different cell types and alterations due to AFER

As in previous chapters the biophysically detailed human atrial cell model developed by Courtemanche *et. al.* (Courtemanche, Ramirez et al. 1998) was chosen for this study. The three main cell types found in the human atrium namely, Crystal Terminalis (CT), Pectinate Muscle (PM), and Atrial Cells (AT) were constructed by modifying the CRN model in accordance with experimental data (Seemann, Hoper et al. 2006). The ionic changes due to cell types are summarized in Table 7.1. In brief the changes are in PM muscle g_{CaL} is increased minutely from 0.012375 nS/pF to 01238 nS/pF. In CT g_{to} is increased 30.2% from 0.1625 nS/pF to 0.2115 nS/pF and gCaL is increased 67.0% from 0.12375 nS/pF to 0.2067 nS/pF. Each of these cells types were further modified in accordance with a previous study to incorporate AFER from a period of 1 (Bosch) and 6 (Workman) months (Bosch, Zeng et al. 1999; Workman, Kane et al. 2001). The ionic channel remodelling in Bosch is by modeled by a 235% increase in I_{K1}, 74% down regulation of $I_{Ca,L}$, 85% down regulation of I_{to}, a shift of -16 mV in the I_{to} steady-state activation, and a -1.6 mV shift of sodium current (I_{Na}) steady state activation. Fast inactivation kinetics of I_{CaL} is slowed down, and was implemented as a 62% increase in the time constant. The ionic channel remodelling in Workman is simulated by a 90% increase in the inward rectifier potassium current (I_{K1}), 64% down regulation of the L-type calcium current ($I_{Ca,L}$), 65% down regulation of the transient outward current (I_{to}), 12% up regulation of the sustained outward potassium current (I_{Ksus}), and a 12% down regulation of the sodium potassium pump ($I_{Na,K}$). The effects of these electrophysiological changes have on the properties of the cell are quantified through single cell and 1D simulations as outlined in Chapter 1.

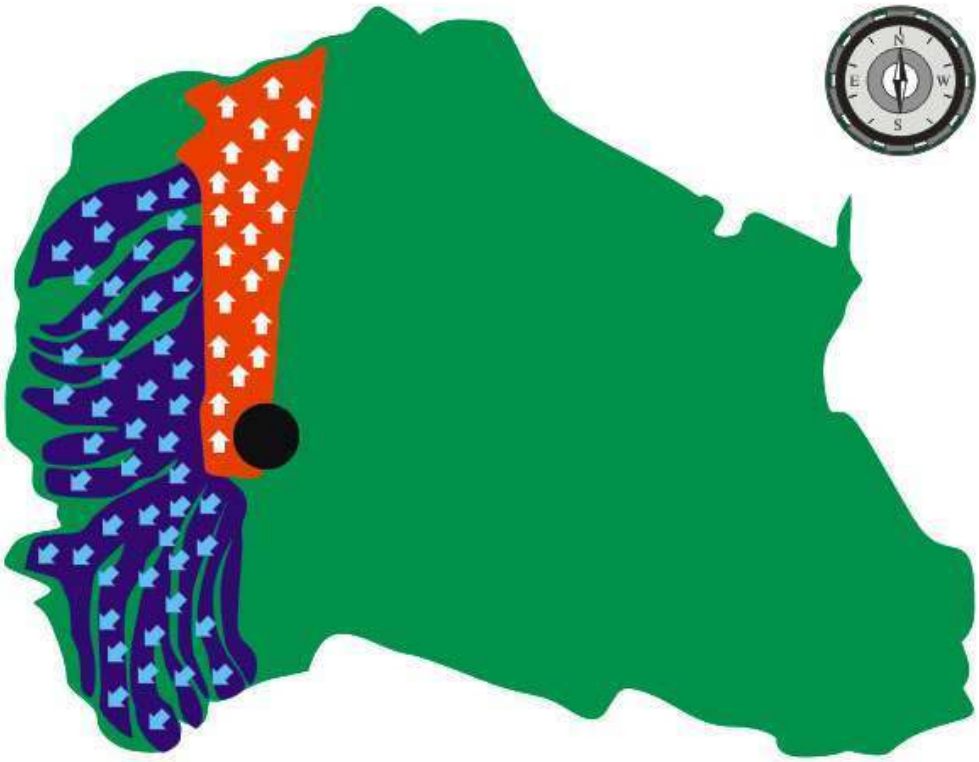

Figure 7.1 Schematic of the 2D atria showing the location AT cells (green), CT cells (red), and PM cells (blue), and the approximate location of the SA node in indicated as a black circle. Fiber orientation is represented by arrows. The fiber orientation is indicated by arrows, in AT tissue there is no fiber orientation, in CT tissue the fiber orientation in runs north to south, and in PM the fiber orientation as running south-west to north-east.

7.2.2 Construction of 2D geometry to simulate re-entry

To simulate the spatial heterogeneity of cell types within the RA a laboratory photograph of the RA was digitised at a spatial resolution of 0.1 mm. The constructed 2D sheet is shown in Figure 7.1. Different cell types were identified via visual inspection and thus the image was segmented into the distinct tissue types AM, PM and CT. Fibre orientation is assumed to be uniform in the AT tissue, running north to south in CT tissue, and north east to south west in PM tissue. The complete 2D sheet has a size of 130 x 100 mm and consisted of approximately 1 million active grid points. Propagation of action potential across the 2D sheet was calculated using the diffusion equation as shown in Equation 1.3. Incorporating a non-uniform diffusion tensor in to the 2D diffusion equation simulates fiber orientation. This tensor is altered depending on the fibre orientation of the region in which the cell is located (Panfilov and Keener).

7.2.3 2D Simulation and initiation of re-entry with an ectopic beat

To study the effects of electrical and spatial heterogeneities on re-entry four different 2D simulation setups were constucted, electrically and spatially homogenous (Hom-Hom), electrically heterogeneous and spatially homogenous (Het-Hom), electrically homogenous and spatially heterogeneous (Hom-Het), and electrically and spatially heterogeneous (Het-Het). Re-entry was initiated with a S1-S2 stimulation protocol which is shown in Figure 7.2 where an initial circular stimulus was applied with a radius r and stimulation strength 2 nS/pF for duration of 2 ms at the approximate location of the SA node. After a short delay a second stimulus S2 with a similar size and strength is applies close to the site of the S1 stimulus to initiate re-entry; simulations were performed for duration of 6 s.

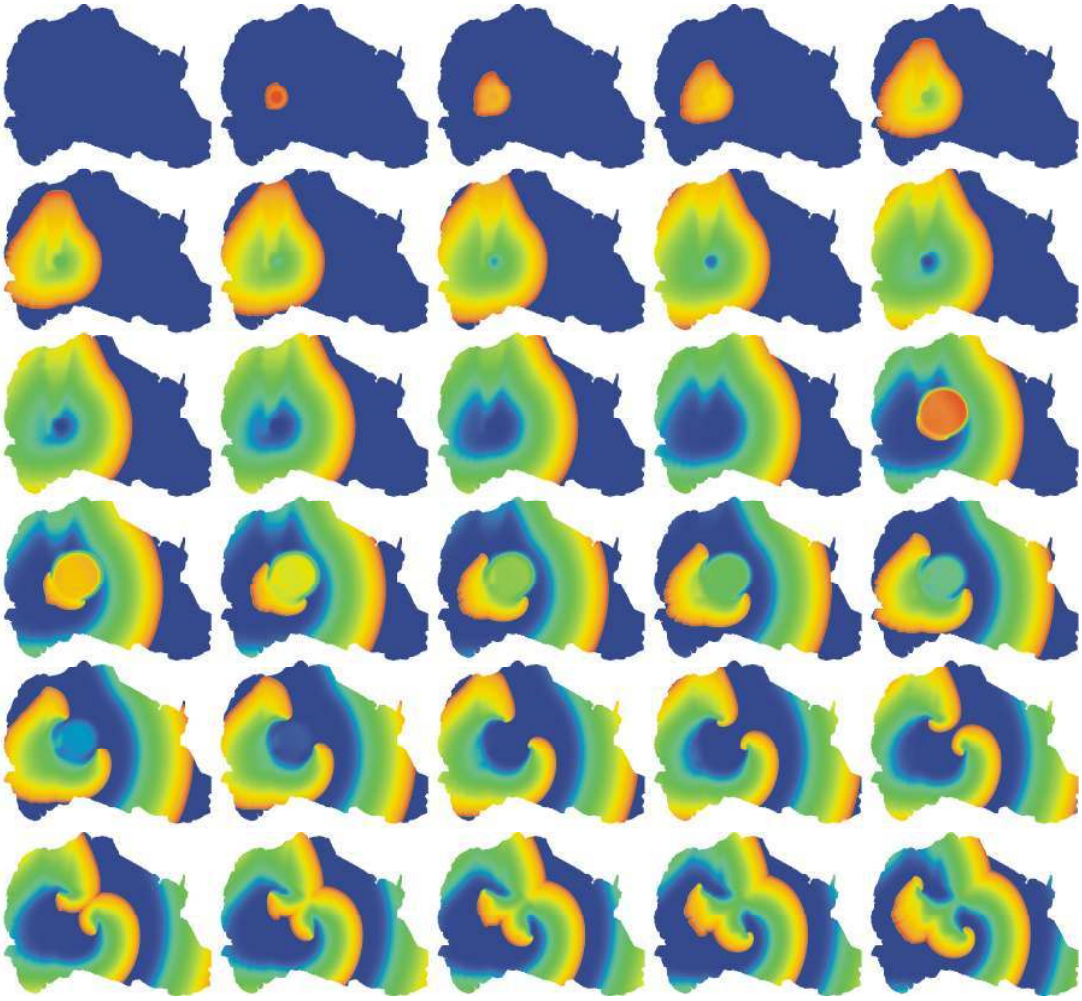

Figure 7.2 Stimulation protocol to initiate re-enrty in an electrically and spatially heterogeneous 2D construct of the RA. Snapshots of re-enrty protocol begin in the top left hand corner and progress in consecutive rows from left to right. An initial circular stimulus (S1) located near the location of the SA node is applied, a time later (ΔT) a second stimulus (S2) of similar size and strength is applied initiated to simulate an ectopic beat.

Table 7.1 Alterations to CRN parameters to simulate AT, PM, and CT cells under Control, Bosch, and Workman conditions

	AT			PM			CT		
Parameter	Control	Bosch	Workman	Control	Bosch	Workman	Control	Bosch	Workman
g_{to} (nS/pF)	0.1652	0.0248 (85% ↓)	0.0578 (65% ↓)	0.1652 (0%)	0.0248 (85% ↓)	0.0578 (65% ↓)	0.2115 (28% ↑)	0.0317 (80.8% ↓)	0.0740 (55.2% ↓)
g_{CaL} (nS/pF)	0.1238	0.0322 (74% ↓)	0.0446 (64% ↓)	0.1238 (0%)	0.0322 (74% ↓)	0.0446 (64% ↓)	0.2067 (67% ↑)	0.0537 (56.6% ↓)	0.0744 (39.9 %↓)
g_{K1} (nS/pF)	0.09	0.3015 (235%↑)	0.1710 (90% ↑)	0.09 (0%)	0.3015 (235%↑)	0.1710 (90% ↑)	0.09 (0%)	0.3015 (235%↑)	0.1710 (90% ↑)
g_{Kur}* (nS/pF)	g_{Kur}	g_{Kur}	1.12*g_{Kur}	g_{Kur}	g_{Kur}	1.12*g_{Kur}	g_{Kur}	g_{Kur}	1.12g_{Kur}
I_{NaK} (max) (nS/pF)	0.06	0.06 (0%)	0.0528 (12% ↓)	0.06	0.06 (0%)	0.0528 (12% ↓)	0.06	0.06 (0%)	0.0528 (12% ↓)
$I_{to\text{-}act\text{-}shift}$	0	- 16	0	0	-16	0	0	-16	0
$I_{na\text{-}act\text{-}shift}$	0	-1.6	0	0	-1.6	0	0	-1.6	0
τ_f	τ_f	τ_f	0.38τ_f	τ_f	τ_f	0.38τ_f	τ_f	τ_f	0.38τ_f

7.3. Results of multi-scale simulations

This section describes how alterations to ion channel kinetics due to differing cell types and AFER alter the behaviour of cell and provides measurements which indicate the cells susceptibility to the onset of AF at a single cell and 1D level, a summary of which is shown in Table 7.2. Simulations showing the results of incorporating electrical and spatial heterogeneities into the 2D atrial sheet are also described.

7.3.1 Single cell simulations

AP profiles and calcium transients for AT cells can be seen in Figure 7.3Ai and 7.3Aii respectfully. Under Control conditions the APD_{90} is measured to be 312.9 ms. This is reduced drastically under Workman conditions to 147.6 ms (52.8% reduction) and is further reduced in the Bosch case to 108.5 ms (65.3% reduction). PM cells APD_{90} is similar to that of AF due to their similar electrophysiology. For CT cells under Control conditions the APD_{90} was measured to be 333.1 ms which is a prolongation of 6.4% compared to the AT Control case. Under Workman conditions the APD_{90} is shortened to 181.0 ms (45.6% reduction) and 136.6 ms (41.0% reduction) for Bosch conditions. These results indicate that AFER is arrhythmogenic due to the shortening of APD. However, it is noted that reductions to APD_{90} for CT cells result in a less dramatic shortening of APD_{90} which indicated CT cells may be more resistant to the genesis of AF than its AT and PM cell counterparts.

The RP for AT cells under Control conditions is measure to be -81.2 mV. AFER results in a hyperpolarized RP from -83.9 mV (3.8% reduction) under Workman conditions and (5.4% reduction) to -85.2 mV for Bosch conditions. PM cells show similar alterations as AT cells due to near identical electrophysiology. CT cells under SR conditions have in a hypo-polarised RP of -80.3 mV (1.1% increases) compared to AT cells under Control conditions. Under AFER conditions for Workman and Bosch conditions the RP are measured to be -83.8 ms (6.2% reduction) and -85.2 mV (6.2% reduction) respectfully. These results show that under SR conditions the CT cells have a hypopolarised RP which increases the cells excitability to stimulus. However, for cells which have undergone AFER there is little difference in RP between cell types.

For AT cells under SR conditions the dV/dt_{max} was measured to be 217.1 mV/ms. In cells which have undergone AFER the dV/dt_{max} for Workman and Bosch cells was found to be

206.66 mV/ms (4.8% reduction) and 205.56 mV/ms (5.3% reduction) respectfully. The PM cells show similar results due to near identical electrophysiology. In CT cells under conditions the dV/dt_{max} was measured to be 215.23 mV/ms; a modest reduction from the AT cell SR case of 0.8%. However, in the AFER CT cell dV/dtmax remained similar in value to AT cells measuring 206.6 mV/ms and 205.52 mV/ms for Workman and Bosch respectfully.

Table 7.2 Summary of quantitative results for AT, PM, and CT cells under Control, Bosch, and Workman conditions

		AT			PM			CT		
Model	Quantity	Control	Workman	Bosch	Control	Workman	Bosch	Control	Workman	Bosch
Cell	Resting potential (mV)	-81.2	-83.90	-85.23	-81.2	-83.90	-85.23	-80.25	-83.84	-85.20
	APD_{90} (ms)	312.9	147.63	108.53	312.9	147.65	108.55	333.09	181.01	136.64
	Overshoot (mV)	24.8	25.01	24.88	24.8	25.01	24.88	24.86	25.10	24.91
	dV/dt_{max} (mV/ms)	217.1	206.66	205.65	217.1	206.66	205.65	215.23	206.59	205.52
	APDr maximal slope	1.3	1.7	4.1	1.3	1.7	4.1	1.6	2.3	4.9
	ERP (ms) (stimulus interval ~ 1 s)	327.9	165.1	122.1	327.9	165.1	122.1	344.0	189.2	146.0
	ERP cut off (ms)	324	163	110	324	163	110	329	193	132
1D	CV (mm/ms)	0.266	0.255	0.247	0.266	0.255	0.247	0.267	0.255	0.247
	CVcut off (ms)	303.5	184.4	142.7	303.6	184.4	142.7	318.5	209.8	161.7
	VW (ms)	14.6	12.9	12.5	14.6	12.9	12.5	13.3	12.8	12.7
	Wavelength (mm)	83.2	37.6	26.8	83.2	37.6	26.8	88.9	46.2	33.8

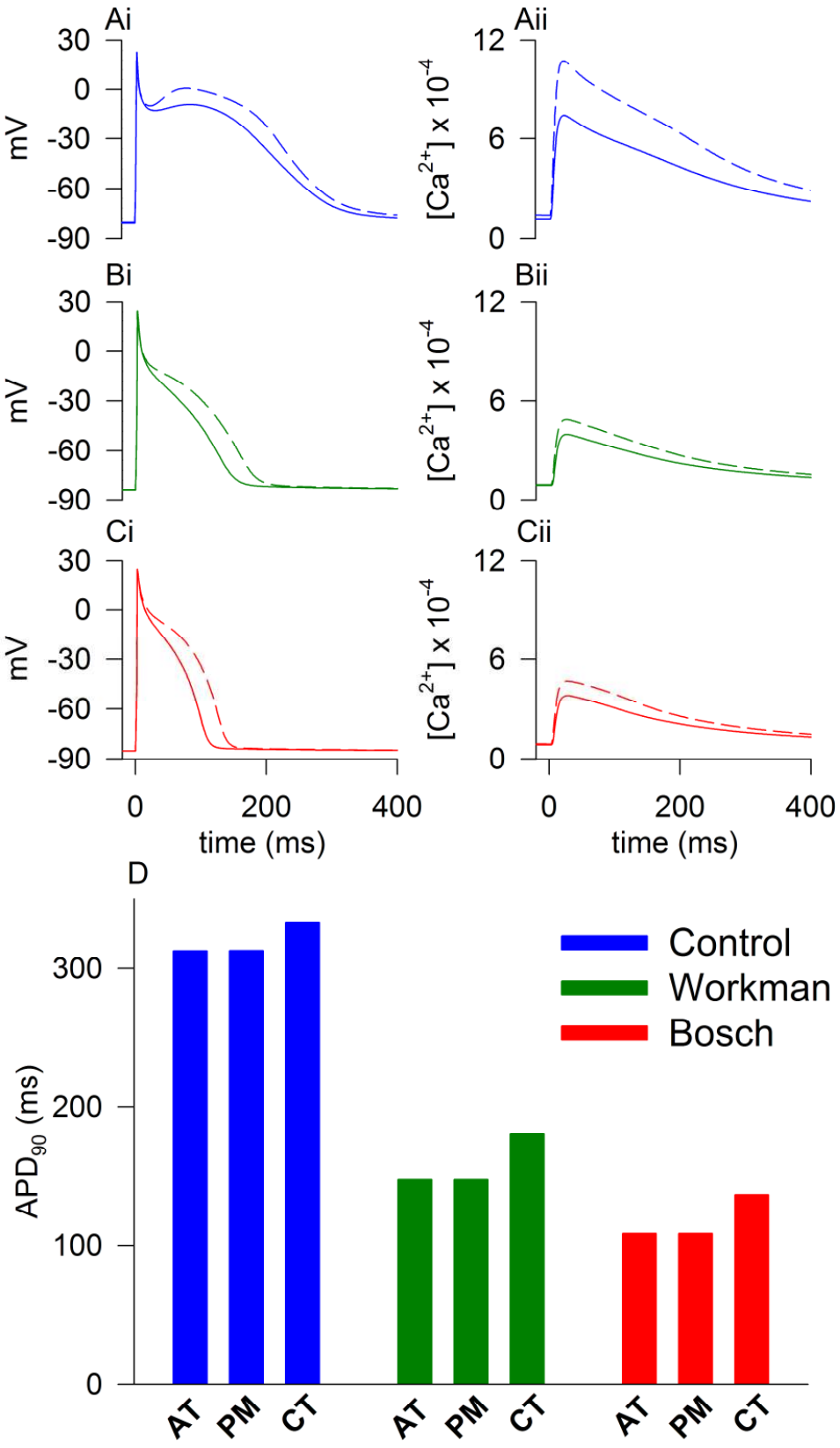

Figure 7.3 Simulated AP profiles and calcium transient current traces where Ai: Control AP profile. Aii: Control Ca^{2+} current trace. Bi: Workman AP profile. Bii: Workman Ca^{2+} current trace. Ci: Bosch AP profile. Cii: Bosch Ca^{2+} current trace. D: Bar chart showing APD_{90} for AT, PM, and CT under Control, Bosch, and Workman conditions.

7.3.2 APD, ERP, and CV restitution curves

APDr curves in Figure 7.4A show that for AT cells the APD is reduced over the full spectrum of DI when the cells undergo AFER cases, it is also noted that under Bosch conditions the APD_{90} is reduced still further over the range of measured DIs. For PM cells the restitution curves are not visible as they lie beneath the AT cell curves due to their similar electrophysiology. For AT and PM cells the maximal slope under SR conditions is measured to be 1.3, under Workman conditions this is increased by 66.9% to 1.7 and for Bosch still further by 413.1% to 4.1. For CT cells the maximal slope under SR conditions was 1.6, a 61.5% increase from the AT SR case. Under Workman conditions this increased by 42.9% to 2.3 and further increased by 305.7% to 4.9 in the Bosch case. An increase in maximal slope indicates that a stable spiral wave is more likely to manifest its self indicating the tissues increased susceptibility to AF. If is observed that the AFER increased the maximal slope substantially in the remodeled cells of Bosch and Workman. However, the ionic changes to model the electrophysiology of the CT cell under SR conditions result in an increased maximal slope, this suggests that tissue constructed of CT cells will be able to sustain re-entry.

ERPr curves are shown in Figure 7.4B. Workman conditions result in a leftward shift of the curves indicating increased excitability at higher pacing frequencies, Bosch conditions result in a greater shift that Workman indicating Bosch further increases excitability at even higher pacing lengths. For AT and PM cells under SR conditions the ERP is measured to be 327.9 ms. For CT cells this is increased by 5.0% to 344.0 ms. Under Workman conditions the EPR for AT and PM cells is reduced from Control conditions by 49.6% to 165.1 ms and 42.2% to 189.2 ms for CT cells. In the Bosch case the ERPs are reduced further where AT and PM are reduced by 62.7% to 122.1 ms and CT was reduced by 55.4% to 146.0 ms. Reductions in ERP due to AFER indicate the tissues ability to maintain wave propagation in a high pacing regime. It is also noted that changes to the electrophysiology of CT cells increases the ERP modestly therefore may provide conduction block in a high pacing regime. The EPR curve cut off points also shows a leftward shift further indicating that the cell had increased ability for maintaining wave propagation in a high pacing regime due to AFER. There was a modest shift in cut off ERPs in CT cells which may also provide conduction block in a high pacing regime.

The CVr curves are shown in Figure 7.4C. For AT, PM and CT cells the CV at PCL of 1000 ms under SR conditions was measured to be 0.266 mm/ms, under Workman conditions this is reduced by 4.1% to 0.255 mm/ms, and in the Bosch case the CV is

further reduced by 7.1% to 0.247 mm/ms. These results indicate that AFER reduced the CV of wave propagations which therefore reduces the wavelength at which the tissue can sustain a re-entrant circuit increasing the ability of the tissue to sustain re-entrant waves. However, in a low pacing regime it was noted that there is no difference between the various cell types. For AT and PM cells the electro physical change due to AFER result in a leftward shift of the CVr curve. Under SR condition the cut off PCL was measured to be 303.5 ms, under Workman conditions this was shifted leftward by 39.2% to 184.4 ms, and further still in the Bosch case by 52.9% to 142.7 ms. For the CT cells under SR conditions the cut of PCL is measured to be 318.5 ms, this is a shift in the positive direction of 4.9% when compared to the cut off PCL of AT cells. Under Workman conditions CT cut off PCL is measured to be 209.8 ms, this is a shift in the positive direction of 13.7% when compared to the cut off PCL of AT cells under Workman condition. Under Bosch conditions CT cut off PCL is measured to be 161.7 ms, this is a shift in the positive direction of 13.3% when compared to the cut off PCL of AT cells under Bosch condition. This left ward shift of CVr curves indicate the possibility of AF genesis as the tissues increased its ability of wave propagation in a high pacing regime. Interestingly, electrophysical changes due to the CT cells result in a rightward shift of the CVr curves for cells which have undergone AFER.

The TVW shown in Figure 7.4D for AT and PM cells under SR conditions was measured to be 14.6 ms. Under Workman conditions the VW is reduce by 11.4% to 12.9 ms. This is further reduced under Bosch conditions by 14.5% to 12.5 ms. The TVW for CT cells under SR conditions was 13.3 ms which is 9.0% shorter than the AT SR case. Under Workman conditions TVW is 12.8 ms, a reduction 4.0% from SR CT case. In the Bosch case the TVW is further shortened by 4.6% to 12.7 ms.

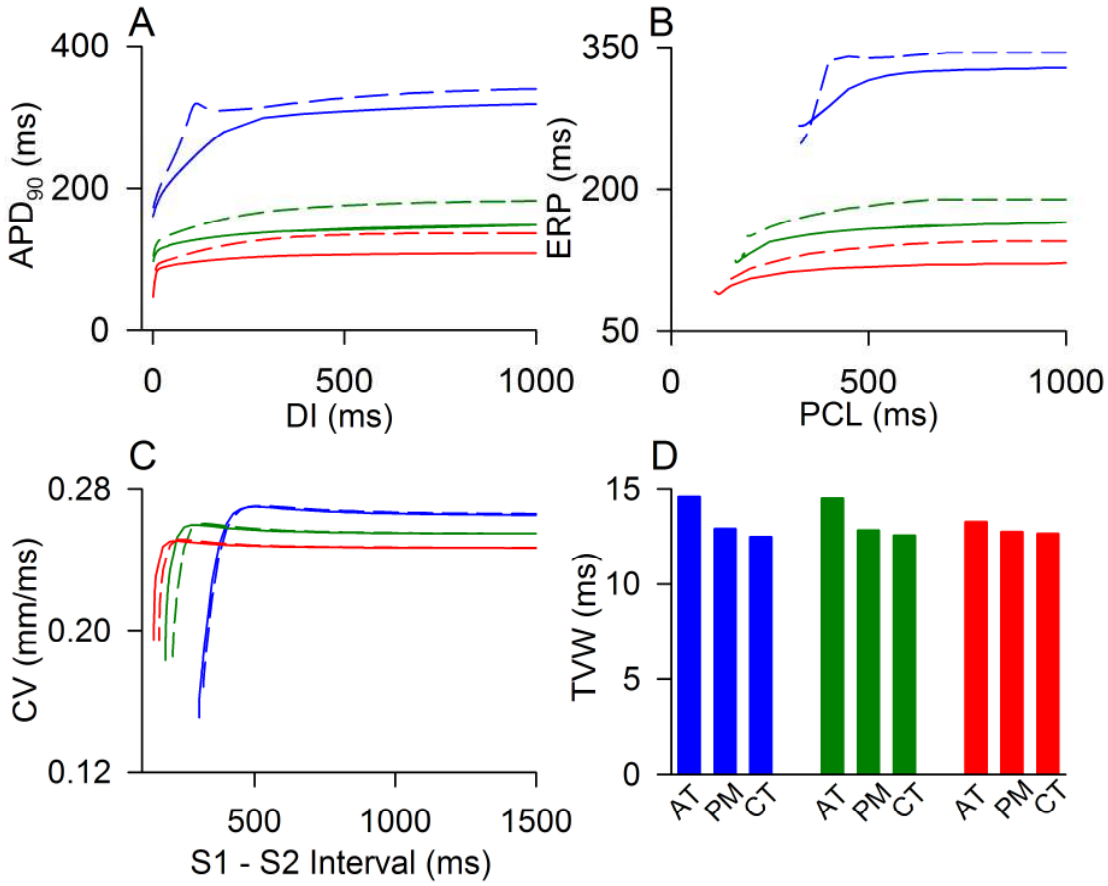

Figure 7.4 Simulated restitution curves for AT (solid lines), PM (dotted lines), and CT (dashed lines) cells under Control (blue lines), Workman (green lines), and Bosch (red lines) conditions where (A) shows APDr curves. (B) Shows ERPr curves. (C) Shows ERPr curves. (D) Shows TVW.

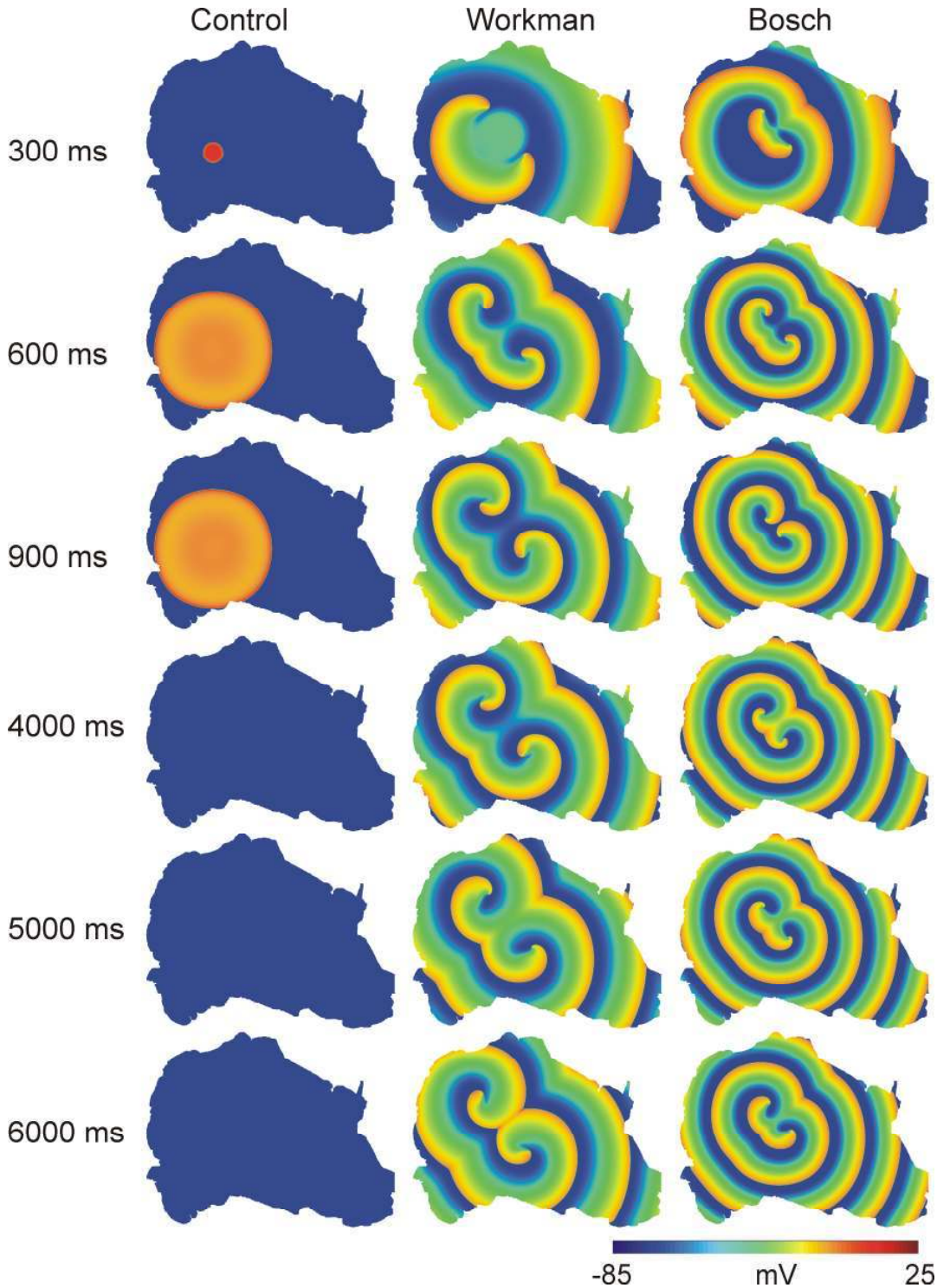

Figure 7.5 Shows snapshots from electrically and spatially homogeneous 2D atrial sheet simulations consisting of only AT cells at time steps of 300 ms, 600 ms, 900 ms, 3000 ms, 4000 ms and, 5000 ms under Control, Bosch, and Workman conditions.

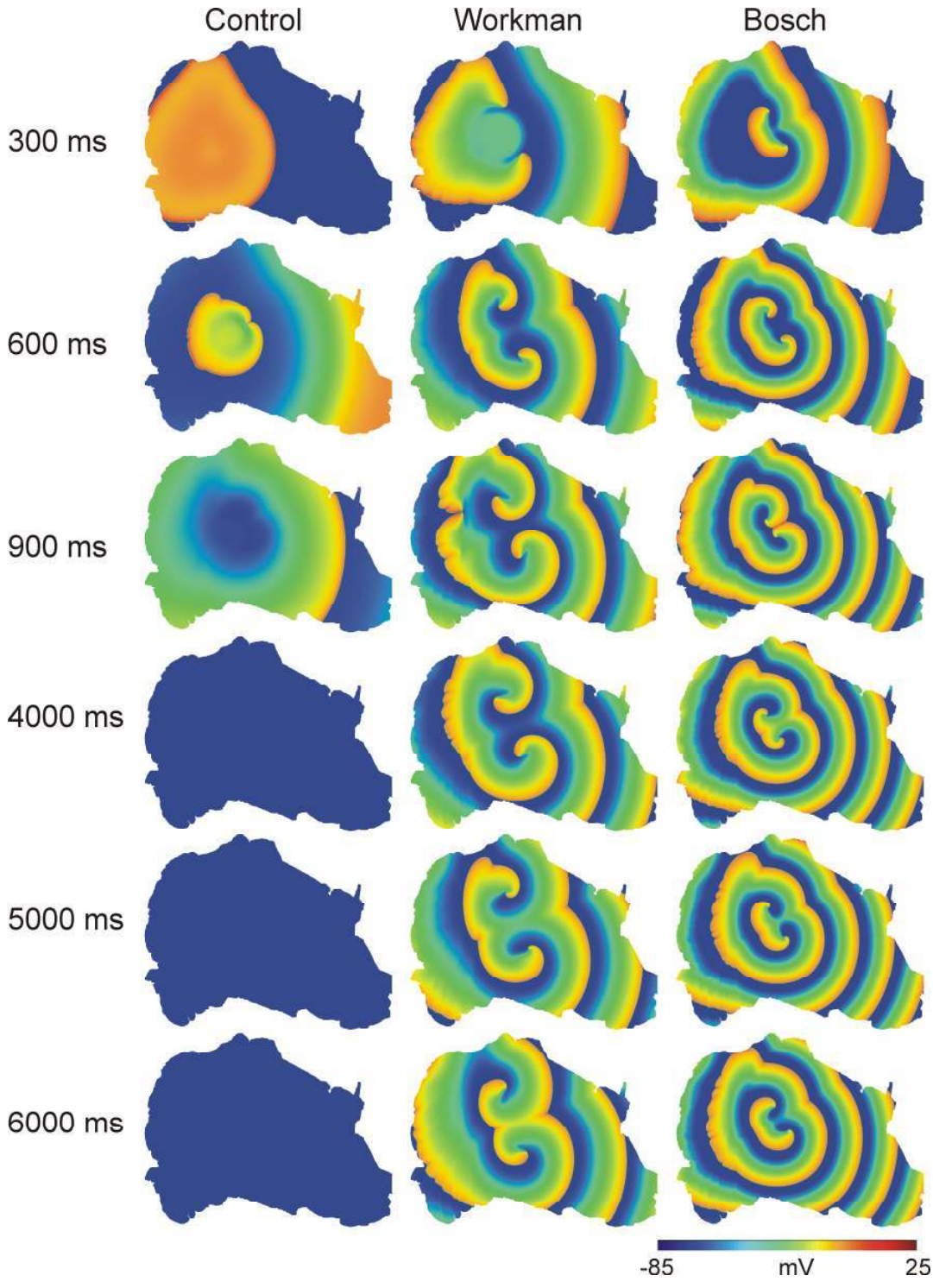

Figure 7.6 Shows snapshots from electrically homogeneous and spatially heterogeneous 2D atrial sheet simulation where only AT cells are present but with fiber orientation in included at time steps of 300 ms, 600 ms, 900 ms, 3000 ms, 4000 ms and, 5000 ms under Control, Bosch, and Workman conditions.

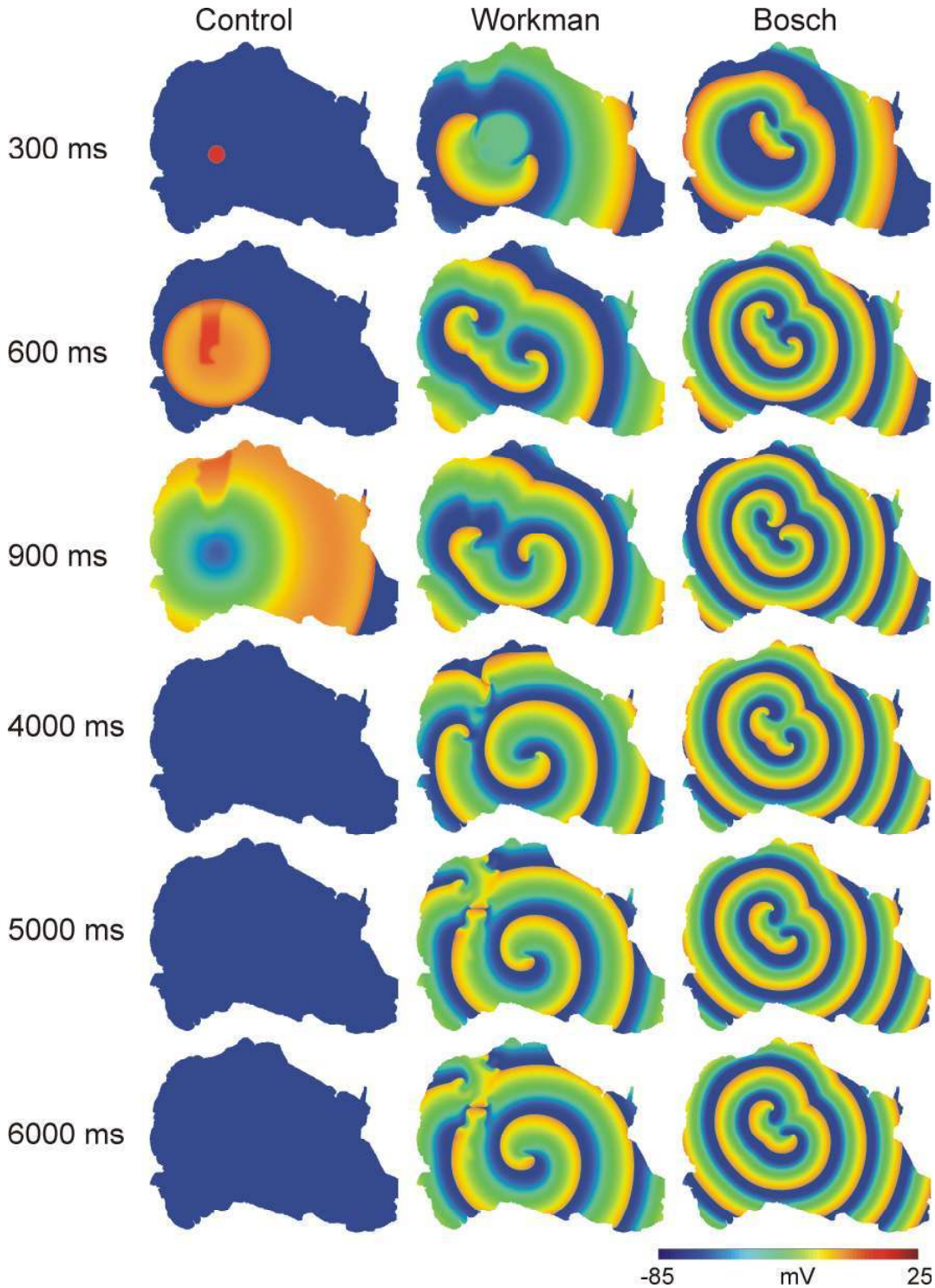

Figure 7.7 Shows snapshots from electrically heterogeneous and spatially homogenous 2D sheet simulation where the atrium consisting of AT, CT, and PM cells and fiber orientations included at time steps of 300 ms, 600 ms, 900 ms, 3000 ms, 4000 ms and, 5000 ms under Control, Bosch, and Workman conditions.

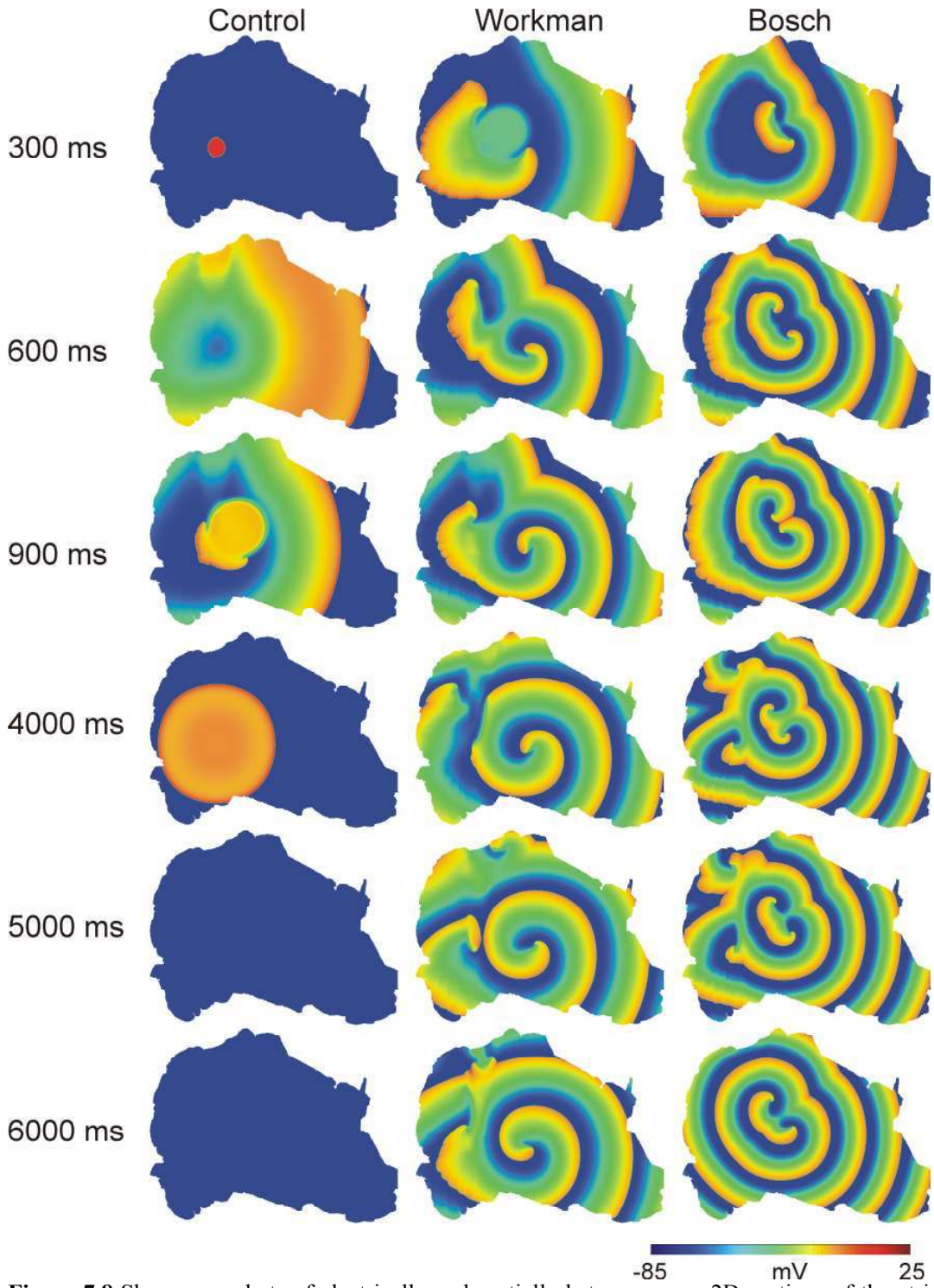

Figure 7.8 Shows snapshots of electrically and spatially heterogeneous 2D sections of the atrium consisting of AT, CT, and PM cells and with fiber orientation incorporated at time steps of 300 ms, 600 ms, 900 ms, 3000 ms, 4000 ms and, 5000 ms under Control, Bosch, and Workman conditions.

7.3.3 2D atrial sheet simulations

Simulations performed on a 2D atrial sheet under a combination of electrical and spatial heterogeneities are shown in Figures 7.6-9 and associated power spectrums are shown in Figure 7.9. Electrically and spatially homogenous simulations where the 2D atrial construct consists of only AT cells are shown in Figure 7.5. Under Control conditions the ectopic beat fails to initiate persistent re-entry. In both Workman and Bosch cases the ectopic beat initiates stable re-entrant waves which persist for the duration of the simulation (6 s). Tissue simulations for electrically homogenous and spatially heterogeneous where the tissue consists of only atrial cells are shown in Figure 7.6. In the Control case the initiation of the ectopic beat again fails to initiate re-entry. In Workman and Bosch cases stable spiral waves are born which persist for the period for the period of the simulation. It is observed that the fiber orientation present in the PM result in a non uniform wave propagation, again this effect is most noticeable in the Bosch case. Tissue simulations for electrically heterogeneous and spatially homogenous are shown in Figure 7.7. In the Control case the ectopic beat fails to initiate re-entry but and re-enrty is observed to be born and persists in the Workman and Bosch cases for the duration of the simulation. It is observed that the boundary between AT can CT results in multiple wavelets being born. Tissue simulations for electrically heterogeneous and spatially heterogeneous are shown in Figure 7.8. Heterogeneities in the SR conditions aid spiral wave break up. However these heterogeneities in the AF cases result in multiple spiral wavelets being born due to fiber orientation and difference in cell properties. In conclusion it is observed that heterogeneities present in the RA may aid in the termination of AF when the cells are healthy. However, if the cells have undergone AFER then the heterogeneities allow for genesis of multiple wavelets. The power spectrum in Figure 7.9 shows that the DF under Control conditions is 3 Hz, under Workman conditions this is augmented to 8 Hz and in the Bosch case the DF is increased to 10 Hz. These results indicate that electrophysiological changes due to AFER allow for higher frequency oscillations.

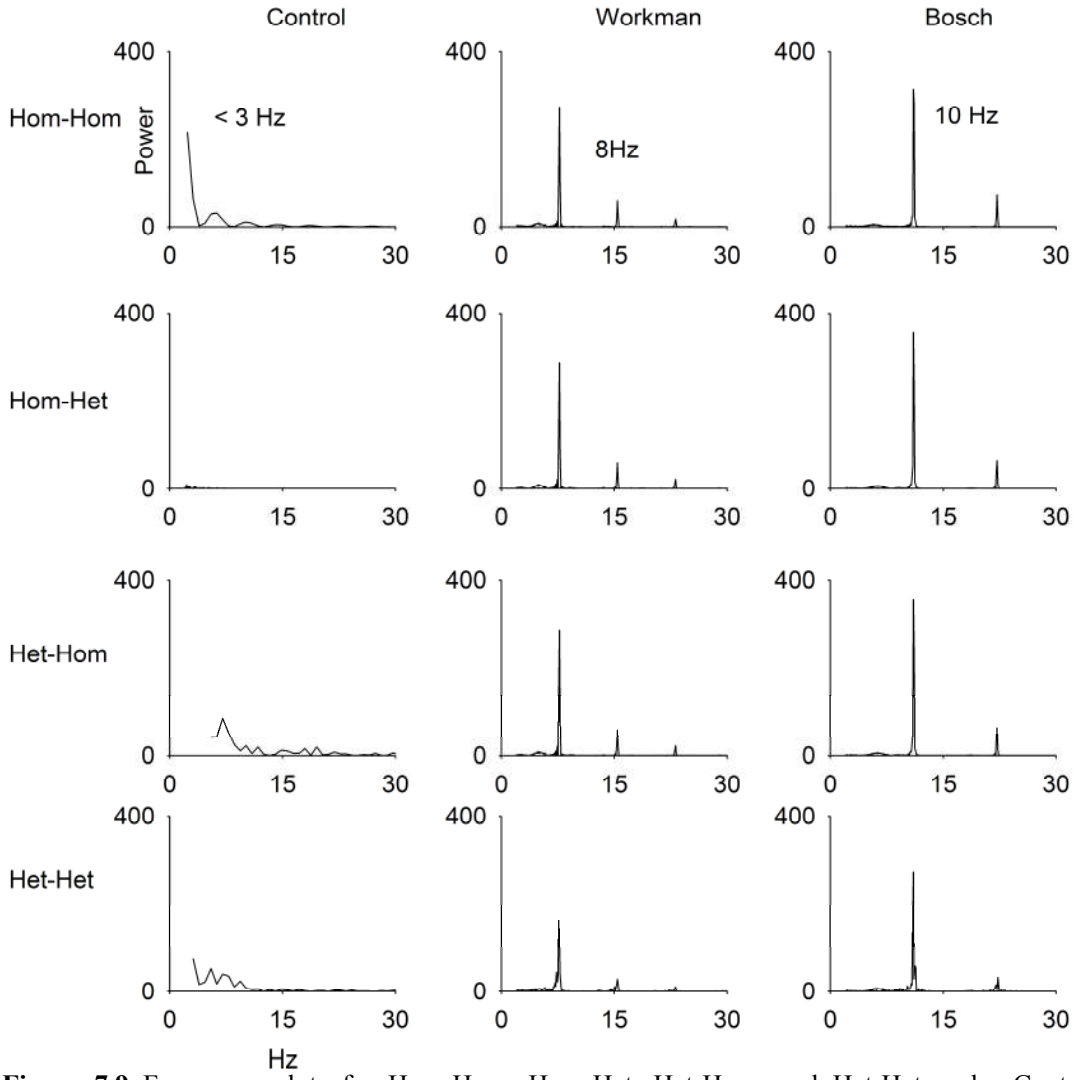

Figure 7.9 Frequency plots for Hom-Hom, Hom-Het, Het-Hom, and Het-Het under Control, Workman, and Bosch conditions. DF under Control conditions is 3 Hz, under Workman conditions this is augmented to 8 Hz and in the Bosch case the DF is increased to 10 Hz. This indicates that electrophysiological changes due to AFER allow for higher frequency oscillations.

7.4. Conclusion and discussion

7.4.1 Main findings

The single cell simulations indicate the pro-arrhythmic effects of AFER in AT, CT, and PM cells are characterised by a shortening of APD, increase in $dV/dT_{max,}$ reduction or ERP, and shortening of VW. In addition electrophysiological changes due to varying cell type results in a diversion of APDs. Recent clinical work has identified that structures within the atrium are an important consideration when studying the generation and maintenance of AF (Wu, Yashima et al. 1998). These structures present themselves as a catalyst for the genesis of re-entrant waves due to their differing electrophysiological properties. The borders between regions between cell types has been identified as to provide an anchor point for spiral rotors (Wieser, Nowak et al. 2008). When performing simulations in the 2D atrial sheet the variations in APD between AT, PM and CT cells at the borders provide a mechanism by which re-entrant waves are initiated. It is observed that these modest variations in between cell types aid in the breakup of re-entry waves under SR conditions. However, under Workman and Bosch conditions the heterogeneities between cell types in increased aiding in maintenance of AF where the CT cells appear to act as an anchor for the re-entrant circuit.

7.4.2 Limitations of simulations

As in the other chapters the CRN model was implemented, the suitability of using this model has been discussed previously. Limitations in the study arise on the assumption that the three different cell types lie in distinct regions separated by a clear boundary. In reality these borders have a transition of cell type density between the regions. In addition these simulations only incorporated cell types for which there is available experimental data. In reality there are multiple cell type regions in the cell all with unique electrophysiological properties. The incorporation of fiber orientation was very basic, with the fibers simulated in the PM and CT region simulated as lying parallel to one another. In the actual myocardium the fibers follow a more free flowing non-descript path. In addition the model of the atria is a single cell in depth; in reality the atria had varying depth through its structure which may alter the CV of the propagating wave.

7.4.3 Clinical relevance

This study has identified the role that electrical and spatial heterogeneities play in the genesis and prevention of AF. Importantly, this study has identified how the effects of

AFER alter the properties of various cells in different ways. For example CT cells seem to resist the effects of AFER more effectively than their PM and AT counter parts. These differences in behaviour of electrophysiology need to be taken into account when developing pharmacological therapies.

Chapter 8

Conclusions, discussion, and future Work

This final chapter outlines the major conclusions drawn from the multiple case studies performed in this thesis and their relevance to the field of study of AF as a whole. The limitations of these studies are discussed along with the possible short and long term direction of future work.

8.1 Conclusions

This section reiterates the major conclusions drawn from the multiple case studies performed in this thesis. The significance of these conclusions are discussed in relation to how they fit into the hypothesis that "AF begets AF", which is outlined in Figure 8.1. Firstly, this includes how AF may be initiated by alterations in the electrophysical properties of the cell due to some underlying etiology, such as the KCNQ1 S140G mutation, or elevated levels of the Hcy hormone. Secondly, how simulations show that AFER increases the tissues susceptibility to the genesis and maintenance of AF. Thirdly, that current clinical treatment using drugs such as BB are not substantially effective at significantly reducing the occurrence of AF, and finally how theoretical simulations allow for conclusions to be drawn about possible future directions of drug developments in regards to atrial specific treatments such as the augmentation of I_{CaL} with the 5HT hormone or blocking of I_{Kur}.

8.1.1 AF genesis in relation to ion-channel remodelling

AF provides a particular problem for clinicians due to its multi-faceted and self perpetuating nature. The hypothesis that "AF begets AF", which is shown in Figure 8.1, provides an indication to the overall complexity of the condition. For AF to occur in a previously healthy patient there must be an underlying mechanism that allows a paroxysmal AF episode to be initiated. The gene mutation KCNQ1 S14G, which is studied in detail in Chapter 2, identified how an alteration to repolarisation K^+ current I_{ks} due to said mutation could result in a substrate that could initiate an AF episode (Chen, Xu et al. 2003). However, while there is a strong link between heart-disease and heredity each

individual genetic mutation would require a tailored pharmacological treatment for each genetic mutation. Unless a mutation was sufficiently prevalent in the population then tailored pharmacological treatments would not be cost effective. In Chapter 3 elevated levels of the Hcy hormone altered the electrophysical propertied of several repolarisation K^+ currents (Cai, Gong et al. 2007). Homocystein levels naturally increase with age but levels may be reduced by increasing vitamin B levels in the diet (Brattstrom, Israelsson et al. 1988). When ionic changes due to the KCNQ1 S140G mutation and elevated levels of the Hcy hormone were incorporated into multi scale models to simulate their effects, re-enrty was observed. While KCNQ1 mutation and Hcy hormone both had differing alterations to ion channel properties both studies resulted in shortened APD and ERP which increased the tissues susceptibility to the genesis of AF.

In addition to the afore mentioned conditions which increase the susceptibility of the atrial tissue to the initiation of AF it has also been observed that rapid pacing of the atrial myocardium for prolonged periods results in AFER (Wijffels, Kirchhof et al. 1995). While the exact mechanism by which AFER occurs is not clear, its identification was a major advancement in the understanding of the progression of AF from paroxysmal to persistent. It was the experimental observation that pacing atrial cells at sufficiently high rates (>600 bpm) resulted in electrical remodelling of the cells at the ion-channel level. In the short term any changes are observed to be protective and reversible. However, under prolonged periods of high pacing the effects are seen to be long tern and irreversible (Wijffels, Kirchhof et al. 1995). This was first observed in a study on goats wjiffles *et. al.* and subsequently in canine (Yue, Melnyk et al. 1999). Theses studies showed that when atrial cells are subjected to a high pacing regime the I_{CaL} current in reduced resulting in a shortened APD and ERP. A hypothesis for why such a reduction in the I_{CaL} current occurs is that it is a protective mechanism against calcium overload. However, the cost to the cell is a reduced ERP which placed the atrial tissue at increased risk of re-entry. If the atrial tissue is subjected to high pacing rates for a short periods the reduction in I_{CaL} in observed to be reversible. However, experimental data suggests that extended periods at high pacing rates the cells are permanently remodelled due to a loss of transcription of the alpha subunit which makes up the I_{CaL} pore forming protein (Yue, Melnyk et al. 1999).

In this thesis I have simulated two separate cases AFER based on available experimental data provided by Bosch *et al* and Workman *et al* in which they studied ionic changes under AF patients who suffered AF for 3 and 6 months respectively (Bosch, Zeng et al. 1999; Workman, Kane et al. 2001). The studies identified that atrial myocyte isolated from AF

patients showed comparable electrophysiological alteration to that observed in sheep. In these studies it was concluded that ionic changes particularly the down regulation of I_{CaL} and up regulation of I_{K1} lowered ERP and which favoured the onset of AF, which is supported in the simulations in this thesis.

8.1.2 Pharmacological treatment of AF

BBs are typically prescribed as a rate control strategy for the management of AF and are routinely prescribed due to their recognised cardio-protective properties (Ishiguro, Ikeda et al. 2008). In Chapter 5, a computational approach was adopted to gain insights into the anti- fibrillatory effects of BBs at tissue and organ levels via the incorporation of experimental data on the effects of BB into a cell under Control conditions and AFER (Workman, Kane et al. 2003). The principal findings were that the application of BB moderately prolonged APD and atrial ERP in when applied to both Control cells and those which have undergone AFER. It was concluded that BBs have a cardio-protective effect of human atrial AP and electrical conduction behaviour, but cannot restore electrical properties of AF affected atrial tissue to SR conditions and therefore have limited applicability in the diseased stages.

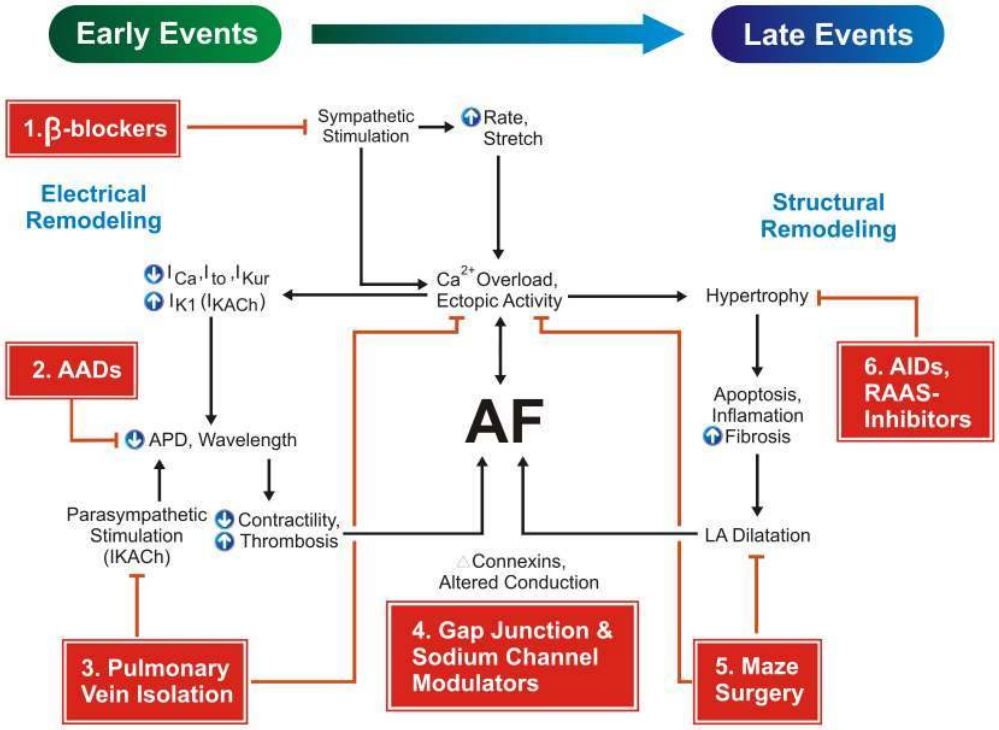

Figure 8.1 Schematic showing the mechanisms for AF and targets for possible therapeutic treatments. Electrical remodeling (left side) occurs on a time scale of hours to days and structural remodeling (right side) occurs over months. The initiation AF due to an ectopic beat results in rapid pacing of the atrial cells allowing AFER to occur. The shortening of APD and atrial ERP increase the tissues susceptibility to AF being initiated. Structural remodeling occurs as rapid pacing results causing hypertrophy and LA dilation, increasing the myocardial volume and therefore increasing the tissues susceptibility to re-entry. Possible treatments options and are numbered and indicate present and future treatment interventions, these include β-Blockers, antiarrhythmic drugs (AADs), pulmonary vein isolation, gap junction and sodium channel modulators, maze surgery, anti-inflammatory drugs (AIDs), rennin-angiontensin-aldosterone system (RAAS).

8.1.3 Theoretical treatment of AF

As previously described current pharmacological treatment strategies for the management of AF are limited in their effectiveness; therefore the development of new drug therapies is vital to improve the prognosis of AF patients (Reiffel 2009). In Chapters 4 and 6 two possible treatment options are simulated, the application of the 5HT hormone which is observed to increase the current density of I_{CaL} in the atria only, and the blocking of the atrial specific repolarisation K^+ current I_{Kur} (Wettwer, Hala et al. 2004; Pau, Workman et al. 2007). Investigating and developing these into a possible pharmacological treatment strategy in the traditional methods would be an extremely expensive process with no guarantee of success (Johnson 2009). However, incorporating the effects of these agents in atrial cells into computer models may give an indication of their effectiveness, thereby possibly reducing the overall cost of drug development.

The ionic changes due to the 5HT hormone as described by Workman *et al.* were incorporated into an atrial myocyte model under Control and AFER conditions, where AFER is simply modeled as a reduction in the I_{CaL} density. Elevated levels of 5HT are know to be arrhythmogenic (Dobrev 2007). However, the augmented I_{CaL} current in tissue which had undergone AFER resulted in a restored I_{CaL} and therefore provide a cardio protective effect. It can be concluded that targeting the 5-HT_4 receptors in tissue which has undergone AFER may provide a possible target for the development of drug treatments. As 5HT is used in multiple other processed in the human body there may be significant side effects when pursuing such a treatment strategy

Though the reduction of I_{CaL} was sufficient to allow re-entry in the 3D geometry this is not an accurate representation of AFER as multiple channels are remodeled which may alter the tissues susceptibility to maintain re-enrty significantly (Bosch, Zeng et al. 1999; Workman, Kane et al. 2001). It is also noted that in experiments atrial myocytes extracted from healthy tissue and subjected to elevated levels of 5HT displayed DAD and EADs which are arrhythmogenic in nature. Simulations to test the cells susceptibility to these phenomena were performed. In cells which where modeled in accordance with AFER as described by Workman *et al.* DADs and EADs were not observed (Pau, Workman et al. 2007). However, in cells under Control conditions it was possible to illicit DADs and EADs.

The blocking of I_{Kur} which is simulated in Chapter 6 is of interest when developing a treatment for AF as it is atrial specific which would limit any adverse effects on the function of the ventricles. Blocking of the I_{Kur} channel has been show experimentally and with simulations to prolongs APD in cardiac myocytes which have undergone AFER and conversely shorten APD and ERP in healthy tissue which may result in increase the tissues susceptibility to AF (Kharche, Seemann et al. 2007). Our simulations confirm that the blocking of I_{Kur} for patients who have undergone electrical remodelling may limit the occurrence of AF and aid in rhythm control, although this is not effective once AF has been initiated. Current pharmacological agents available to block I_{Kur}, such as Vernakalant and AZD7009, also block the sodium current (I_{Na}) (Persson, Carlsson et al. 2005). Another agent, AVE0118, also blocks the transient outward current (I_{to}) in high concentration and are therefore unsuitable to be administered to patients (Gogelein, Brendel et al. 2004). However, if an agent was developed which avoided the blocking of these ion channels it may be a promising rhythm control treatment for AF.

8.1.4 Role of heterogeneity

The single cell simulations indicate the pro-arrhythmic effects of AFER in AT, CT and PM cells are characterized by a shortening of APD, increase in dV/dT_{max} reduction or ERP, and shortening of VW. In addition electrophysiological changes due to varying cell type results in a diversion of APDs. Recent clinical work has identified that structures within the atrium are an important consideration when studying the generation and maintenance of AF (Wu, Yashima et al. 1998). These structures present them selves as a catalyst for the genesis of re-entrant waves due to their differing electrophysiological properties. The borders between regions between cell types has been identified as to provide an anchor point for spiral rotors (Wieser, Nowak et al. 2008). When performing simulations in the 2D atrial sheet the variations in APD between AT, PM and CT cells at the borders provide a mechanism by which re entrant waves are initiated. It is observed that these modest variations in between cell types aid in the breakup of re-entry waves under SR conditions. However, under Bosch and Workman conditions the heterogeneities between cell types in increased aiding in maintenance of AF where the CT cells appear to act as an anchor for the re-entrant circuit.

8.2 Discussion

This discussion section outlines some of the areas which are not included in this thesis but are important when considering the topic of AF as a whole. This includes a description in to the structural and mechanical aspects of AF and possible alternative treatment targets. A discussion into the suitability of cardiac modelling is also included.

8.2.1 Alternative causes and treatments for AF

This thesis has primarily focused on the genesis and maintenance of AF due to changes to the electrophysiology of the cardiac myocyte resulting from a range of external factors. Investigations into structural and mechanical component in the genesis and maintenance of AF are not in the scope of this thesis. However, it is vital area of investigation if the overall understanding of AF is to progress. Structural changes include cardiomegaly, which causes a stretching of the cardiac wall, increasing its size (Levy, Breithardt et al. 1998). This results in an increased area in which re-entrant circuits can occur. In addition fibrosis of the cardiac tissue results from ageing or local fibrosis resulting from a myocardial infarction. Fibrosis is the process where the fibroblast density is increases impeding electrical wave propagation causing a reduced CV. These structural changes also provide the opportunity for the development of drug therapies which target the junction gap coupling allowing for restoration of CV. In any next generation of models it will be vital to incorporate their effects.

8.2.2 Can modelling provide the answers?

The traditional techniques to develop treatment for are an expensive and time consuming process, in addition there are also many ethical considerations (DiMasi, Hansen et al. 2003). In recent years developing new drugs for the treatment of AF had becoming increasingly inefficient, with fewer new drugs being approved (Kola and Landis 2004). As computer simulations are relatively cheap to implement when compared to their traditional counterparts the development of cardiac modelling to study AF may help improve the

efficiency of the development of new pharmacological treatments, therefore modelling provides an attractive tool for drug development.

The power of modelling lies in its ability to predict the out come of how alterations to the electrophysiology of a cell are manifested at whole heart level. In the near future modelling could provide insight into possible drug therapies direction and in the far future modelling may play a role in tailoring treatment to patients in real time at the clinical setting. The field of cardiac modelling has advanced substantially over the past 50 years. However, the current state of modelling is still in the developmental stage whereby models are developed empirically based on available experimental data. These models are then validated by altering the parameters of the equations to reproduce observed experimental results. If models fail to reproduce experimental data then the models need to be improved. While current single cell models accurately reproduce single APs in healthy human tissue they sometimes fail to fully reproduce effects of diseases observed in the clinical setting. This was observed to some degree in modelling of the I_{ks} current in Chapter 2. The KCNQ1 S140G mutation was simulated by adding a voltage dependant leakage current to the Hodgkin-Huxley formulation provided in the CRN model. This modification to the model may not provide an accurate description of the ion channel mutation. Recent work by Abraham *et al.* has suggested that the replacement of the I_{ks} formulation by a series of ODEs representing a markov chain may more accurately represent the complexity of states the ion channel may lie in (Abraham, Yang et al.). However, simulation of markov chains proves to be a problematic in terms of the computation expense required for them to be solved numerically. As the CRN model consists of a series of 24 ODEs incorporating the I_{Ks} markov chain suggested by Abraham *et al.* would required an additional of 17 ODEs to be solved. While this is feasible to implement simulations at a single cell level for a single ion-channel the expansion of this to multi-dimensions and would significantly increase computation power required. If all ion channels were modelled using markov chains the increase in the complexity of the system would be prohibitive. In addition to the increase in number of ODSs to be solved markov chains are problematic to solve numerically due to the large range of time scales involved in the ODE system very are extremely stiff and require advanced ODE solver methods which further escalated the computation expense required. To improve simulation methods employing such techniques are necessary therefore more creative computation techniques are required.

8.3 Future work

This section will outline the possible extensions of projects in this thesis which include the addition of a SA node in to the 3D structure and 2D heterogeneous sheet, improvements to anatomical structure.

8.3.1 Simulating SA node activity

In multi-scale simulations performed on the 3D atria and the 2D heterogeneous sheet re-entry was initiated by a S1-S2 protocol, this allowed for the studies to focus on the tissues ability to permit the formation of sustainment of re-entrant waves. However, the presence of the continuous depolarisation of the SA node is neglected in these studies. The incorporation of a SA node (Chandler, Greener et al. 2009) into the multi-scale simulations would improve understanding of the in the interaction between the beats of the SA node and any re-entrant waves which are present in the atria. The genesis of AF could also be studied in relation to the cardiac tissue being subjected to a high pacing regime. In addition, simulations of cardioversion could be implemented on 2D and 3D geometries to simulate the effects of various protocols which would aid in the breakup of re-enrty and restore normal SR. Future studies may also consider mechanism involving malfunctioning of intracellular $[Ca^{2+}]_i$ handling (Hove-Madsen, Prat-Vidal et al. 2006), spontaneous firing at atrial blood vessel ostia, interaction between SAN and atria.

8.3.2 Improving Anatomical Structures

The anatomical 3D structure used in simulations was taken from the human heart project. However, the resolution of the image is low and does not include fibre orientation or differentiate between differing cell types present in the myocardium, which are know to exhibit differing electrophysiology. Therefore obtaining detailed MRI images is vital to identify fibre orientations and also identify different regions of atrial cell tissue type. There could also be the possibility of subjecting tissue to dissection and imunostaining to help identify different regions of tissues. The case studies in this thesis focused on macro re-entrant waves. However, micro re-entry is also an important factor responsible for AF (Markowitz, Nemirovksy et al. 2007) and the inclusion of the electrical and spatial heterogeneities in the various tissue sub-types in the atrium will further our understanding the genesis of AF, especially the micro-entry due to heterogeneity boundaries

Bibliography

Abraham, R. L., T. Yang, et al. "Augmented potassium current is a shared phenotype for two genetic defects associated with familial atrial fibrillation." J Mol Cell Cardiol **48**(1): 181-90.

Abriel, H. (2007). "Cardiac sodium channel Nav1.5 and its associated proteins." Arch Mal Coeur Vaiss **100**(9): 787-93.

Abriel, H. and R. S. Kass (2005). "Regulation of the voltage-gated cardiac sodium channel Nav1.5 by interacting proteins." Trends Cardiovasc Med **15**(1): 35-40.

Amani, F. and E. S. Smith, 3rd (2005). "Atrial fibrillation: rate versus rhythm control." J Ark Med Soc **102**(4): 110-2.

Andersson, A., L. Brattstrom, et al. (1992). "Plasma homocysteine before and after methionine loading with regard to age, gender, and menopausal status." Eur J Clin Invest **22**(2): 79-87.

Antzelevitch, C. and A. Burashnikov (2009). "Atrial-selective sodium channel block as a novel strategy for the management of atrial fibrillation." J Electrocardiol **42**(6): 543-8.

Aronow, W. S. (2009). "Management of atrial fibrillation in the elderly." Minerva Med **100**(1): 3-24.

Banville, I., N. Chattipakorn, et al. (2004). "Restitution dynamics during pacing and arrhythmias in isolated pig hearts." J Cardiovasc Electrophysiol **15**(4): 455-63.

Bellocq, C., A. C. van Ginneken, et al. (2004). "Mutation in the KCNQ1 gene leading to the short QT-interval syndrome." Circulation **109**(20): 2394-7.

Bernus, O., C. W. Zemlin, et al. (2005). "Alternating conduction in the ischaemic border zone as precursor of reentrant arrhythmias: a simulation study." Europace **7 Suppl 2**: 93-104.

Bettoni, M. and M. Zimmermann (2002). "Autonomic tone variations before the onset of paroxysmal atrial fibrillation." Circulation **105**(23): 2753-9.

Biktashev, V. N. (2002). "Dissipation of the excitation wave fronts." Phys Rev Lett **89**(16): 168102.

Blanc, O., N. Virag, et al. (2001). "A computer model of human atria with reasonable computation load and realistic anatomical properties." IEEE Trans Biomed Eng **48**(11): 1229-37.

Boriani, G., I. Diemberger, et al. (2004). "Pharmacological cardioversion of atrial fibrillation: current management and treatment options." Drugs **64**(24): 2741-62.

Bosch, R. F., X. Zeng, et al. (1999). "Ionic mechanisms of electrical remodeling in human atrial fibrillation." Cardiovasc Res **44**(1): 121-31.

Brattstrom, L. E., B. Israelsson, et al. (1988). "Folic acid--an innocuous means to reduce plasma homocysteine." Scand J Clin Lab Invest **48**(3): 215-21.

Brendel, J. and S. Peukert (2003). "Blockers of the Kv1.5 channel for the treatment of atrial arrhythmias." Curr Med Chem Cardiovasc Hematol Agents **1**(3): 273-87.

Buch, E. and K. Shivkumar (2009). "Epicardial catheter ablation of atrial fibrillation." Minerva Med **100**(2): 151-7.

Burashnikov, A. and C. Antzelevitch "New developments in atrial antiarrhythmic drug therapy." Nat Rev Cardiol **7**(3): 139-48.

Burashnikov, A. and C. Antzelevitch (2008). "Can inhibition of IKur promote atrial fibrillation?" Heart Rhythm **5**(9): 1304-9.

Burashnikov, A. and C. Antzelevitch (2009). "New pharmacological strategies for the treatment of atrial fibrillation." Ann Noninvasive Electrocardiol **14**(3): 290-300.

Burashnikov, A., J. M. Di Diego, et al. (2008). "Atrial-selective effects of chronic amiodarone in the management of atrial fibrillation." Heart Rhythm **5**(12): 1735-42.

Cai, B., L. Shan, et al. (2009). "Homocysteine modulates sodium channel currents in human atrial myocytes." Toxicology **256**(3): 201-6.
Cai, B. Z., D. M. Gong, et al. (2007). "Homocysteine inhibits potassium channels in human atrial myocytes." Clin Exp Pharmacol Physiol **34**(9): 851-5.
Callahan, T. D. t., L. Di Biase, et al. (2009). "Catheter ablation of atrial fibrillation." Cardiol Clin **27**(1): 163-78, x.
Chaldoupi, S. M., P. Loh, et al. (2009). "The role of connexin40 in atrial fibrillation." Cardiovasc Res **84**(1): 15-23.
Chandler, N. J., I. D. Greener, et al. (2009). "Molecular architecture of the human sinus node: insights into the function of the cardiac pacemaker." Circulation **119**(12): 1562-75.
Chen, P. S., B. Joung, et al. (2009). "The Initiation of the Heart Beat." Circ J.
Chen, Y. H., S. J. Xu, et al. (2003). "KCNQ1 gain-of-function mutation in familial atrial fibrillation." Science **299**(5604): 251-4.
Cheng, J. W. and M. Nayar (2009). "A review of heart failure management in the elderly population." Am J Geriatr Pharmacother **7**(5): 233-49.
Cherry, E. M. and S. J. Evans (2008). "Properties of two human atrial cell models in tissue: restitution, memory, propagation, and reentry." J Theor Biol **254**(3): 674-90.
CK Friedberg (1966). "Diseases of the Heart." W.B Saunders.
Coronel, R., F. J. Wilms-Schopman, et al. (1992). "Reperfusion arrhythmias in isolated perfused pig hearts. Inhomogeneities in extracellular potassium, ST and TQ potentials, and transmembrane action potentials." Circ Res **71**(5): 1131-42.
Courtemanche, M., R. J. Ramirez, et al. (1998). "Ionic mechanisms underlying human atrial action potential properties: insights from a mathematical model." Am J Physiol **275**(1 Pt 2): H301-21.
Danicek, V., N. Theodorovich, et al. (2008). "Sinus rhythm restoration after atrial fibrillation: the clinical value of N-terminal pro-BNP measurements." Pacing Clin Electrophysiol **31**(8): 955-60.
Das, S., S. Makino, et al. (2009). "Mutation in the S3 segment of KCNQ1 results in familial lone atrial fibrillation." Heart Rhythm **6**(8): 1146-53.
Dawber, T. R., F. E. Moore, et al. (1957). "Coronary heart disease in the Framingham study." Am J Public Health Nations Health **47**(4 Pt 2): 4-24.
De Bree, A., W. M. Verschuren, et al. (2002). "Homocysteine determinants and the evidence to what extent homocysteine determines the risk of coronary heart disease." Pharmacol Rev **54**(4): 599-618.
de Denus, S., C. A. Sanoski, et al. (2005). "Rate vs rhythm control in patients with atrial fibrillation: a meta-analysis." Arch Intern Med **165**(3): 258-62.
DiMasi, J. A., R. W. Hansen, et al. (2003). "The price of innovation: new estimates of drug development costs." J Health Econ **22**(2): 151-85.
Dobrev, D. (2007). "5-hydroxytryptamine and atrial arrhythmogenesis: a "culprit mechanism" or bystander in patients with chronic atrial fibrillation?" J Mol Cell Cardiol **42**(1): 51-3.
Dobrev, D. and S. Nattel (2008). "Calcium handling abnormalities in atrial fibrillation as a target for innovative therapeutics." J Cardiovasc Pharmacol **52**(4): 293-9.
Ehrlich, J. R. (2008). "Inward rectifier potassium currents as a target for atrial fibrillation therapy." J Cardiovasc Pharmacol **52**(2): 129-35.
Ehrlich, J. R., S. Nattel, et al. (2007). "Novel anti-arrhythmic drugs for atrial fibrillation management." Curr Vasc Pharmacol **5**(3): 185-95.
Fitzgerald, J. D. (1975). "Beta blocking drugs as anti-arrhythmic agents." Int J Clin Pharmacol Biopharm **11**(3): 235-44.
Ford, J. W. and J. T. Milnes (2008). "New drugs targeting the cardiac ultra-rapid delayed-rectifier current (I Kur): rationale, pharmacology and evidence for potential therapeutic value." J Cardiovasc Pharmacol **52**(2): 105-20.

Fuster, V., L. E. Ryden, et al. (2001). "ACC/AHA/ESC guidelines for the management of patients with atrial fibrillation. A report of the American College of Cardiology/American Heart Association Task Force on Practice Guidelines and the European Society of Cardiology Committee for Practice Guidelines and Policy Conferences (Committee to develop guidelines for the management of patients with atrial fibrillation) developed in collaboration with the North American Society of Pacing and Electrophysiology." Eur Heart J **22**(20): 1852-923.

Gillespie, D. T. (1977). "Exact stochastic simulation of coupled chemical reactions." The Journal of Physical Chemistry **81**(25): 2340-2361.

Gogelein, H., J. Brendel, et al. (2004). "Effects of the atrial antiarrhythmic drug AVE0118 on cardiac ion channels." Naunyn Schmiedebergs Arch Pharmacol **370**(3): 183-92.

Gould, P. A., M. Yii, et al. (2006). "Evidence for increased atrial sympathetic innervation in persistent human atrial fibrillation." Pacing Clin Electrophysiol **29**(8): 821-9.

Gray, H. (1918). "Anatomy of the Human Body." Philadelphia: Lea & Febiger.

Haghjoo, M. (2007). "A computer simulation study: the role of multiple wavelets, rotors, and snakes in initiation and maintenance of atrial fibrillation." J Electrocardiol **40**(4): 335 e1.

Haissaguerre, M., P. Jais, et al. (1998). "Spontaneous initiation of atrial fibrillation by ectopic beats originating in the pulmonary veins." N Engl J Med **339**(10): 659-66.

Harvey, W. and Lederle Laboratories. (1987). The anatomical exercises of Dr. William Harvey first published in 1653. [United States], DevCom.

Hodgkin, A. L. and A. F. Huxley (1952). "The components of membrane conductance in the giant axon of Loligo." J Physiol **116**(4): 473-96.

Hodgkin, A. L. and A. F. Huxley (1952). "The dual effect of membrane potential on sodium conductance in the giant axon of Loligo." J Physiol **116**(4): 497-506.

Hollander, W., A. L. Michelson, et al. (1957). "Serotonin and antiserotonins. I. Their circulatory, respiratory, and renal effects in man." Circulation **16**(2): 246-55.

Hong, K., D. R. Piper, et al. (2005). "De novo KCNQ1 mutation responsible for atrial fibrillation and short QT syndrome in utero." Cardiovasc Res **68**(3): 433-40.

Hove-Madsen, L., C. Prat-Vidal, et al. (2006). "Adenosine A2A receptors are expressed in human atrial myocytes and modulate spontaneous sarcoplasmic reticulum calcium release." Cardiovasc Res **72**(2): 292-302.

Huang, T. (1949). The Yellow Emperor's Classic of Internal Medicine
(Translated by Veith I). Baltimore, USA, Williams and
Wilkins.

Hundal, M. and R. K. Garg (2009). "Dronedarone - A New Alternative for Management of Atrial Fibrillation." Recent Pat Cardiovasc Drug Discov.

Ishiguro, H., T. Ikeda, et al. (2008). "Antiarrhythmic effect of bisoprolol, a highly selective beta1-blocker, in patients with paroxysmal atrial fibrillation." Int Heart J **49**(3): 281-93.

Jacquemet, V. (2007). "Steady-state solutions in mathematical models of atrial cell electrophysiology and their stability." Math Biosci **208**(1): 241-69.

Johnson, S. G. (2009). "Improving cost-effectiveness of and outcomes from drug therapy in patients with atrial fibrillation in managed care: role of the pharmacist." J Manag Care Pharm **15**(6 Suppl B): S19-25.

Jongsma, H. J. and R. Wilders (2000). "Gap junctions in cardiovascular disease." Circ Res **86**(12): 1193-7.

Kalus, J. S. (2009). "Pharmacologic management of atrial fibrillation: established and emerging options." J Manag Care Pharm **15**(6 Suppl B): S10-8.

Kaumann, A. J. and F. O. Levy (2006). "5-hydroxytryptamine receptors in the human cardiovascular system." Pharmacol Ther **111**(3): 674-706.

Kemeny-Suss, N., A. Kasneci, et al. (2009). "Alendronate affects calcium dynamics in cardiomyocytes in vitro." Vascul Pharmacol **51**(5-6): 350-8.

Kharche, S., C. J. Garratt, et al. (2008). "Atrial proarrhythmia due to increased inward rectifier current (I(K1)) arising from KCNJ2 mutation--a simulation study." Prog Biophys Mol Biol **98**(2-3): 186-97.

Kharche, S., G. Seemann, et al. (2007). Scroll Waves in 3D Virtual Human Atria: A Computational Study. LNCS. F. B. S. a. G. Seemann. **4466:** 129–138.

Kharche, S., G. Seemann, et al. (2008). "Simulation of clinical electrophysiology in 3D human atria: a high-performance computing and high-performance visualization application." Concurrency and Computation: Practice and Experience **20**(11): 10.

Kharche, S. and H. Zhang (2008). "Simulating the effects of atrial fibrillation induced electrical remodeling: a comprehensive simulation study." Conf Proc IEEE Eng Med Biol Soc **2008**: 593-6.

Kharche, S. P. R. L., H Zhang (2009). Studying Ion Channel Dysfunction and Arrythmogenesis in the Human Atrium: A Computational Approach. Recent Advances in Biomedical Engineering, InTech.

Kneller, J., J. Kalifa, et al. (2005). "Mechanisms of atrial fibrillation termination by pure sodium channel blockade in an ionically-realistic mathematical model." Circ Res **96**(5): e35-47.

Kola, I. and J. Landis (2004). "Can the pharmaceutical industry reduce attrition rates?" Nat Rev Drug Discov **3**(8): 711-5.

Kozlowski, D., S. Budrejko, et al. (2009). "Vernakalant hydrochloride for the treatment of atrial fibrillation." Expert Opin Investig Drugs **18**(12): 1929-37.

Kozlowski, D., S. Budrejko, et al. (2009). "Lone Atrial Fibrillation - What Do We Know?" Heart.

Kuhlkamp, V., A. Schirdewan, et al. (2000). "Use of metoprolol CR/XL to maintain sinus rhythm after conversion from persistent atrial fibrillation: a randomized, double-blind, placebo-controlled study." J Am Coll Cardiol **36**(1): 139-46.

Kumagai, K., C. Khrestian, et al. (1997). "Simultaneous multisite mapping studies during induced atrial fibrillation in the sterile pericarditis model. Insights into the mechanism of its maintenance." Circulation **95**(2): 511-21.

Lafuente-Lafuente, C., S. Mouly, et al. (2006). "Antiarrhythmic drugs for maintaining sinus rhythm after cardioversion of atrial fibrillation: a systematic review of randomized controlled trials." Arch Intern Med **166**(7): 719-28.

Lally, J. A., E. M. Gnall, et al. (2007). "Non-antiarrhythmic drugs in atrial fibrillation: a review of non-antiarrhythmic agents in prevention of atrial fibrillation." J Cardiovasc Electrophysiol **18**(11): 1222-8.

Lambert, D. M. (1972). "Beta-blockers and life expectancy in ischemic heart-disease." Lancet **1**(7754): 793-4.

Laurent, G., G. Moe, et al. (2008). "Experimental studies of atrial fibrillation: a comparison of two pacing models." Am J Physiol Heart Circ Physiol **294**(3): H1206-15.

Lemessurier, D. H., C. J. Schwartz, et al. (1959). "Cardiovascular effects of intravenous infusions of 5-hydroxytryptamine in man." Br J Pharmacol Chemother **14**(2): 246-50.

Levi, G. F. and C. Proto (1972). "Combined treatment of atrial fibrillation with quinidine and beta-blockers." Br Heart J **34**(9): 911-4.

Levy, S. (2006). "Do we need pharmacological therapy for atrial fibrillation in the ablation era?" J Interv Card Electrophysiol **17**(3): 189-94.

Levy, S., G. Breithardt, et al. (1998). "Atrial fibrillation: current knowledge and recommendations for management. Working Group on Arrhythmias of the European Society of Cardiology." Eur Heart J **19**(9): 1294-320.

Liang, X., H. Xie, et al. (2008). "Ryanodine receptor-mediated Ca2+ events in atrial myocytes of patients with atrial fibrillation." Cardiology **111**(2): 102-10.

Lindblad, D. S., C. R. Murphey, et al. (1996). "A model of the action potential and underlying membrane currents in a rabbit atrial cell." Am J Physiol **271**(4 Pt 2): H1666-96.

Liu, P., J. H. Guo, et al. (2009). "Vagal effects on the occurrence of focal atrial fibrillation originating from the pulmonary veins." Circ J **73**(1): 48-54.

Lundby, A., L. S. Ravn, et al. (2007). "KCNQ1 mutation Q147R is associated with atrial fibrillation and prolonged QT interval." Heart Rhythm **4**(12): 1532-41.

Markowitz, S. M., D. Nemirovksy, et al. (2007). "Adenosine-insensitive focal atrial tachycardia: evidence for de novo micro-re-entry in the human atrium." J Am Coll Cardiol **49**(12): 1324-33.

McCully, K. S. (1969). "Vascular pathology of homocysteinemia: implications for the pathogenesis of arteriosclerosis." Am J Pathol **56**(1): 111-28.

Mudd, S. H., J. D. Finkelstein, et al. (1964). "Homocystinuria: An Enzymatic Defect." Science **143**: 1443-5.

Nanda, S., S. M. Siddique, et al. (2009). "Atrial Fibrillation - Advances in Drug Therapy." Recent Pat Cardiovasc Drug Discov.

Nattel, S., C. Matthews, et al. (2000). "Dose-dependence of 4-aminopyridine plasma concentrations and electrophysiological effects in dogs : potential relevance to ionic mechanisms in vivo." Circulation **101**(10): 1179-84.

Nygren, A., C. Fiset, et al. (1998). "Mathematical model of an adult human atrial cell: the role of K+ currents in repolarization." Circ Res **82**(1): 63-81.

Olshansky, B. (2005). "Rate versus rhythm control strategies for AF." Curr Treat Options Cardiovasc Med **7**(5): 371-81.

Olson, T. M., A. E. Alekseev, et al. (2006). "Kv1.5 channelopathy due to KCNA5 loss-of-function mutation causes human atrial fibrillation." Hum Mol Genet **15**(14): 2185-91.

Olson, T. M., V. V. Michels, et al. (2005). "Sodium channel mutations and susceptibility to heart failure and atrial fibrillation." JAMA **293**(4): 447-54.

Osaka, T., A. Itoh, et al. (2000). "Action potential remodeling in the human right atrium with chronic lone atrial fibrillation." Pacing Clin Electrophysiol **23**(6): 960-5.

Otway, R., J. I. Vandenberg, et al. (2007). "Stretch-sensitive KCNQ1 mutation A link between genetic and environmental factors in the pathogenesis of atrial fibrillation?" J Am Coll Cardiol **49**(5): 578-86.

P Wood (1968). "Disease of the Heart and Circulation." J.B Lippincott Company.

Page, R. L. and D. M. Roden (2005). "Drug therapy for atrial fibrillation: where do we go from here?" Nat Rev Drug Discov **4**(11): 899-910.

Panfilov, A. and J. P. Keener "Re-entry in an anatomical model of the heart." Chaos, Solitons & Fractals **5**(3-4): 681-689.

Pau, D., A. J. Workman, et al. (2003). "Electrophysiological effects of 5-hydroxytryptamine on isolated human atrial myocytes, and the influence of chronic beta-adrenoceptor blockade." Br J Pharmacol **140**(8): 1434-41.

Pau, D., A. J. Workman, et al. (2007). "Electrophysiological and arrhythmogenic effects of 5-hydroxytryptamine on human atrial cells are reduced in atrial fibrillation." J Mol Cell Cardiol **42**(1): 54-62.

Persson, F., L. Carlsson, et al. (2005). "Blocking characteristics of hERG, hNav1.5, and hKvLQT1/hminK after administration of the novel anti-arrhythmic compound AZD7009." J Cardiovasc Electrophysiol **16**(3): 329-41.

Plewan, A., G. Lehmann, et al. (2001). "Maintenance of sinus rhythm after electrical cardioversion of persistent atrial fibrillation; sotalol vs bisoprolol." Eur Heart J **22**(16): 1504-10.

Priebe, L. and D. J. Beuckelmann (1998). "Simulation study of cellular electric properties in heart failure." Circ Res **82**(11): 1206-23.

Quan, W. and Y. Rudy (1990). "Unidirectional block and reentry of cardiac excitation: a model study." Circ Res **66**(2): 367-82.
Rahme, M. M., B. Cotter, et al. (1999). "Electrophysiological and antiarrhythmic effects of the atrial selective 5-HT(4) receptor antagonist RS-100302 in experimental atrial flutter and fibrillation." Circulation **100**(19): 2010-7.
Ravens, U. and E. Cerbai (2008). "Role of potassium currents in cardiac arrhythmias." Europace **10**(10): 1133-7.
Ravn, L. S., Y. Aizawa, et al. (2008). "Gain of function in IKs secondary to a mutation in KCNE5 associated with atrial fibrillation." Heart Rhythm **5**(3): 427-35.
Reiffel, J. A. (2009). "Cardioversion for atrial fibrillation: treatment options and advances." Pacing Clin Electrophysiol **32**(8): 1073-84.
Restier, L., L. Cheng, et al. (2008). "Mechanisms by which atrial fibrillation-associated mutations in the S1 domain of KCNQ1 slow deactivation of IKs channels." J Physiol **586**(Pt 17): 4179-91.
Reumann, M., J. Bohnert, et al. (2007). "Multiple wavelets, rotors, and snakes in atrial fibrillation--a computer simulation study." J Electrocardiol **40**(4): 328-34.
Roy, D., M. Talajic, et al. (2008). "Rhythm control versus rate control for atrial fibrillation and heart failure." N Engl J Med **358**(25): 2667-77.
Saltman, A. E. and A. M. Gillinov (2009). "Surgical approaches for atrial fibrillation." Cardiol Clin **27**(1): 179-88, x.
Sanjay R Kharche, P. R. L., Henggui Zhang (2009). "Recent Advances in Biomedical Engineering."
Schouchoff, B. (2007). "Surgical approaches for atrial fibrillation." Crit Care Nurs Q **30**(3): 233-42; quiz 243-4.
Seemann, G., C. Hoper, et al. (2006). "Heterogeneous three-dimensional anatomical and electrophysiological model of human atria." Philos Transact A Math Phys Eng Sci **364**(1843): 1465-81.
Shamiss, Y., Y. Khaykin, et al. (2009). "Dofetilide is safe and effective in preventing atrial fibrillation recurrences in patients accepted for catheter ablation." Europace **11**(11): 1448-55.
Shaw, R. M. and Y. Rudy (1995). "The vulnerable window for unidirectional block in cardiac tissue: characterization and dependence on membrane excitability and intercellular coupling." J Cardiovasc Electrophysiol **6**(2): 115-31.
Singh, B. (2009). "Atrial fibrillation: from ion channels to bedside treatment options." J Electrocardiol.
Sinha, S., M. D. Schwartz, et al. (2009). "Self-reported and actual Beta-blocker prescribing for heart failure patients: physician predictors." PLoS One **4**(12): e8522.
Slocum, J., A. Sahakian, et al. (1992). "Diagnosis of atrial fibrillation from surface electrocardiograms based on computer-detected atrial activity." J Electrocardiol **25**(1): 1-8.
Smelley, M. P. and B. P. Knight (2009). "Approaches to catheter ablation of persistent atrial fibrillation." Heart Rhythm.
Sobieraj-Teague, M., M. O'Donnell, et al. (2009). "New anticoagulants for atrial fibrillation." Semin Thromb Hemost **35**(5): 515-24.
Steeds, R. P., A. S. Birchall, et al. (1999). "An open label, randomised, crossover study comparing sotalol and atenolol in the treatment of symptomatic paroxysmal atrial fibrillation." Heart **82**(2): 170-5.
Syed, Z., E. Vigmond, et al. (2005). "Suitability of Genetic Algorithm Generated Models to Simulate Atrial Fibrillation and K⁺Channel Blockades." Conf Proc IEEE Eng Med Biol Soc **7**: 7087-90.
Tamargo, J., R. Caballero, et al. (2009). "I(Kur)/Kv1.5 channel blockers for the treatment of atrial fibrillation." Expert Opin Investig Drugs **18**(4): 399-416.

Tanabe, Y., Y. Kawamura, et al. (2009). "Blood pressure control and the reduction of left atrial overload is essential for controlling atrial fibrillation." Int Heart J **50**(4): 445-56.

ten Tusscher, K. H., A. Mourad, et al. (2009). "Organization of ventricular fibrillation in the human heart: experiments and models." Exp Physiol **94**(5): 553-62.

Turley, A. J., S. Murray, et al. (2008). "Pre-excited atrial fibrillation triggered by intravenous adenosine: a commonly used drug with potentially life-threatening adverse effects." Emerg Med J **25**(1): 46-8.

Tveito, A. and G. T. Lines (2008). "A condition for setting off ectopic waves in computational models of excitable cells." Math Biosci **213**(2): 141-50.

van der Velden, H. M., J. Ausma, et al. (2000). "Gap junctional remodeling in relation to stabilization of atrial fibrillation in the goat." Cardiovasc Res **46**(3): 476-86.

van der Velden, H. M. and H. J. Jongsma (2002). "Cardiac gap junctions and connexins: their role in atrial fibrillation and potential as therapeutic targets." Cardiovasc Res **54**(2): 270-9.

Viswanathan, M. N. and R. L. Page (2009). "Pharmacological therapy for atrial fibrillation: current options and new agents." Expert Opin Investig Drugs **18**(4): 417-31.

Voigt, N., A. Maguy, et al. (2008). "Changes in I K, ACh single-channel activity with atrial tachycardia remodelling in canine atrial cardiomyocytes." Cardiovasc Res **77**(1): 35-43.

Watanabe, H., D. Darbar, et al. (2009). "Mutations in sodium channel beta1- and beta2-subunits associated with atrial fibrillation." Circ Arrhythm Electrophysiol **2**(3): 268-75.

Watanabe, I., R. Masaki, et al. (2002). "Rate-dependent changes in atrial action potential duration after short- duration rapid atrial pacing in humans." Circ J **66**(9): 874-5.

Weerasooriya, R., P. Jais, et al. (2009). "Catheter ablation of atrial tachycardia following atrial fibrillation ablation." J Cardiovasc Electrophysiol **20**(7): 833-8.

Wettwer, E., O. Hala, et al. (2004). "Role of IKur in controlling action potential shape and contractility in the human atrium: influence of chronic atrial fibrillation." Circulation **110**(16): 2299-306.

Wetzel, U., G. Hindricks, et al. (2009). "Atrial fibrillation in the elderly." Minerva Med **100**(2): 145-50.

Whiteley, J. P. (2007). "Physiology driven adaptivity for the numerical solution of the bidomain equations." Ann Biomed Eng **35**(9): 1510-20.

Wieser, L., C. N. Nowak, et al. (2008). "Mother rotor anchoring in branching tissue with heterogeneous membrane properties." Biomed Tech (Berl) **53**(1): 25-35.

Wijffels, M. C. and H. J. Crijns (2003). "Recent advances in drug therapy for atrial fibrillation." J Cardiovasc Electrophysiol **14**(9 Suppl): S40-7.

Wijffels, M. C. and H. J. Crijns (2004). "Rate versus rhythm control in atrial fibrillation." Cardiol Clin **22**(1): 63-9.

Wijffels, M. C., C. J. Kirchhof, et al. (1995). "Atrial fibrillation begets atrial fibrillation. A study in awake chronically instrumented goats." Circulation **92**(7): 1954-68.

Williams, K. T. and K. L. Schalinske "Homocysteine metabolism and its relation to health and disease." Biofactors **36**(1): 19-24.

Workman, A. J. (2009). "Cardiac adrenergic control and atrial fibrillation." Naunyn Schmiedebergs Arch Pharmacol.

Workman, A. J., K. A. Kane, et al. (2001). "The contribution of ionic currents to changes in refractoriness of human atrial myocytes associated with chronic atrial fibrillation." Cardiovasc Res **52**(2): 226-35.

Workman, A. J., K. A. Kane, et al. (2003). "Chronic beta-adrenoceptor blockade and human atrial cell electrophysiology: evidence of pharmacological remodelling." Cardiovasc Res **58**(3): 518-25.

Wouters, M. G., M. T. Moorrees, et al. (1995). "Plasma homocysteine and menopausal status." Eur J Clin Invest **25**(11): 801-5.
Wu, T. J., M. Yashima, et al. (1998). "Role of pectinate muscle bundles in the generation and maintenance of intra-atrial reentry: potential implications for the mechanism of conversion between atrial fibrillation and atrial flutter." Circ Res **83**(4): 448-62.
Xia, M., Q. Jin, et al. (2005). "A Kir2.1 gain-of-function mutation underlies familial atrial fibrillation." Biochem Biophys Res Commun **332**(4): 1012-9.
Xie, F., Z. Qu, et al. (2002). "Electrical refractory period restitution and spiral wave reentry in simulated cardiac tissue." Am J Physiol Heart Circ Physiol **283**(1): H448-60.
Yang, T., D. J. Snyders, et al. (1997). "Rapid inactivation determines the rectification and [K+]o dependence of the rapid component of the delayed rectifier K+ current in cardiac cells." Circ Res **80**(6): 782-9.
Yang, Y., J. Li, et al. (2009). "Novel KCNA5 loss-of-function mutations responsible for atrial fibrillation." J Hum Genet.
Yin, S., X. Zhang, et al. (2005). "Measuring single cardiac myocyte contractile force via moving a magnetic bead." Biophys J **88**(2): 1489-95.
Yue, L., P. Melnyk, et al. (1999). "Molecular mechanisms underlying ionic remodeling in a dog model of atrial fibrillation." Circ Res **84**(7): 776-84.
Yusuf, S., N. Al-Saady, et al. (2003). "5-hydroxytryptamine and atrial fibrillation: how significant is this piece in the puzzle?" J Cardiovasc Electrophysiol **14**(2): 209-14.
Yusuf, S., R. Peto, et al. (1985). "Beta blockade during and after myocardial infarction: an overview of the randomized trials." Prog Cardiovasc Dis **27**(5): 335-71.
Zhang, H., C. J. Garratt, et al. (2009). "Remodelling of cellular excitation (reaction) and intercellular coupling (diffusion) by chronic atrial fibrillation represented by a reaction-diffusion system." Physica D: Nonlinear Phenomena **238**(11-12): 8.
Zhang, H., C. J. Garratt, et al. (2005). "Role of up-regulation of IK1 in action potential shortening associated with atrial fibrillation in humans." Cardiovasc Res **66**(3): 493-502.
Zhang, H., S. Kharche, et al. (2008). "Repolarisation and vulnerability to re-entry in the human heart with short QT syndrome arising from KCNQ1 mutation--a simulation study." Prog Biophys Mol Biol **96**(1-3): 112-31.
Zhang, S. (2009). "Atrial fibrillation in mainland China: epidemiology and current management." Heart **95**(13): 1052-5.
Zhao, J., M. L. Trew, et al. (2009). "A tissue-specific model of reentry in the right atrial appendage." J Cardiovasc Electrophysiol **20**(6): 675-84.